

*New Platform Designs for Enabling Atomic
Interactions in Solid and Gaseous States*

by

Omar Alshehri

A dissertation

presented to the University of Waterloo

in fulfillment of the

thesis requirement for the degree of

Doctor of Philosophy

in

Mechanical and Mechatronics Engineering (Nanotechnology)

Waterloo, Ontario, Canada, 2023

© Omar Alshehri 2023

Examining Committee Membership

The following served on the Examining Committee for this thesis. The decision of the Examining Committee is by majority vote.

Chair	Urs Hengartner Associate Professor, Cheriton School of Computer Science
External Examiner	Thomas Thundat Professor, School of Engineering and Applied Sciences University at Buffalo, The State University of New York
Supervisor(s)	William Melek Professor of Mechanical and Mechatronics Engineering
Internal Member	Kevin Musselman Associate Professor of Mechanical and Mechatronics Engineering
Internal-external Member	Omar Ramahi Professor of Electrical and Computer Engineering
Internal-external Member	David Yevick Professor of Physics and Astronomy

Author's Declaration

This thesis consists of material all of which I authored or co-authored (see Statement of Contributions included below). This is a true copy of the thesis, including any required final revisions, as accepted by my examiners.

I understand that my thesis may be made electronically available to the public.

Statement of Contributions

The work involved in this PhD was done by Omar Alshehri at five different institutions: University of Waterloo, King Abdullah University for Science and Technology (KAUST), King Abdulaziz City for Science and Technology (KACST), King Saud University (KSU), and King Fahad University for Petroleum and Minerals (KFUPM). These visits were approved by the concerned authorities of these institutions.

Omar Alshehri was the sole author for this dissertation. However, for the 1st project of this thesis (Microsystems/MEMS project), Figure 28 and Figure 46 were captured and provided by M. Arabi (an alumnus from System Design Engineering Department, University of Waterloo) who also helped in drawing the design submitted to MEMSCAP®. These figures were co-authored and published with him. For the 2nd project of this thesis (Nanophotonics project), Jeremy Flannery (an alumnus from Physics Department, University of Waterloo) contributed to the simulations part (Figure 107, Figure 109 & Figure 111 which were co-authored and published). Also, some written content co-authored and published with him was used in the context of these figures.

The following is a list of publications published during this course of this PhD project:

- O. Alshehri, Z-H Li, and M. Al-Amri “Basics of Quantum Communications”, a book chapter within the book “Structured Light for Optical Communication”, *Elsevier* (2021).
- O. Alshehri, M. Al-Ghamdi, M. Arabi, M. Khater, M. Bakri-Kassem, & D. Yevick "Prospect of New AFM Probe Design Enabled by Stress Gradient. *IEEE Transducers* (2021).
- J. Flannery, G. Bappi, S. V. Bhaskara, O. Alshehri, M. Bajcsy, "Implementing Bragg mirrors in a hollow-core photonic-crystal fiber", *Optical Materials Express* 7, 1198 (2017).

- C. Haapamaki, J. Flannery, G. Bappi, R. Al Maruf, S. V. Bhaskara, O. Alshehri, T. Yoon, M. Bajcsy, "Mesoscale cavities in hollow-core waveguides for quantum optics with atomic ensembles", *Nanophotonics* 5, 392 (2016).
- T. Yoon, C. Haapamaki, J. Flannery, G. Bappi, R. Al Maruf, O. Alshehri, M. Bajcsy "Laser cooled cesium atoms confined in a fiber-guided magic-wavelength dipole trap" *APS Division of Atomic, Molecular and Optical Physics Meeting* (2016).
- C. Haapamaki, T. Yoon, J. Flannery, G. Bappi, R. Al Maruf, O. Alshehri, M. Bajcsy "Cold Cs atoms inside a hollow-core photonic crystal fiber" *46th Annual Meeting of the APS Division of Atomic, Molecular, and Optical Physics*, Volume 60, number 7 (2015).

Abstract

This dissertation is composed of two projects that explored two new platforms for measuring atomic interactions using simpler designs than in the literature. The first project of this dissertation designed a platform that enables the measurement of Lennard-Jones interaction between two solid surfaces in the form of Atomic Force Microscope (AFM) probe, using different techniques from Micro electrical Mechanical Systems (MEMS). MEMS by definition implies a mechanical and electrical parts of a system. There are many defects and imperfections that emerges on both sides of the system. On the mechanical side, one of the most common imperfections is residual stress, where most fabrication recipes are designed to eliminate it. Residual stress on films causes curvature (manifested as buckling, bending, etc.) for structures that are meant to be straight. On the electrical side, fringing field is considered very complicated to model, and too small to experimentally detect and separate from the main direct electrostatic field; hence, mostly it gets ignored in modelling. This project will try to make a benefit of these two unwanted phenomena combined (residual stress and fringing field) to make a new design for an Atomic Force Microscope (AFM) probe (tip). The tip behavior is first analyzed and modeled statically using COMSOL software, then dynamically using Mathematica software. Both models were combined and compared with the experimental results obtained by an optical profilometer, scanning electron microscope, and a vibrometer. It was found that the model gave good predictions of the experimental behaviors, except with higher displacement amplitude of the model than that of experiment. The reason is due to the purposeful curvature of the probe (cantilever) induced by residual stress, which caused some parts of the probe not to be on the same level with the electrode; hence, weakened its actual response experimentally. Since use of correction factors to account for

fringing field is nothing new, a correction reduction factor was introduced to lower the model response to match that of the experiment. The results show that the structure of the actuator (parallel plate or a single comb finger) is not of importance in modeling fringing field, as we have applied literature force modeled for non-curved parallel plate capacitors for our curved comb-finger structure and got identical response to our comb-finger derived new force with a matter of just a correction factor (i.e. free parameter). We have also shown that the curvature equation is unnecessary in the model, and the behavior of the curved probe can be modeled as a straight one.

The second project of this dissertation is another simple design for enhancing light-matter interaction between a single laser beam and an atomic gas (cesium) in what is known as cavity Quantum Electrodynamics (QED). Increasing the interaction between light and matter is inspired by the desire to unravel more understanding about the nature of both interacting entities: light and matter. This can be enabled by engineering necessary platforms where such maximally interacting light and matter can be realized. Usually there are two ways to increase such interaction: 1) increase transverse confinement, and 2) increase the interaction time (in addition to increasing the number of atoms). Each of these two ways is done in a separate platform design. This second project proposes a new platform that can have both ways: increasing both transverse confinement and interaction time by using the hollow core of photonic crystal fiber as the interaction host (hence blocking light from propagating transversally by the photonic bandgap effect), while the light will be bounced back and forth against the atomic gas, not by the conventional Fabry-Perot cavity, but instead by inscribing a Bragg grating mirror on the walls of the hollow core (hence, increase interaction time). The unblocked hollow core will allow easier atomic gas insertion. Different mirror inscription methods were studied, and the best method was employed using a photoresist-assisted layer, instead of direction inscription on the core silicon wall. Initial numerical modeling

was done using *Lumerical* software that gave the Bragg parameters corresponding to the best Bragg mirror reflection which was up to 99.99% reflectivity from only about 3×10^2 Bragg periods (shorter mirror) corresponding to only ~ 100 μm penetration depth. Moreover, since the hollow core photonic crystal fiber is of a high cost, an injection port was designed and built to enable low fiber material loss caused by conventional injection.

Acknowledgment

This PhD dissertation was done over the period of a whole decade. It was done in two countries, and at five different institutions. This PhD survived a sudden sponsorship termination, a conflict between my country (Saudi Arabia) and Canada, and a global pandemic (COVID 19) with a worldwide lockdown and a travel ban. I could have never survived this Hollywood-style, almost fictional story without the support from a higher power (God Almighty), then by standing on the shoulders of tens of giant friends, family members, professors, colleagues, public sector employees, and so on. Unlike regular PhD dissertations, I am not going to acknowledge them here because listing their names and contributions will take a whole book constituting the story of this PhD. I hope to write it one day where they will be fully acknowledged.

Table of Contents

Author's Declaration	iii
Statement of Contributions	iv
Abstract	vi
Acknowledgment	ix
List of Figures	xiii
List of Tables	xxv
Project 1: New Electrostatic AFM Probe Design Enabled by Stress Gradient.....	1
Chapter 1: Introduction	2
1.1 Motivation	3
1.2 Curvature in MEMS Structures.....	7
a) Undesired curvature.....	7
b) Purposefully induced curvature.....	9
1st: Temperature variance based.....	10
2 nd : Pressure variance based.....	13
3rd: Photoisomerization.....	14
4th: Tip-Controlled Electrodeposition.....	15
5 th : 3D printing.....	16
6 th : Shape-locking.....	17
7 th : Using multi-materials.....	17
Chapter 2: Statics Modelling vs. Related Experiments	20
2.1 Building the COMSOL Model.....	20
2.2 Static DC Voltage-Induced Displacement	29
2.2.1 The Curved Cantilever Case.....	32
2.3 Fringing Field Forcing Equations	34
2.3.1 Existing Literature Force Equations	34
Kambali et al	35
2.3.2 The Approach to Find the New Forcing Equation	38
Chapter 3: Dynamics Modeling with Related Experiment	43
3.1 Equation of Motion	45

3.1.1 The Deflection Revisited	47
3.1.2 Forcing Equations Revisited $f(t)$	49
3.1.3 The effective rigidity EI_{eff}	50
3.2 Solving the Equation of Motion by Galerkin’s Weighted Residual Method	52
3.2.1 Finding the mode shape	53
Chapter 4: Experimental Results vs Related Models.....	56
Chapter 5: Conclusion and Recommendations for Project 1	64
Project 2: Light-Matter Interaction Using 1D Mirror Inscribed in a 2D Photonic Crystal Fiber .	72
Chapter 1: Introduction	73
1.1 Light-Matter Interactions	73
1.1.1 The Proposed Platform	76
1.2 Photonic Bandgap Effect and the Light Matter Similarities	77
1.2.1 Photonic Crystals and Photonic Bandgap.....	80
1.2.1.1 The Mechanism of 1D Photonic Bandgap: Bragg Reflection	81
1.3 Modified Optical Fibers (MOFs)	82
1.3.1 The Bandgap Mechanism of 2D Photonic Crystal Fiber.....	84
1.3.2 Fabrication of HC-PCF.....	87
Chapter 2: Experimental	89
2.1 Inscribing 1D PC into 2D PC.....	89
2.1.1 The Proposed Platform	92
2.2 Experimental Procedures.....	93
2.2.1 Blocking the Cladding Photonic Crystal	93
a) Femtosecond laser drilling [99].....	93
b) UV-assisted cleaving [100].	94
c) Lateral access filling [103, 104].	96
d) Manual gluing [106, 107]	97
e) Air-holes collapse [102].	98
f) 4.1.7 Capillary splicing [109, 110].	100
2.2.2 Resist Injection	104
a) Drop held on Single Mode Fiber.	104
b) Syringe.....	105
c) Custom-Made Injection Port	106

2.2.3 Laser Interference Pattern Inscription	108
a) Direct ablation/burning (also called point by point) [112].	108
b) Interferometer-mask coupling [115].	109
c) Bare phase mask [117].	109
d) Bare interferometer [118, 119].	110
2.2.4 Bragg Grating Material and Parameters	111
2.2.5 Grating Characterization.....	115
a) SEM imaging.....	115
b) Custom Built Optics Table Setup.	116
Chapter 3: Numerical Simulations.....	118
3.1 Bragg Mirror Reflectivity.....	120
3.1.1 Resist Thickness	121
3.1.2 Resist-based FBG compared to FBG by bare silica modulation	125
Chapter 4: Future Work for Project 2	126
4.1 Selective Injection	126
4.2 Laser Interference Inscription	126
4.3 Characterization	126
References.....	128
Appendix (Permissions).....	141

List of Figures

Figure 1: Lateral (left) [3] and vertical (right) [4] actuation movement of cantilevers towards actuation electrodes. Note the existence for two side stoppers to prevent cantilever-electrode stiction (pull-in) in the lateral case (left) [3]. No reuse permission was required from [3] & [4]).3

Figure 2: Schematics of the probe's different components (top). The probe has to be flipped when integrated with other AFM components (bottom). 4

Figure 3: Electrostatically actuated AFM by Brugger et al [6]. Note the tip at the cantilever's end as an attachment, not as an integrated part of it. Used with permission from [6]..... 5

Figure 4: An AFM tip (FASTSCAN-A model) by Bruker company, which is sold for \$98.175 a piece. Reused with permission from Bruker Nano Surfaces and Metrology [7]. 5

Figure 5: An extremely bent cantilever which makes it mostly out of the effect of the fringing field if actuated by a side electrode. Used with permission from [10]..... 7

Figure 6: Undesired curvature induced by fabrication process [11]. Used under Fair Use Doctrine. 8

Figure 7: Control of the curvature of bi-layered cantilever made of poly and gold through heating. No reuse permission was required by the publisher of [12] that referred to Fair Use under US Copyright Law. 8

Figure 8: Non-structural, stationary curved side electrodes. Used with permission from [13]. 9

Figure 9: Schematics (left) and optical microscope images (right) for the curved cantilevers with their corresponding electrodes. Used with permission from [14]. 9

Figure 10: An SEM image of self-rolling beams on a suspended plate. Used with permission from [15]. 10

Figure 11: Schematics of grain sizes gradience effect in inducing curvature (after removing the sacrificial layer). 10

Figure 12: Stress-temperature relation made by Yang et al [25] as a summary of four works where, + from [29], x from [30], ° from [31], Δ from [32]. Used with permission from [25]. 12

Figure 13: The borderline between etching and deposition for the reduction of silicon tetrachloride gas by hydrogen in a PECVD. Used with permission from [24]. 14

Figure 14: Trans to cis isomerizations of of a molecule (a) and how it induces cantilever curvature (b). Used with permission from [33]. 15

Figure 15: AFM-enabled electrodeposition of curved microbeams. Used with permission from [34]. 15

Figure 16: Voltage as applied to the AFM probe to enable electrolyte breakdown and deposition to form the desired structure. Used with permission from [35]. 16

Figure 17: SEM images for slanted 3D printed tips/probes (top [37] and bottom [36]). Bottom imaged was used with permission from [36] (no reuse permission was required for the top image from [36] & [37]). 16

Figure 18: How magnetic shape memory polymers locks at curvature after turning off the magnetic field. This was done on a cantilever made of polymer that is embedded with soft (Fe_3O_4) and hard (NdFeB) magnetic particles. Used with permission from [38]. 17

Figure 19: A schematics of the bi-material cantilever (left) and an SEM image of the induced curvature after removing the sacrificial/release layer (right). Used with permission from [14]. . 18

Figure 20: Schematics of the cross-sectional view showing different layers of the PolyMUMPs process. Used with permission from [39]. 19

Figure 21: The Physics tree defined for the Electromechanics module used to simulate the actuator.
..... 20

Figure 22: 3D view of the actuator as designed in COMSOL..... 22

Figure 23: The electric potential distribution across the length of the cantilever with a 1 DC volt.
..... 23

Figure 24: von Mises stress matrix for the gold layer as entered in COMSOL. Poly layer was assumed with no stress, so a matrix was not introduced..... 25

Figure 25: The initial curvature profile as found by COMSOL. 25

Figure 26: Table-Top JEOL Scanning Electron Microscope. 26

Figure 27: SEM images of the curved long cantilever (top) and the short one (bottom). The image was co-published by the student in [41] and was reused here with permission. 27

Figure 28: The curvature profile of the long (top) and short (bottom) cantilevers as produced by the optical profilometer. The image was co-published by the student in [41] and was reused here with permission..... 27

Figure 29: von Mises stress profile across the short cantilever. Enlarged above is the cantilever post which holds the highest stress point. The image was co-published by the student in [41] and was reused here with permission. 28

Figure 30: Actuation voltage vs tip displacement for long cantilever as obtained by COMSOL. The voltage was applied to the side electrode, with a sweep range from 0-190 V. The image was co-published by the student in [41] and was reused here with permission..... 29

Figure 31: Actuation voltage (X axis) vs Tip Displacement in μm (Y axis) for the short cantilever. The voltage was applied to the side electrode, with a sweep range from 0-190 V. The image was co-published by the student in [41] and was reused here with permission..... 30

Figure 32: Cross sectional view of the potential contours (dashed lines) and electric fields (solid arrows) of a cantilever (single comb finger) under levitation force [43]. Note that both the cantilever (movable finger) and bottom electrode are grounded, similar case to our actuator. No reuse permission was required by the publisher of [43] that referred to Fair Use under US Copyright Law. 31

Figure 33: (Top) The type of force acting on a movable finger between two side electrodes and a fixed bottom electrode. (Bottom) The force passes from being repulsive (a) to attractive (c) through a threshold point (b). Used with permission from [44]..... 33

Figure 34: The parallel plate actuator modeled by Osterberg and Senturia. Used with permission from [45]. 35

Figure 35: Different configurations studied by Kambali et al [46]. The configuration of interest to us is (i) as it closely resembles ours. Used with permission from [46]. 35

Figure 36: The beam configuration corresponding to our actuator [46]. Note that the bias between cantilever and bottom electrode, which is absent in our case: due changes in the forcing equation to count for that. Used with permission from [46]..... 36

Figure 37: Actuation Voltage (X axis) vs Tip Displacement in μm (Y axis) for the short cantilever. The voltage was applied to the side electrode, with a sweep range from 0-190 V..... 39

Figure 38: The overall capacitance (Y axis) vs applied actuation voltage (X axis). 40

Figure 39: The combined chart of capacitance values (y axis) and their corresponding tip deflection (x axis). Note the fitting function y in the middle of the chart. The black dots (with green borders) represents the COMSOL data points, while the red line is the trend line which is represented by the fitting function y (at the middle of the chart). 41

Figure 40: Total beam deflection $w(x,t)$ including the initial curvature due to stress gradient. 48

Figure 41: The original cross section of the beam (left) transformed into a new equivalent cross section (right) made of polysilicon only. 50

Figure 42: Wire clips (red) as they are connected to the PCB connectable pins. One pin connects the side electrode to the voltage source, the other connects the cantilever and bottom electrode to external grounding. The chip was covered with glass lid, mounted by the golden tape for protection. 56

Figure 43: The drawing and dimensions of the chip on which the device was fabricated (top), a closer view showing the bond pads and their numbering for cantilever identification (bottom right), and a 3D view showing the cavity inside which the cantilevers are protected with the lid (bottom left). Used with permission from [49]..... 57

Figure 44: The Polytec vibrometer. The photos show the device and its computer interface. 58

Figure 45: (Left) The chip as mounted on the PCB and subjected to the laser beam. (Right) The laser beam pointer directed to the cantilever's tip as observed under the vibrometer's optical microscope. 58

Figure 46: First three natural frequencies experimentally obtained in air medium. The image was co-published by the student in [41] and was reused here with permission..... 59

Figure 47: An example of time history response for the cantilever at excitation frequency of 22 kHz using 10 AC-10 DC forcing (on Mathematica) showing the transient response in nondimensional time units (x-axis). Note that the deflection amplitude was taken for the last three periods..... 60

Figure 48: Different curvatures for different DC voltages in a sweep from 0-190 Volts using COMSOL. Different lines here represent cantilevers with different curvatures. 61

Figure 49: Experimental frequency sweeps (blue) as compared with the theoretical ones: Osterberg and Senturia (red) and our new force (brown)..... 62

Figure 50: Capacitance for curved structure turned into slices. Note how COMSOL only measures one capacitance per whole structure despite the defined slices and defined corresponding probes. 65

Figure 51: The thick wire bonding (right of the image) which might have produced more field onto the cantilever..... 66

Figure 52: The lock-in amplifier user interface (LabOne) for 10 DC - 7 AC (top) and the transimpedance amplifier (bottom)..... 67

Figure 53: The probe connections to the lock-in amplifier via the chip carrier pins. Note that there exist only two clamps connected to the pins (red wire): one is for connecting the side electrode, and the other is for connecting both the probe and bottom electrode to ground. 68

Figure 54: The proposed lock-in amplifier connection and the description of its mechanism with numbered steps..... 69

Figure 55: The peel force acting on the cantilever's tip due to the shear stress induced force imbalance caused by the sacrificial layer below it. Used with permission from [16]. 71

Figure 56: Single photon-multi atoms interaction. 74

Figure 57: Schematic of a cross section of a fiber core confining one photon and one atom. 74

Figure 58: Schematic of a cavity confining one photon and one atom allowing the photon to go through multiple passes..... 75

Figure 59: Schematic of a cavity cross section confining one photon and one atom both longitudinally and transversally..... 75

Figure 60: Schematic of fiber cross section confining one photon and one atom with an impeded cavity of two Bragg mirrors inscribed on the core’s wall. Hence, it allows the photon to go through multiple passes while keeping the core unobstructed. 76

Figure 61: Cartoon visualization of the HC-PCF (left) [51] and an optical microscope image of the HC-PCF used in this project (right) [52]. Used with permission from [51] and [52]..... 76

Figure 62: a) Photograph of the beetle. b) Optical micrograph of few scales. c) Cross section SEM image of a single scale. d) Higher magnification of SEM image of a region of a scale. Used with permission from [72]..... 80

Figure 63: 1D PBG crystal [73], 2D PBG crystal [74], and 3D PBG crystal [75], respectively. Modified and reused with permission from [74] and Fair Use Doctrine. 81

Figure 64: Schematic showing the mechanism of Bragg reflection: no forward propagation, and only backward reflection for the resonant wavelength. The rest of wavelengths will cause both forward and backward propagations. 82

Figure 65: The first two proposed MOF as shown in [77] which were slightly modified from [78]. Used with permission from [78]. 83

Figure 66: The first HC-PCF demonstrated experimentally [82]. No reuse permission was required from [82]. 83

Figure 67: A tree showing different kinds of fibers and how it relates to HC-PCF. 84

Figure 68: Guidance by TIR between two glasses with different refractive indices (left). Guidance by TIR coupled with PBG caused by transversely destructive interference of certain light frequencies, allowing light to confine and propagate longitudinally along the core. Note that the core here is shown as hollow, though the same mechanism applies for solid core also (right). Adopted and modified with permission from [85]. 84

Figure 69: The band diagram of the out of plane light propagation into a 2D photonic crystal fiber (PCF) showing the bandgaps. Used with permission from [86]. 85

Figure 70: Five-by-Five grid for a neutral cesium atom-based quantum-computer prototype built at Penn State University. Used with permission from [89]. 86

Figure 71: Near field intensity profile at the core of the HC-PCF with $7.5 \pm 1 \mu\text{m}$ hollow core diameter. Used with permission from [52]. 87

Figure 72: Fabrication process of HC-PCF. Compiled from references. Figure composed from [91] and [92]. Used with permission from [91] (no permission was required from [92]). 87

Figure 73: The FBG as should look inside the hollow core from front (a) and cross sectional (b) views (not to scale). The image was co-published by the student in [95] and no reuse permission was required. 89

Figure 74: Schematic showing the small portion of the propagating light that interacts with the grating (top). The light mode field diameter compared to the fiber core’s diameter (bottom). Bottom image was reused with permission from [96]. 90

Figure 75: For the same amount of light incident into both cavities (top and bottom) and a given reflectivity, the lower index contrast mirror (top) requires more layers to achieve the given reflectivity; hence, longer penetration depth which in turn distributes the light volume over larger area as seen by the intensity distribution curve above. The higher index contrast mirror (bottom) requires less layers; hence, shorter penetration depth which in turn allows for a tighter confinement of the light in the cavity and can thus lead to stronger light-matter interactions. 91

Figure 76: The index modulation as it appears in a cross section of the fiber (top) and the “effective” index modulation as experienced by the propagating light (bottom). 93

Figure 77: Sequential steps from top to bottom of creating a cap for selective injection using femtosecond laser cleaving. No reuse permission is required from [99].	94
Figure 78: Optical microscope images of the different steps towards opening the lateral hole in the wall of the fiber. No reuse permission was required [103].	96
Figure 79: A hole drilled on the fiber side wall by FIB drilling. No reuse permission was required from [105].	96
Figure 80: PC-holes manual blocking using a UV-curable glue. Used with permission from [107].	97
Figure 81: Blocking photonic crystal holes using a glue carried on another fiber. Used with permission from [106].	98
Figure 82: Air holes' collapse by splicing arc-induced heating. No reuse permission is required from [102].	99
Figure 83: Optical microscope image (a) and SEM image (b) of NOA74-filled central hole PCF. No reuse permission is required from [102].	99
Figure 84: Capillary splicing assisted infiltration. a) The steps to make the infiltration cap. b) optical microscope image of the infiltration cap. Used with permission from author of [110].	100
Figure 85: The splicer screen showing a top view of the HC-PCF & capillary interface (left of the screen) and a side view of the interface (right of the screen).	101
Figure 86: The HC-PCF as spliced to a capillary of the same diameter (top) and a closer image (bottom). Fiber diameter is 120 microns, hole diameter is 7 ± 2 microns. The central hole can still be seen continuous across the cap.	102
Figure 87: The cleaver used.	102
Figure 88: Schematics of the proper HC-PCF loading onto the V groove holder.	103

Figure 89: The capped HC-PCF (left) and the bare HC-PCF (right). The cap successfully blocked fiber outgoing light except at the hollow core, as intended.	104
Figure 90: SMF-based fluid delivery system. Used with permission from [111].	105
Figure 91: Injection of photoresist inside the fiber hollow core using an epoxy-sealed syringe.	105
Figure 92: Schematic of the designed injection port.	106
Figure 93: The injection port we designed and assembled.	107
Figure 94: SEM image of the SU-8 fully blocked core (left) and the post nitrogen blow ring formed by the high viscosity SU-8 photoresist (right).	107
Figure 95: Long Period Grating made into HC-PCF by splicing arc, air pump, and a micro-stepper. The air pump is used to prevent hole's collapse by the arc partially maintaining the hollow structure. Used with permission from [114].	108
Figure 96: Mirror inscription into the nanofiber by both a phase mask and an interferometer (dual beam interferometer here). No reuse permission is required from [116].	109
Figure 97: A schematic showing the full light beam where the lower half of the beam is directly projected onto the substrate, while the upper half reaches the substrate reflected from the mirror; hence forming the interference pattern when interfering with the directly projected light. Used with permission from [122].	110
Figure 98: The assembled Lloyd Interferometer. The holder on the right is covered with partially sticking tape for easier loading and unloading of samples (the setup is enclosed in a box to minimize airflow avoiding optical path differences).	111
Figure 99: Parameters for Lloyd interference lithography. Used with permission from [125]. .	112
Figure 100: Beam cleanliness enhancement as a result of the pinhole. Used with permission from [126].	114

Figure 101: Cross section of a solid core fiber with FBG inscribed on its core. Used and modified from [97]. No reuse permission was required [97]. 115

Figure 102: Experimental setup for characterizing the FBG formation showing light power distribution due to transmission, reflection, and refraction due to beam sampler and the fiber. 116

Figure 103: SEM image of the HC-PCF (left) and the imported image to Lumerical (right). ... 118

Figure 104: The Lumerical software interface showing the initial model built with circular holes. 118

Figure 105: The light attenuation curve as a function of the propagating wavelength into the HC-800-02 HC-PCF as provided by the manufacturer (left) and as simulated by Lumerical (right). Used with permission from [52]. 119

Figure 106: The penetration depth components, z_1 and z_2 , in which the blue arrow represents the light beam/photon penetrating the hollow core. The penetration depth basically is how far this beam/photon “penetrates” the core which is simply the sum of z_1 and z_2 121

Figure 107: The attenuation as a function of the photoresist film thickness for photoresist indices of 1.61 (black line) 1.45 (red) and 1.3 (green). The image was co-published by the student in [95] and no reuse permission was required. 122

Figure 108: Visualization of the 300 periods made of AZ-701 photoresist and air that spans across 100 μm inside the fiber, in order to cause the 99.99% reflectivity. 122

Figure 109: FBG reflectivity as a function of the photoresist film thickness. The image was co-published by the student in [127] and no reuse permission was required. 123

Figure 110: Visualization of the index modulation of the first layer of PCF holes surrounding the hollow core, in which the photonic crystal holes are selectively filled with a polymer then exposed

to interference pattern-based index contrast. The image was co-published by the student in both [95] and [127] and no reuse permission was required. 123

Figure 111: The corresponding maximum reflectivities that can be achieved using a perfect Bragg reflector with optical losses associated with the fiber are shown for polymer in the photonic crystal region (in which the holes in the first layer are filled one at a time in a counter-clockwise direction). The image was co-published by the student in [127] and no reuse permission was required. ... 124

List of Tables

Table 1: Residual stress and microstructure of as-deposited (top) and annealed (bottom) silicon films as a function of both deposition temperature and pressure, where (a) stands for amorphous and (c) for crystalline. Used with permission from [18].	13
Table 2: Dimensions of the side electrode, cantilever, air box, and bottom electrode.	21
Table 3: The mechanical and electrical parameters of PolyMUMPs process layers. Used with permission from [39].	23
Table 4: Fabrication variation range for the residual stress of all PolyMUMPs layers. The last two are of interest since they constitute the cantilever layers. Used with permission from [39].	24
Table 5: Different forms of F_2 and their corresponding applicable ranges. Note that g is the side gap between the cantilever and the side electrode, while d is the gap between the cantilever and the bottom electrode.	37
Table 6: Parameters used in the dynamics modelling and their values.	44
Table 7: The components needed to calculate the height of the neutral axis.	51
Table 8: Comparative table of natural frequencies of the cantilever as obtained experimentally and analytically.	59
Table 9: Physical and optical properties of the hollow core fiber we are using [52].	86
Table 10: Different steps of introducing a cap on the fiber end-face by UV glue in preparation for selective injection (modified from [100]).	95
Table 11: HC-PCF to capillary splicing parameters. Note that the offset is the distance between the arc and the center of the gap between the fibers.	101
Table 12: Fiber dimensions fed to the Lumerical model.	119

"العلم نقطة كثَّرها الجاهلون"

علي ابن أبي طالب رضي الله عنه

“Knowledge is a speck, multiplied by the ignorant”

Ali ibn Abi Talib (601-661 AD)

Project 1: New Electrostatic AFM Probe

Design Enabled by Stress Gradient

Chapter 1: Introduction

Atomic Force Microscope (AFM) is well known microscope that taps the microstructural surfaces and plot their roughness/profiles. AFM is based on piezoelectric actuation of a microcantilever that will be in close proximity to the surface under study. There are several actuation methods that could be tried for AFM including the following:

- 1- Thermal
- 2- Piezoelectric
- 3- Electromagnetic.
- 4- Electrostatic.

In this project, we try achieving a new method of actuation method: one kind of electrostatic actuation: the fringing field component of the electrostatic field. The benefit of electrostatic actuation (over piezoelectric) is that it gives wider material selection than the fewer piezoelectric. The piezoelectric materials must have strong coupling coefficient while their grains have to be oriented in the right direction: things that the electrostatic actuation does not require. Moreover, electrostatic actuation is less expensive to fabricate and is also energy conserving process (basically a capacitor pushing a conductor both ways). The only energy loss happens through I^2R losses if we have parasitic resistance (in conductor and interconnect) in series with the electrodes which will generate heat losses. Eliminating this resistance will make it loss-less actuation method. It is worth mentioning that the electrostatic actuation is already well-known actuation method that is already applied for various MEMS applications [1, 2]. In these applications, however, usually the movement direction of actuated structure (e.g. cantilever) is towards the electrode direction:

either longitudinally or vertically. Figure 1 shows a longitudinally actuated cantilever [3] and vertically actuated one [4] that are both in the direction towards the actuation electrode.

The problem with such actuation is that it could lead to pull-in phenomena, where the actuator's beam/cantilever is permanently stuck to the electrode when passing a certain actuation threshold voltage. Usually pull-in is eliminated by either avoiding threshold voltage, or by adding a stopper as shown on Figure 1. Avoiding threshold voltage will limit the range of surfaces the AFM can scan, while adding a stopper defies the principle of AFM because the direction of the stopper is the direction of the surface the AFM scans/taps.

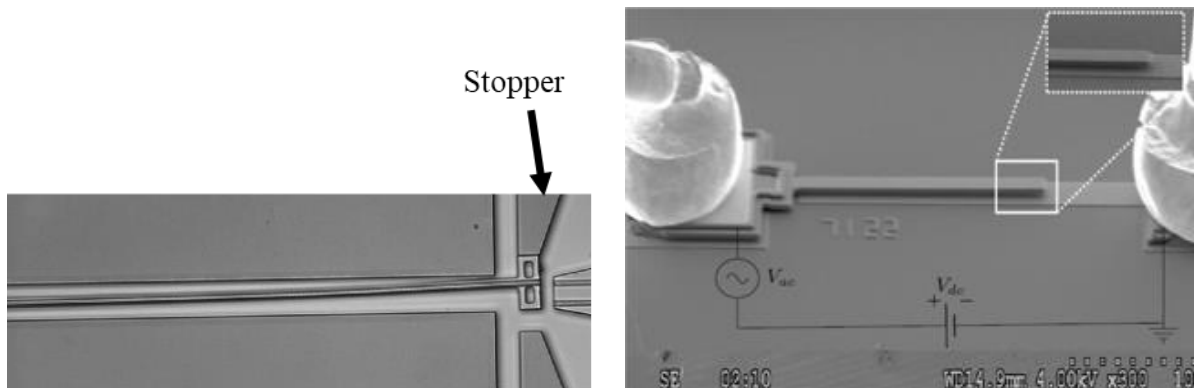


Figure 1: Lateral (left) [3] and vertical (right) [4] actuation movement of cantilevers towards actuation electrodes. Note the existence for two side stoppers to prevent cantilever-electrode stiction (pull-in) in the lateral case (left) [3]. No reuse permission was required from [3] & [4].

1.1 Motivation

Having a pull-in free AFM requires a tip that is allowed to freely vibrate vertically along the surface it measures, while been safe from pull-in. This is attainable by the following requirements:

- 1- A cantilever that moves away from the electrode upon actuation. Reason: to avoid pull-in.
- 2- The cantilever tip that is away far enough from the actuation electrode. Reason: to avoid any interaction between the actuation electrode and the specimen under investigation by

the tip. These interactions are called Lennard-Jones interactions [5] which is supposed to happen only between tip and sample.

Achieving this tip AFM probe design is the goal of this work. The design implemented to achieve this goal is as follows: a curved cantilever (with a sharp tip) centered inside a U-shaped side electrode that actuates the beam upwards by its fringing field by being connected to AC/DC voltage source. An additional bottom electrode will be grounded along with the cantilever that is also grounded. Figure 2 shows a schematic of the structure. Note that the structure has to be flipped upside down to act as AFM tip. Note that the cantilever ends up being curved due to the fact that it is a bi-layered cantilever of polysilicon and gold. Curvature will be thoroughly discussed in the next section.

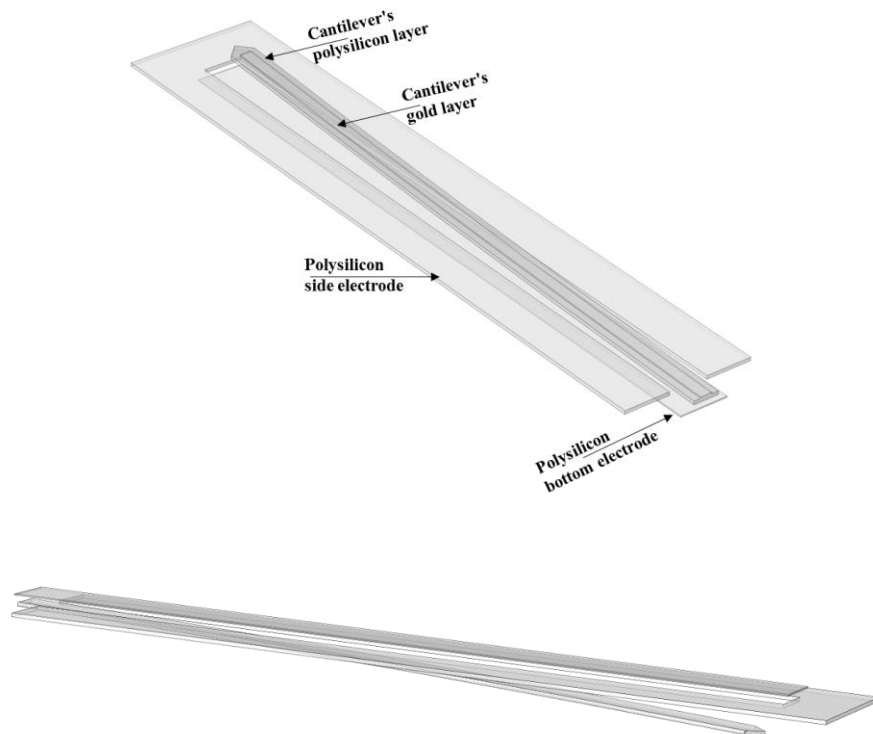


Figure 2: Schematics of the probe's different components (top). The probe has to be flipped when integrated with other AFM components (bottom).

The following list breaks down the benefits of such structure:

- a) The sharp cantilever end will act as the probing tip. This will remove the need for additional tip attachment. Usually in AFM designs, the cantilever acts as a holder for the tip as in Figure 3, while in our probe design the cantilever end acts as the tip itself.

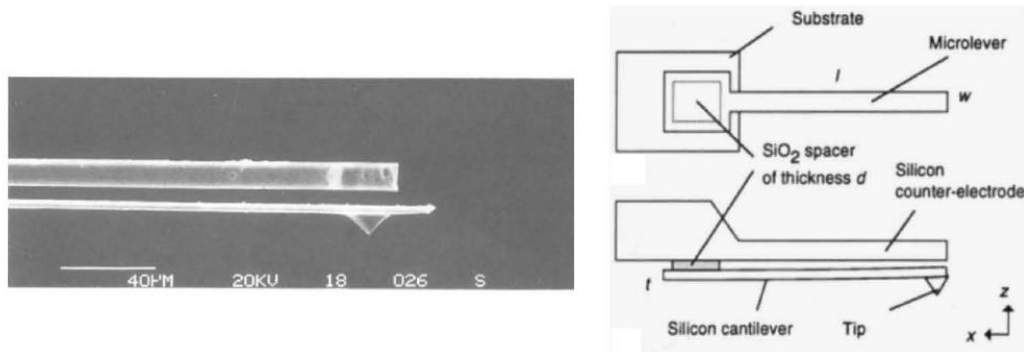


Figure 3: Electrostatically actuated AFM by Brugger et al [6]. Note the tip at the cantilever's end as an attachment, not as an integrated part of it. Used with permission from [6].

This will reduce the fabrication time of the tip. To quantify how much time this design will save in fabrication, we will take the following commercial Bruker AFM tip as an example which is FASTSCAN-A model, which is sold for \$98.175 per cantilever (see Figure 4).

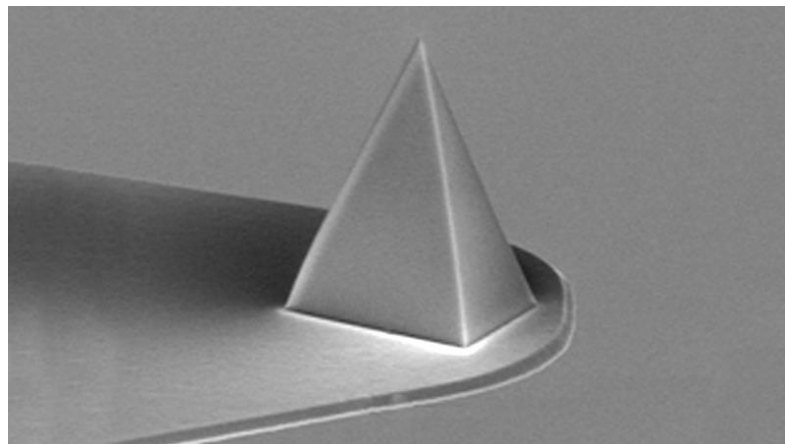


Figure 4: An AFM tip (FASTSCAN-A model) by Bruker company, which is sold for \$98.175 a piece. Reused with permission from Bruker Nano Surfaces and Metrology [7].

We can see that the pyramidal tip height can go up to $8\ \mu\text{m}$ ($80000\ \text{\AA}$). Consequently, if a thicker cantilever is to be etched down to form the tip (top-down method), the etch rate of undoped polysilicon is $714\ \text{\AA}/\text{min}$ in HBr/He plasma without O_2 [8] (for example), which means that the etching required to create such pyramid is 112 min. So, our design will eliminate this 112 min etching time, in addition to saving the corresponding material loss (polysilicon and etchant) and eliminate the associated heat energy required to induce such dry etching. Such elimination will be reflected as a lower tip price. However, if the tip will be deposited (bottom-up method), we can take the silicon deposition rate of a typical LPCVD, which is 5-20 nm/min [9]: we will take the best-case scenario: 20 nm/min. So, for the $8\ \mu\text{m}$ high tip (8000 nm), and 20 nm/min rate, the deposition time for the tip will be 400 min. For our cantilever ($1.5\ \mu\text{m} = 1500\ \text{nm}$), and for the same deposition rate, the tip will just take 75 min, which is just 18.75% of the pyramidal tip deposition time.

- b) The curvature will levitate the tip higher from the side electrode's surface; hence, when the actuator is flipped up-side-down to act as an AFM tip, the tip-sample interaction (Lennard-jones interactions [5]) will happen only between the tip and the sample (away from the effect of the side electrode).
- c) The fact that the beam is in the center of this U-shaped electrode means that the field from both sides will cancel each other in the lateral direction [1]; hence, no lateral movements → minimal to zero chance for pull-in to the side electrodes.

However, the cantilever curvature has to be controlled as not to be extremely bent upward. Extremely bent cantilevers (as shown below in Figure 5 below) won't be of an interest to us as it causes the majority of cantilever to out of range for the field lines; hence, limiting the control of the tip movement.

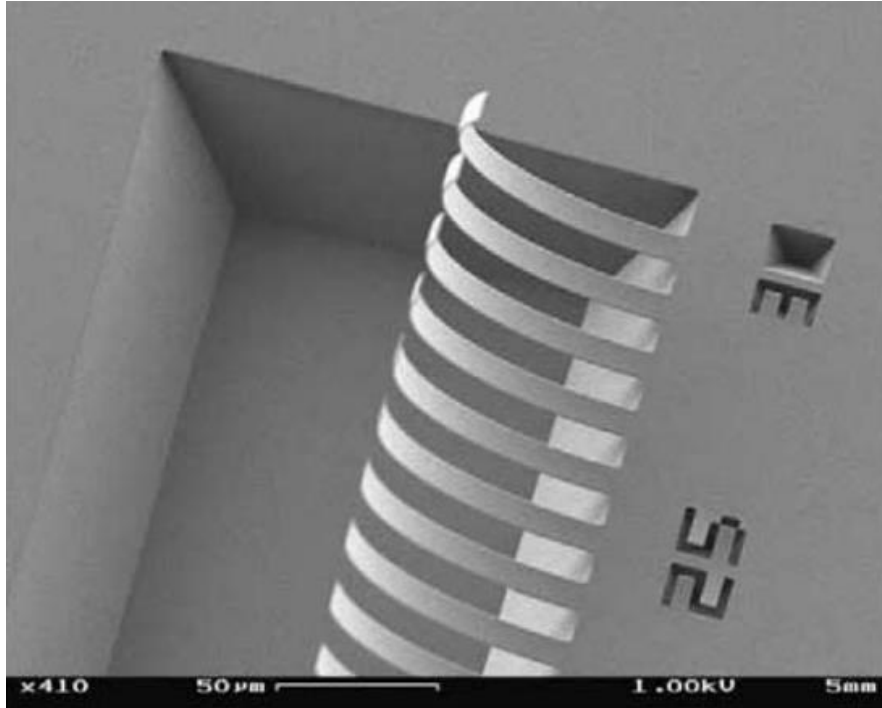


Figure 5: An extremely bent cantilever which makes it mostly out of the effect of the fringing field if actuated by a side electrode. Used with permission from [10].

Note that any curvature will weaken the force sensed by the cantilever: such weakening will be considered in the fringing force equation by multiplication of the equation by a correction factor (free parameter) as will be discussed later in the results. Therefore, it is worth discussing the curvature mechanism in the following section.

1.2 Curvature in MEMS Structures

In MEMS, curvatures are of two types: unwantedly induced curvature (usually due to fabrication imperfection), and a purposefully induced one.

a) Undesired curvature. This curvature is usually due to either the structure design (e.g. made of two layers) or the heat generated during film deposition [11]. Figure 6 shows an example of such unwanted curvature.

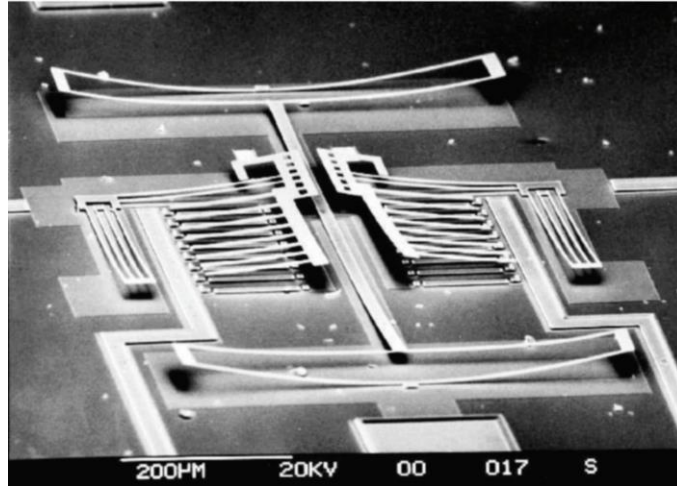


Figure 6: Undesired curvature induced by fabrication process [11]. Used under Fair Use Doctrine¹.

In such cases, curvature could be reduced/ eliminated by controlling the fabrication process. However, for well-established processes (such as PolyMUMPs), the curvature could be reduced post-fabrication. For example, Morrison et al [12] have used heat treatment to reduce the curvature of the structure.

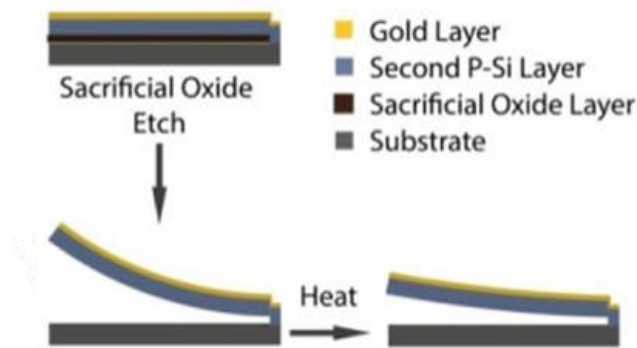


Figure 7: Control of the curvature of bi-layered cantilever made of poly and gold through heating. No reuse permission was required by the publisher of [12] that referred to Fair Use under US Copyright Law.

¹ Jonathan Candelaria, Executive Director of BSAC and BWRC research centers, UC-Berkeley, was sought for permission. He forwarded the matter to Prof. Clark Nguyen who never responded to the multiple email requests. As such, UC Berkeley Library referred to the Fair Use Doctrine.

b) Purposefully induced curvature. This type of curvature was introduced to MEMS structures to investigate the curvature effects on different MEMS related phenomena. The curvature was done to both the main structural part and/or other stationary parts of the design. For example, Legtenberg et al [13] have introduced the curvature to the stationary side electrodes as seen in Figure 8.

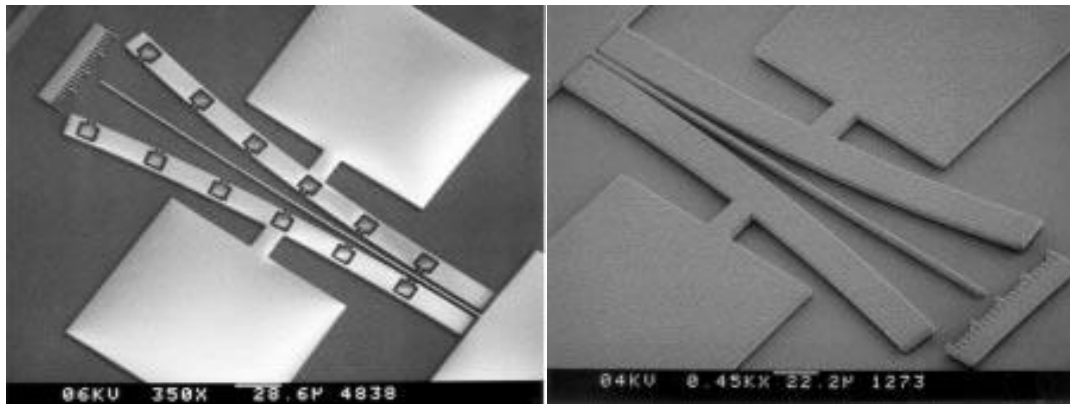


Figure 8: Non-structural, stationary curved side electrodes. Used with permission from [13].

However, Rosa et al [14] have both introduced the curvature to the cantilever as shown in Figure 9.

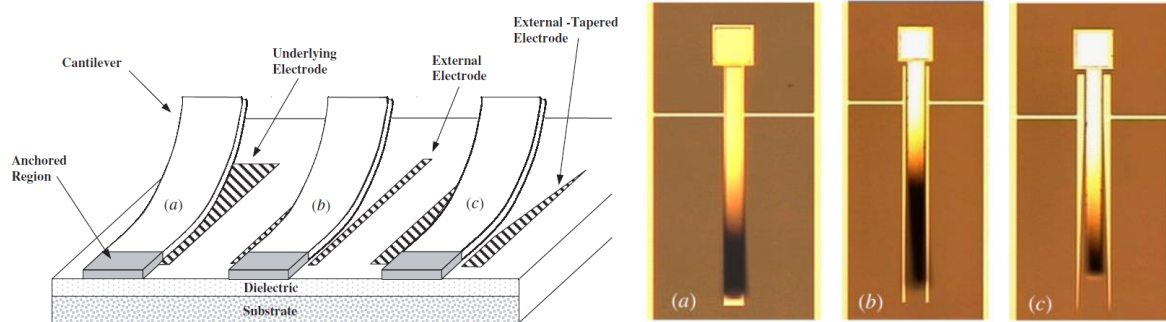


Figure 9: Schematics (left) and optical microscope images (right) for the curved cantilevers with their corresponding electrodes.

Used with permission from [14].

Others have tried different electrode shaping for different functionality enhancements, or as a proof of concept. Most notably, very exotic 3D structures were made possible by carefully engineered beams' and plates' curvature such as the work of Pinto et al [15] where they made a self-rolling beams on top of suspended plates as shown in Figure 10.

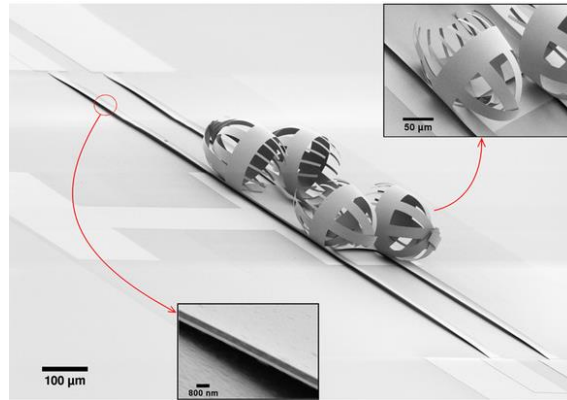


Figure 10: An SEM image of self-rolling beams on a suspended plate. Used with permission from [15].

The reason behind such curvatures is the stress gradient along the vertical Z direction which will force the cantilever bending upwards or downwards to be in an equilibrium, stress-free shape. There are several ways to purposefully introduce curvature to microbeams:

1st: Temperature variance based. Here, we use one single material but with two or more layers of different grains sizes [16]. This is attainable by depositing the beam at different temperatures; hence, inducing different grain sizes at the top and bottom of the cantilever as shown in Figure 11.

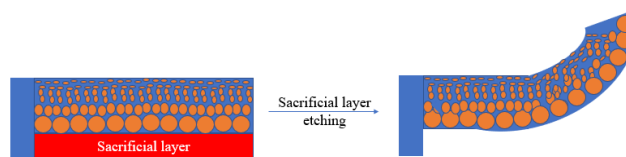
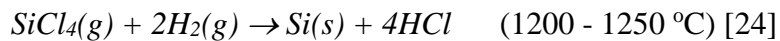


Figure 11: Schematics of grain sizes gradience effect in inducing curvature (after removing the sacrificial layer).

In this scheme, the top surface will have a tensile stress applied to it as a result of the higher crystal density, which will make the upper surface wanting to shrink as an equal and opposite force. On the other hand, the bottom surface will have compressive stress which will make the lower surface wanting to expand as an equal and opposite force. Consequently, the cantilever will be bent upwards to neutralize the stresses applied to both surfaces, and a stress-free curved cantilever will result.

Depending on the desired grain size, polysilicon can be deposited either from a gas or vapor either in epitaxial or non-epitaxial CVD fashions. High-intensity laser has been shown to help in gas decomposition [17]. Generally speaking, polysilicon deposition can be done with low pressure chemical vapor deposition (LPCVD) [18, 19], plasma enhanced chemical vapor deposition (PECVD) [20, 21], magnetron sputtering [22], or e-beam evaporation [23]. There are many reactions that can be implemented to deposit polysilicon, but one of the common ways is by the reduction of silicon tetrachloride gas by hydrogen in a PECVD process as follows:



For MEMS, however, LPCVD is the commonly used method. For LPCVD, the as-deposited films come with high residual stresses and residual stress gradients across the film thickness [25]. However, if the process/device used does not produce such gradient, it can be introduced by varying the deposition temperatures above and below 625 °C [26, 27]. Others [25, 28] set such point to be 610 °C.

Generally speaking in terms of temperature, Yang et al [25] conducted a thorough review where it was found that thin Si films are amorphous at temperatures lower than about 570 °C, display fine ellipsoidally shaped grains (about 0.1 μm diameter) at temperatures between about 570 to 610 °C,

and display columnar (110)-textured grains preceded by a thin fine-grained nucleation layer at temperatures between about 610 to 700 °C. For these columnar crystals, however, crystals grow vertically and in-plane pushing on each other, which implies compressive stresses at the bottom of the film. As we go up through the film thickness, the residual stress tends to be less compressive (hence, more tensile) [25] forming the stress gradient intrinsically imbedded within the deposition process. Consequently, having compressive stress at the bottom of the cantilever and tensile at its top will surely curve/bend the cantilever up upon removal of sacrificial layer. Therefore, for our purpose 610 to 700 °C should be the deposition target which (the temperature) may be lowered through the deposition process to induce more tensile residual stress at the cantilever's top.

Figure 12 shows the residual stress of polysilicon films as a function of the deposition temperature for LPCVD [25].

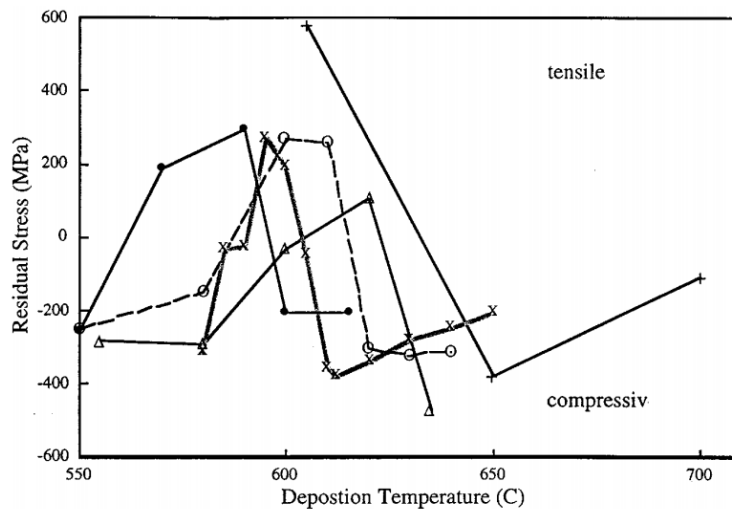


Figure 12: Stress-temperature relation made by Yang et al [25] as a summary of four works where, + from [29], x from [30], ° from [31], Δ from [32]. Used with permission from [25].

Deposition temperature is a limiting factor to the type of material deposited; however, the higher the temperature the greater the uniformity becomes in addition to lower defects.

2nd: *Pressure variance based*. Here, we also use one single material made of multiple layers of different grain sizes. Unlike the previous method, the grain size difference here is induced by varying the deposition chamber pressure. Temple-Boyer et al [18] showed that a low-stress bilayer polysilicon was deposited at 100-mTorr silane which was compressive yet the other layer was tensile at 200-mTorr silane: both layers deposited at the same temperature of 600 °C. Table 1 illustrates the effect of pressure variance on the residual stress of polysilicon deposited by LPCVD in as-deposited (top) and annealed (bottom) states.

Table 1: Residual stress and microstructure of as-deposited (top) and annealed (bottom) silicon films as a function of both deposition temperature and pressure, where (a) stands for amorphous and (c) for crystalline. Used with permission from [18].

	P = 100 mtorr	P = 200 mtorr	P = 300 mtorr
T = 555°C	-280 MPa (a)	-295 MPa (a)	-285 MPa (a)
T = 580°C	-70 MPa (a-c)	-240 MPa (a-c)	-290 MPa (a)
T = 600°C	-450 MPa (c)	+130 MPa (a-c)	-30 MPa (a-c)
T = 620°C	-485 MPa (c)	-490 MPa (c)	+105 MPa (c)
T = 635°C	-490 MPa (c)	-450 MPa (c)	-475 MPa (c)

	P = 100 mtorr	P = 200 mtorr	P = 300 mtorr
T = 555°C	+230 MPa (c)	+200 MPa (c)	+245 MPa (c)
T = 580°C	+225 MPa (c)	+250 MPa (c)	+250 MPa (c)
T = 600°C	-520 MPa (c)	+210 MPa (c)	+240 MPa (c)
T = 620°C	-540 MPa (c)	-490 MPa (c)	+100 MPa (c)
T = 635°C	-480 MPa (c)	-475 MPa (c)	-525 MPa (c)

Either using the temperature induced stress gradient or the pressure induced one, Figure 13 shows a curve combining both temperature and pressure changes which both must be respected in order to control the process not to move from deposition into an etching one.

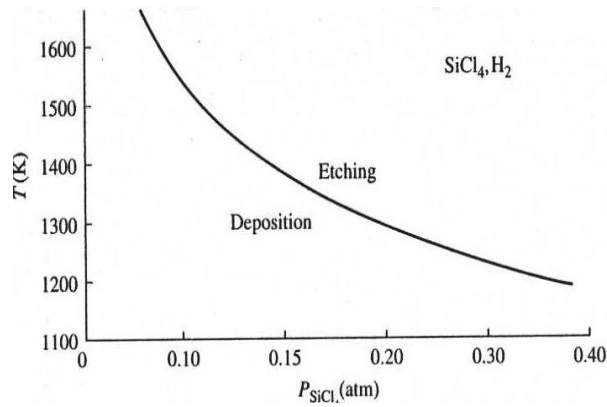


Figure 13: The borderline between etching and deposition for the reduction of silicon tetrachloride gas by hydrogen in a PECVD. Used with permission from [24].

Note that the cantilever material (polysilicon) properties could be controlled by doping (pre-doped or in-situ doped with boron and arsenic for example), however, the cantilever must be annealed post doping to assure homogenous diffusion of the dopant atoms across the cantilever thickness.

3rd: Photoisomerization. This curvature induction method is an organic chemistry method using photoisomerization of a molecule attached to the cantilever. For example, photoisomerization of azobenzene molecule (attached to a cantilever) will cause the molecule to shrink in size when exposed to a light of wavelength 365nm and dragging the cantilever with it on the process; hence, induce curvature. This is called cis isomerization. For the cantilever to come back to the straight original shape, the azobenzene molecule has to go through trans isomerization: expose it to UV light of 420nm wavelength [33]. Figure 14 illustrate such process.

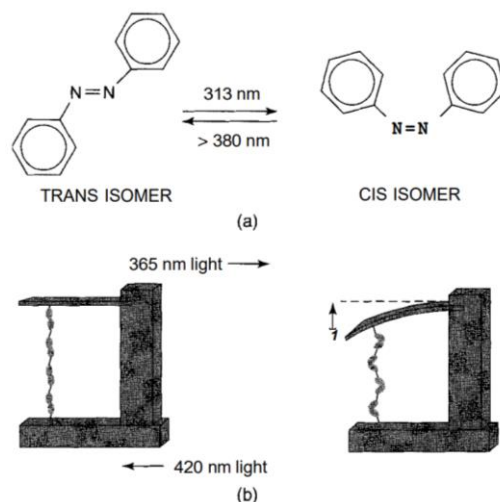


Figure 14: Trans to cis isomerizations of of a molecule (a) and how it induces cantilever curvature (b). Used with permission from [33].

4th: *Tip-Controlled Electrodeposition*. Eliyahu et al [34] have used a non-curved AFM tip to grow curved structures such as the curved microbeam shown in Figure 15.

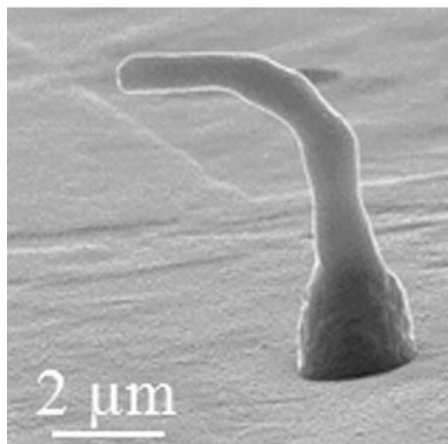


Figure 15: AFM-enabled electrodeposition of curved microbeams. Used with permission from [34].

Some call this method as tip-controlled local breakdown of electrolyte [35] as demonstrated in Figure 16.

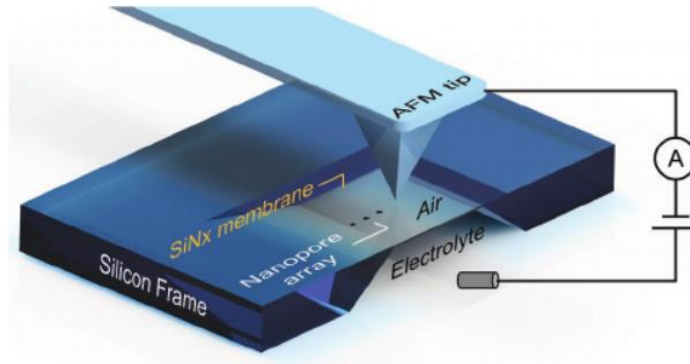


Figure 16: Voltage as applied to the AFM probe to enable electrolyte breakdown and deposition to form the desired structure.

Used with permission from [35].

5th: 3D printing. Curvature can be directly introduced by 3D printing, yet to the best of our knowledge it has not been done yet. However, Dietrich et al [36] and Sun et al [37] substituted curvature by slant in the 3D printed microbeams as shown in Figure 17.

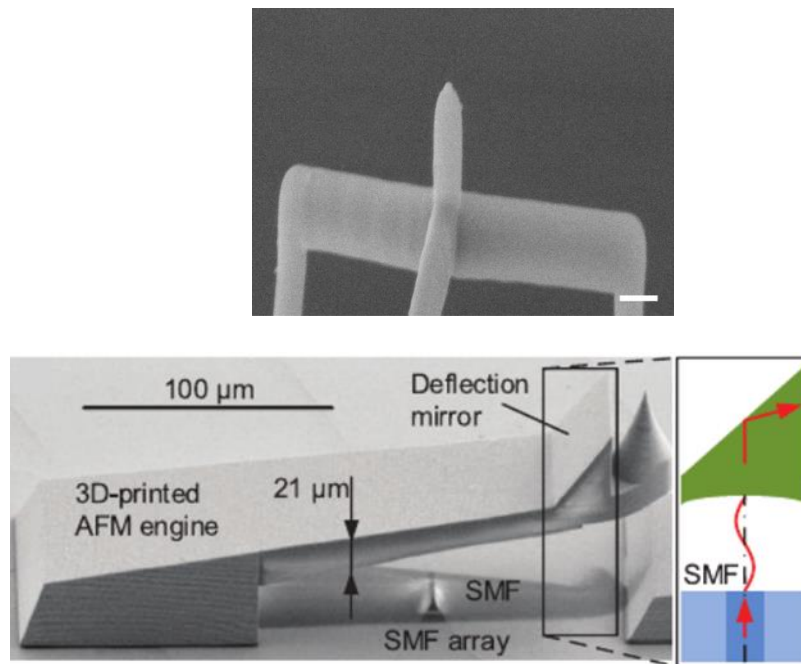


Figure 17: SEM images for slanted 3D printed tips/probes (top [37] and bottom [36]). Bottom imaged was used with permission from [36] (no reuse permission was required for the top image from [36] & [37]).

6th: *Shape-locking*. For example, a shape memory polymer can be mixed with magnetic particles then made into a cantilever shape (for example via 3D printing). The cantilever is then actuated by a magnetic field which will curve it upward (positive field) or downward (negative field). Once removing the field, the cantilever will be locked at its curved state as shown in Figure 18.

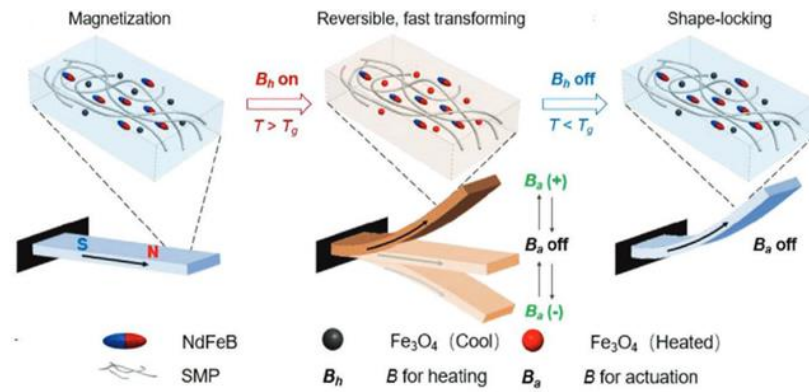


Figure 18: How magnetic shape memory polymers locks at curvature after turning off the magnetic field. This was done on a cantilever made of polymer that is embedded with soft (Fe_3O_4) and hard (NdFeB) magnetic particles. Used with permission from [38].

7th: *Using multi-materials*. This way uses two (or more) different materials to induce curvature. Since each material has different linear thermal expansion coefficient, a stress gradient will bend the cantilever upwards or downwards depending on the thermal expansion coefficient difference, and the order of layers (which is top and which is bottom). Note that these two materials must naturally stick to each other, or an adhesion layer must be sandwiched between them otherwise. Figure 19 shows an example of bilayer bent cantilever [14].

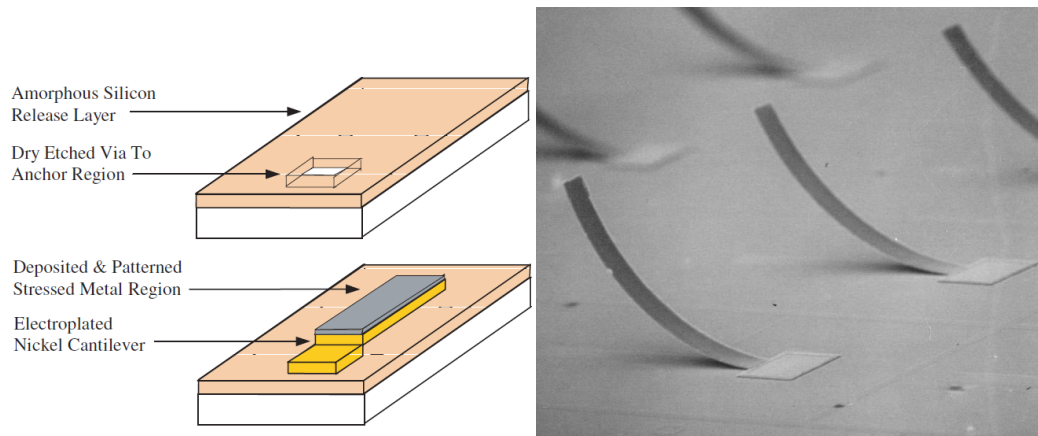


Figure 19: A schematics of the bi-material cantilever (left) and an SEM image of the induced curvature after removing the sacrificial/release layer (right). Used with permission from [14].

Out of all aforementioned methods for inducing curvature, the last method was employed for two reasons: it is the easiest to fabricate through the PolyMUMPS process (or even simple Silicon-On-Insulator), and also easier to numerically simulate by COMSOL.

The L-edit software design of the actuators had been submitted to CMC Microsystems Inc. where they were fabricated by PolyMUMPS process. CMC Microsystems Inc. is a company providing services to research institutions to help academicians and industry focus on new designs and science behind them, while outsource the fabrication pain and the time waste it causes. This process stemmed from work performed at the Berkeley Sensors and Actuators Center (BSAC) at the University of California during the latest years of the 20th century. Note that there exist other companies such as Qzabre.com, which is a spin off from ETH Zürich, Applied Nanotools, and others. As per CMC Microsystems Inc, they provide several fabrication recipes, where the one we benefited from is PolyMUMPs, which stands for Polysilicon Multi-User MEMS Processes. It is a three-layer polysilicon surface micromachining process. Figure 20 shows the different layers deposited throughout the PolyMUMPs process.

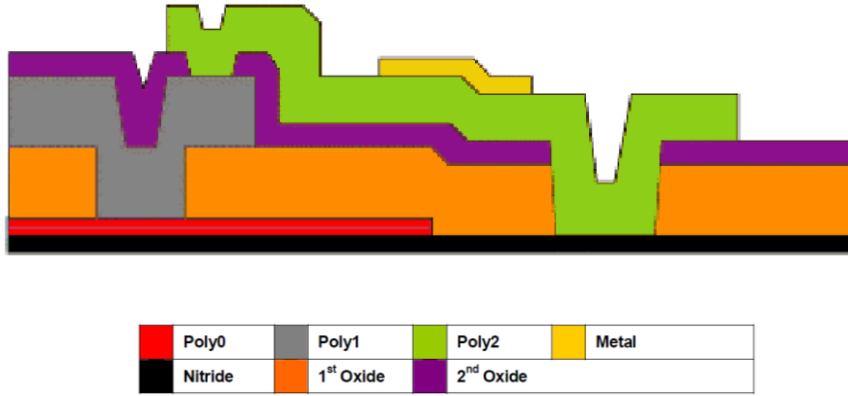


Figure 20: Schematics of the cross-sectional view showing different layers of the PolyMUMPs process. Used with permission from [39].

Chapter 2: Statics Modelling vs. Related

Experiments

2.1 Building the COMSOL Model

Prior to experiments, a numerical modeling of this work was done using COMSOL software in order to give some insights about the device. In order to double check the validity of the model, two COMSOL simulation methods were tried on a preliminary model. First was *Solid Mechanics* module coupled with *Electrostatics* module. Second was the *Electromechanics* module. Both methods gave identical results. However, the latter method was carried on further due to its simpler user interface. The *Electromechanics* tree defined is shown in Figure 21.

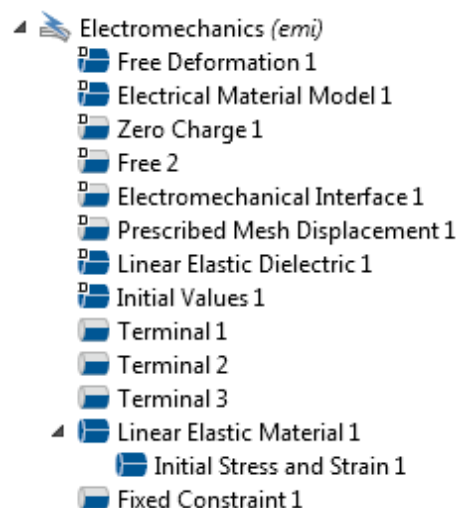


Figure 21: The Physics tree defined for the Electromechanics module used to simulate the actuator.

It was found that it is better to define the grounding of an object, not from the *Ground* sub node, but with a *Terminal* sub node having a $V = 0$. This was done in grounding both the cantilever and the bottom electrode. The reason is that this method gives more flexibility in defining different capacitances, probes and other COMSOL features that cannot be defined with a *Ground* terminal at stake.

As an initial trail to see how different curvatures affect cantilever's statics and dynamics, two cantilever lengths were randomly chosen and investigated: 295 and 245 μm . Dimensions of the different parts of the actuator are shown in Table 2. As per the airbox definition, it was determined based on a COMSOL tutorial [40], where the company gave a recommendation for the airbox to be three times the dimension of the structure under investigation. The interaction area of interest lies within the 17 μm trench in the middle of the side U-shaped side electrode, so the air box must be more three times the maximum deflection. However, the air box was gradually extended vertically and horizontally beyond the COMSOL recommended dimensions. This was done until any further increase in the air box dimensions gave negligible increase in simulation results.

Table 2: Dimensions of the side electrode, cantilever, air box, and bottom electrode.

	Width (μm)	Length (μm)	Thickness (μm)	Note
Side electrode	57	294	1.5	With a 17 μm trench in the middle for the cantilever to fit inside
Cantilever's poly	11	295 (long) 246 (short)	1.5	Two triangles were subtracted from the poly's flat tip to form the sharper tip
Cantilever's gold	5	285 (long) 236 (short)	0.52	Both gold and poly roots were given a fixed boundary condition at the root

Bottom electrode	21	303	0.5	Shifted down by $-3.25 \mu\text{m}$ to form the vertical gap with cantilever
Air box	61	337	100	The width was $10 \mu\text{m}$ more than the minimum requirement

A 3D view of the drawn COMSOL model is shown in Figure 22. Note that all three parts of the actuator were defined as *Linear Elastic Material*, where all side electrode, all bottom electrode, and the cantilever's root were given a *Fixed Constraint* boundary condition to represent their stationary status experimentally. Moreover, the X and Y axis mesh displacements were set to be zero components; hence, allowing only mesh displacements along the vertical Z axis, in order to prevent any undesired side lateral movement of the structure (aka vertical levitation only). This was done as per the COMSOL tutorial for *Electrostatically Actuated Cantilever* [40] so the vertical levitation is only studied.

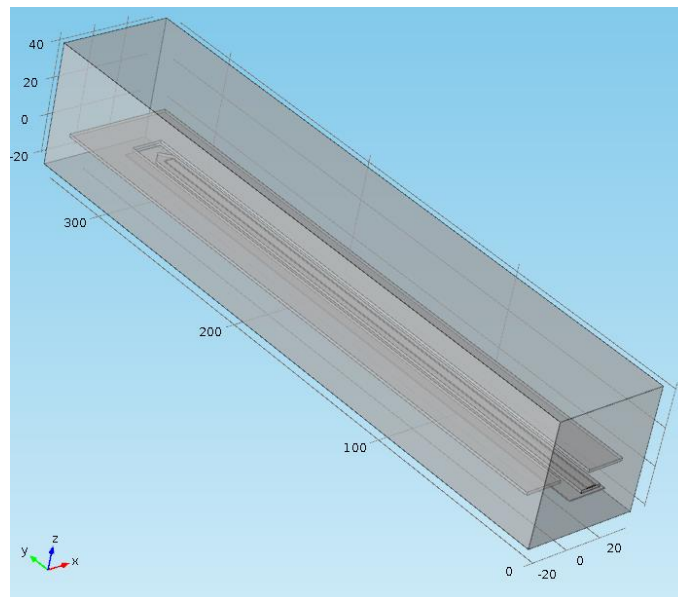


Figure 22: 3D view of the actuator as designed in COMSOL.

The materials of the probe (polysilicon and Au) were not defined from COMSOL library. Instead, they were defined as *Blank Material* where the material properties were fed into the module as provided by CMC Microsystems manual *PolyMUMPs Design Handbook* by Cowen et al [39] as shown in Table 3 and Table 4 (in addition to Young's Modulus of 158 +/- 10 GPa). Whatever property not mentioned by Cowen et al [39], the default COMSOL value was used.

Table 3: The mechanical and electrical parameters of PolyMUMPs process layers. Used with permission from [39].

Film	Thickness(Å)			Residual Stress (Mpa)			Resistance (ohm/sq)		
	Min.	Typ.	Max.	Min.	Typ.	Max.	Min.	Typ.	Max.
Nitride	5300	6000	6700	0	90	180	N/A		
Poly0	4700	5000	5300	0	-25	-50	15	30	45
Oxide1	17500	20000	22500	N/A			N/A		
Poly1	18500	20000	21500	0	-10	-20	1	10	20
Oxide2	6700	7500	8300	N/A			N/A		
Poly2	14000	15000	16000	0	-10	-20	10	20	30
Metal	4600	5200	5800	0	50	100	0.05	0.06	0.07

The potential across the beam was also investigated, and Figure 23 shows that the potential across the cantilever. Note the zero potential by the cantilever and bottom electrode (grounded).

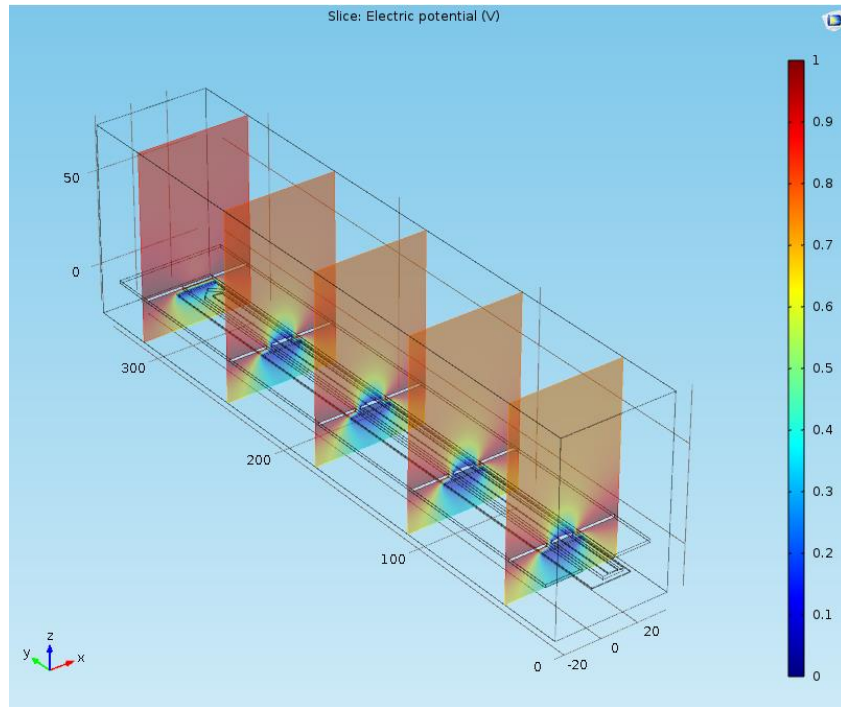


Figure 23: The electric potential distribution across the length of the cantilever with a 1 DC volt.

Having defined the materials and the physics of the model, now remains the induction of the curvature. The equation representing such curvature will be crucial in the dynamics modeling as will be discussed later.

We first tried inducing curvature by introducing stresses to both poly and Au. In our case, the PolyMUMPS-made cantilevers are composite beams made of polysilicon (poly2) and gold, with a fabrication inherited residual stress on both layers. The difficulty lies in the fact the residual stress on both film is not precisely known; instead, Cowen et al [39] gave a range of possible fabrication inherited stresses as shown in Table 4.

Table 4: Fabrication variation range for the residual stress of all PolyMUMPs layers. The last two are of interest since they constitute the cantilever layers. Used with permission from [39].

Film	Residual Stress (Mpa)		
	Min.	Typ.	Max.
Nitride	0	90	180
Poly0	0	-25	-50
Oxide1	N/A		
Poly1	0	-10	-20
Oxide2	N/A		
Poly2	0	-10	-20
Metal	0	50	100

For poly, the stress ranges from 0 to -20 MPa, while for gold from 0 to 100 MPa. Consequently, there is almost infinite possible 3×3 von Mises Stress matrices to be fed in the COMSOL model to produce the curvature. Through trial and error, we have tried to find the best stress matrices that produced a curvature equation that resembles the experimental curvature and static deflection (under DC voltage) as will be discussed in the results chapter. Poly was assumed to have zero residual stress (zero matrix), while gold was given the following von Mises stress matrix

Initial Stress and Strain				
Initial stress:				
S_0	50 [MPa]	50 [MPa]	50 [MPa]	N/m ²
	50 [MPa]	50 [MPa]	50 [MPa]	
	50 [MPa]	50 [MPa]	-50 [MPa]	
Initial strain:				
ϵ_0	0	0	0	1
	0	0	0	
	0	0	0	

Figure 24: von Mises stress matrix for the gold layer as entered in COMSOL. Poly layer was assumed with no stress, so a matrix was not introduced.

Now the model is almost ready for execution. Adding a *Stationary* study with a *Fine* mesh, the initial curvature was found. The *Physics Controlled* mesh was selected, where COMSOL might choose *Coarse* mesh for parts of the model that does not have much deformation or interaction (to save computational power). Figure 25 shows the curvature profile of the cantilever without any applied force/voltage.

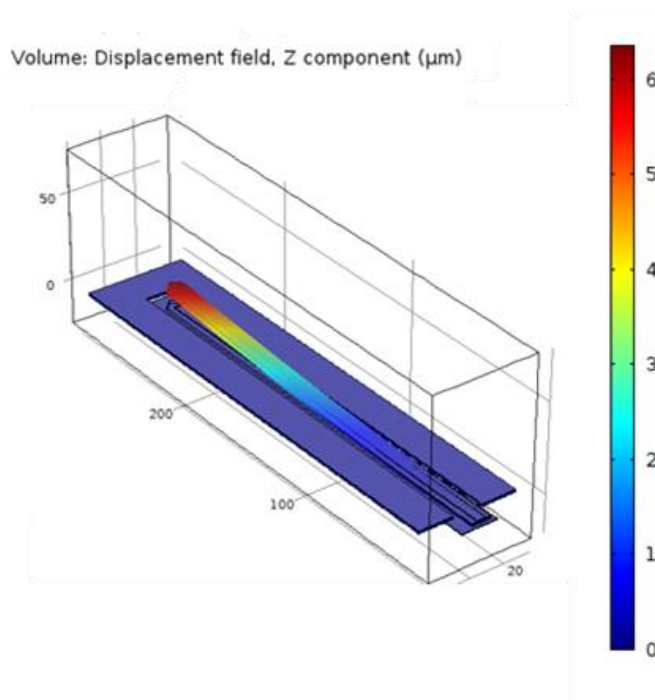


Figure 25: The initial curvature profile as found by COMSOL.

However, another method was applied which is more precise and helps reduce model-experiment differences. It was through using an optical profilometer. The fabricated cantilever was first imaged by table-top Scanning Electron Microscope (SEM), at the Meteorology Lab, Industrial Engineering Department, King Saud University, shown in Figure 26. This makes sure that the cantilever is curved (as per the design).



Figure 26: Table-Top JEOL Scanning Electron Microscope.

Indeed, Figure 27 shows side view SEM images of the curved cantilevers [41].

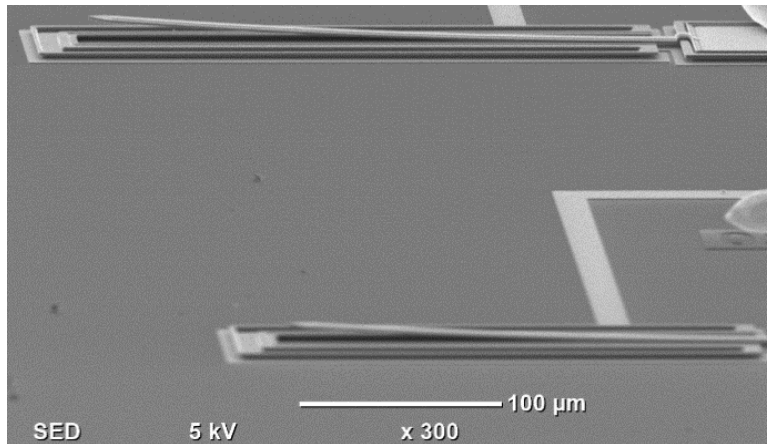


Figure 27: SEM images of the curved long cantilever (top) and the short one (bottom). The image was co-published by the student in [41] and was reused here with permission.

The cantilevers were then subjected to the optical profilometer (see Figure 28), and the profile data points were exported by *Vision64 Map* Software, and then imported to *Microsoft Excel* to produce a fitting equation of the (x,y) series of points representing the curvature of the cantilevers.

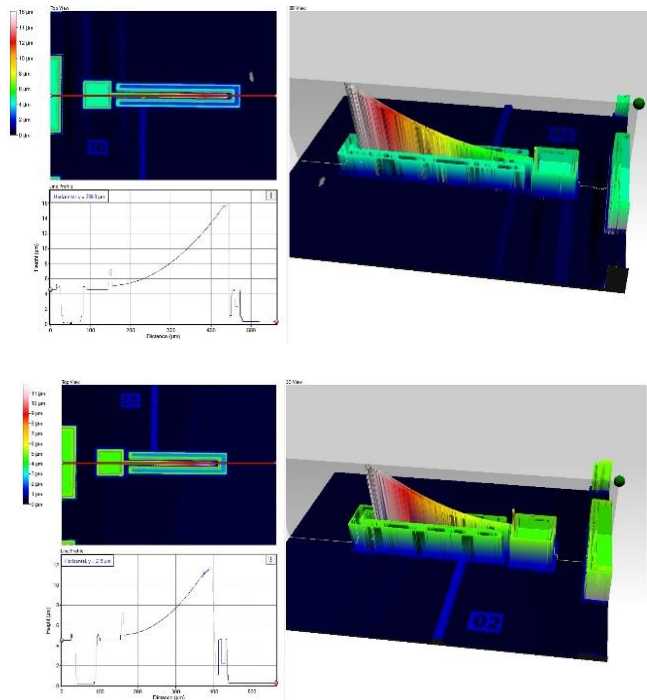


Figure 28: The curvature profile of the long (top) and short (bottom) cantilevers as produced by the optical profilometer. The image was co-published by the student in [41] and was reused here with permission.

The equations for both cantilever curvature are as follows [41]

$$w_0(x)_{Long} = 124.91 x^2 \text{ (m)} \quad (1)$$

$$w_0(x)_{Short} = 129.21 x^2 \text{ (m)} \quad (2)$$

where w_0 is the initial curvature equation, and x is the axial projection along the X axis for any curvature point w along the cantilever curvature. The next step was to re-draw the cantilever in COMSOL using these curvature equations. Due to the simplicity of custom drawing in SolidWorks, the cantilever was drawn by SolidWorks using the equation above, then was imported back into COMSOL, where it was centered inside the U-shaped actuation electrode.

The stress profile for the cantilevers shows stress relief, with maximum stress only at the cantilever's post/root as shown in Figure 29.

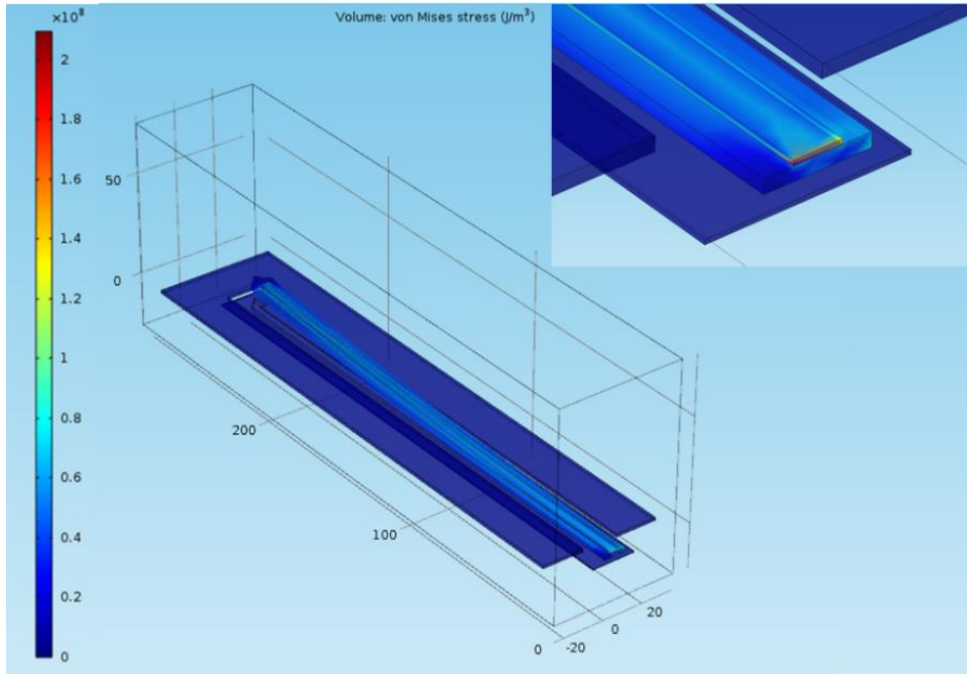


Figure 29: von Mises stress profile across the short cantilever. Enlarged above is the cantilever post which holds the highest stress point. The image was co-published by the student in [41] and was reused here with permission.

2.2 Static DC Voltage-Induced Displacement

The nature of the levitation force was examined via a voltage sweep in COMSOL from 0-190 Volts. The vertical displacement of the tip was plotted against its respective voltage as shown in Figure 30 for the long cantilever and in Figure 31 for the short. For the long cantilever an attractive force was manifested as the tip displacement was going downward across the sweep. For the short cantilever, however, the voltage sweep clearly shows a repulsive force, manifested as an upward tip displacement for the voltage increase across the sweep. This numerical way used here to get tip displacement as a function of voltage, is way much simpler than the conventional ways either through the equivalent circuits or from linearized state equations [42].

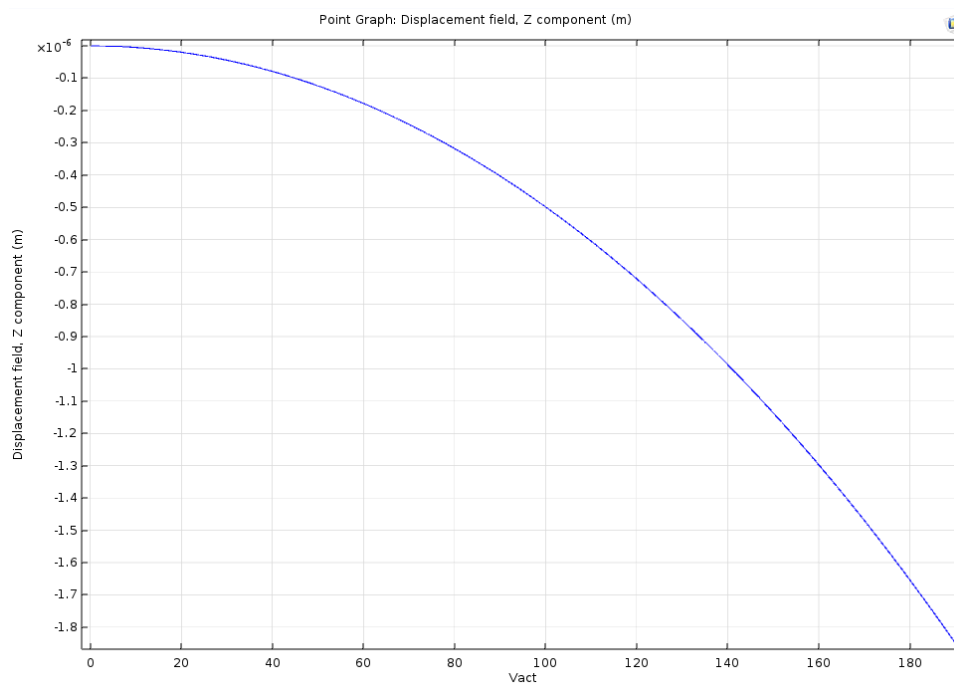


Figure 30: Actuation voltage vs tip displacement for long cantilever as obtained by COMSOL. The voltage was applied to the side electrode, with a sweep range from 0-190 V. The image was co-published by the student in [41] and was reused here with permission.

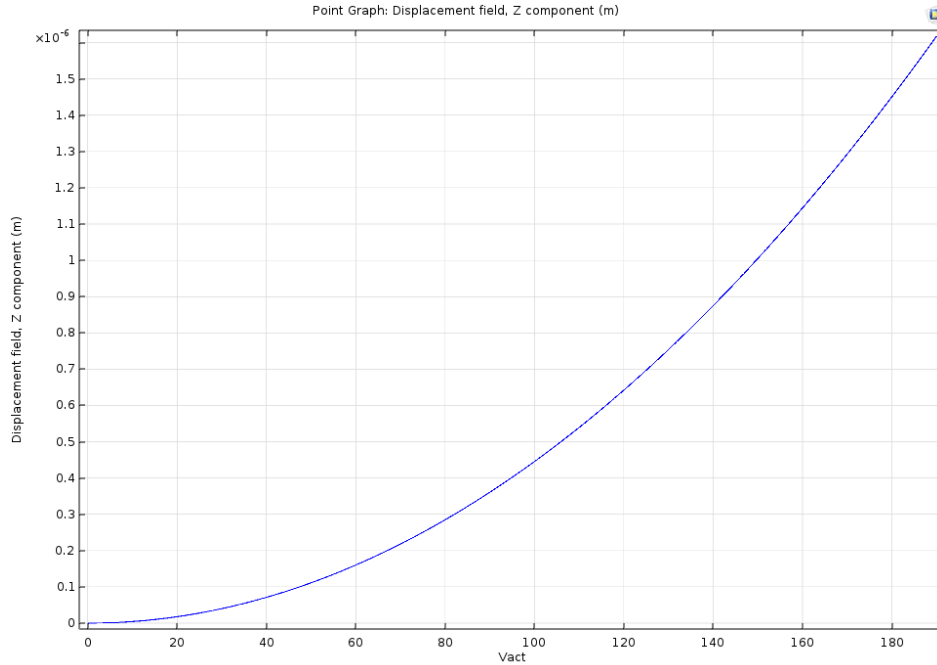


Figure 31: Actuation voltage (X axis) vs Tip Displacement in μm (Y axis) for the short cantilever. The voltage was applied to the side electrode, with a sweep range from 0-190 V. The image was co-published by the student in [41] and was reused here with permission.

The explanation of this transition (from repulsive to attractive) can be well explained by studying the field lines of a straight (non-curved) cantilever. First, the effect on the cantilever from the direct field lines in the lateral direction will be cancelled out [1] since each side will pick a different field sign stemming from their opposing directions. Therefore, we will be left only with the fringing field lines that will be landing on the top of the cantilever's surface in the same arrow direction. The bottom electrode will attract the field lines instead of the bottom surface of the cantilever (the reason will be explained below). Now we will be left with a field lines only affecting the top of the cantilever; hence, create an upward vertical displacement (levitation force) which means it will actuate the cantilever out-of-plane as shown in Figure 32.

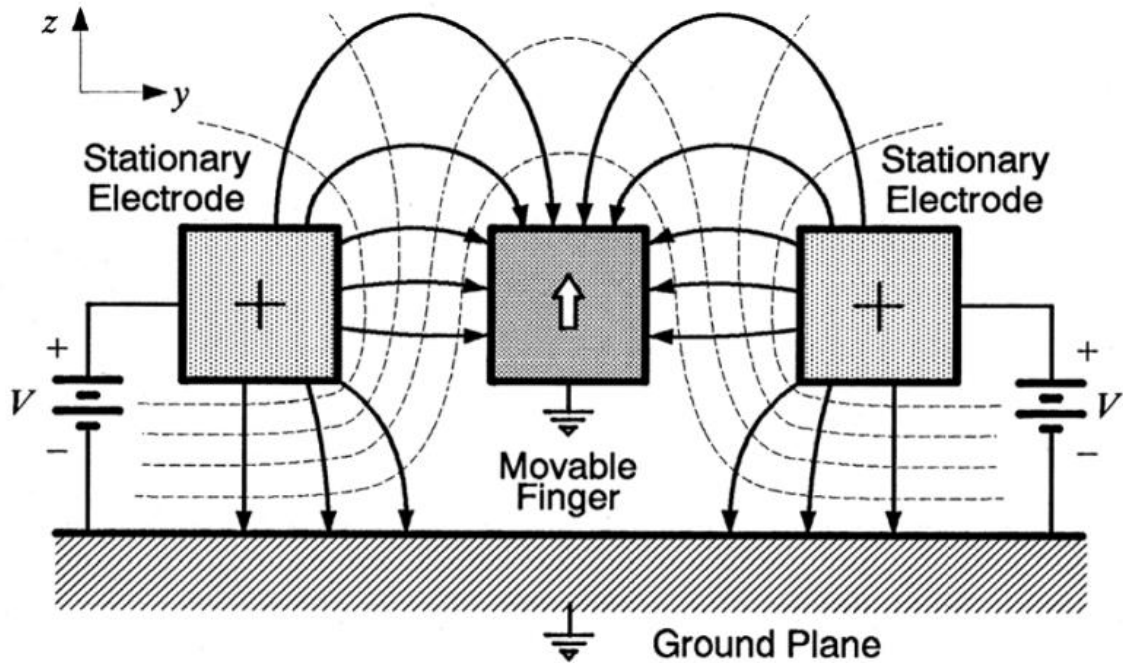


Figure 32: Cross sectional view of the potential contours (dashed lines) and electric fields (solid arrows) of a cantilever (single comb finger) under levitation force [43]. Note that both the cantilever (movable finger) and bottom electrode are grounded, similar case to our actuator. No reuse permission was required by the publisher of [43] that referred to Fair Use under US

Copyright Law.

In other words, the actuator movement comes from the imbalance of field lines of the top surface of the movable finger (cantilever) versus those at its bottom surface of the finger/cantilever. The imbalance comes from the fact that there is a bottom electrode, but no opposing top electrode. Therefore, the lack of top electrode will make the field lines stemmed from the upper surface of the U-shaped side electrode landing on the *upper* surface of the cantilever. On the other side, the presence of a grounded bottom electrode will make the field lines stemmed from the *lower* surface of the U-shaped side electrode land on the bottom electrode instead of landing on the lower surface of the cantilever. Now we are left with a cantilever that has field lines only on its top surface (remember that left and right field lines cancel each other's [1]). Consequently, this imbalance results in a net vertical electrical force lifting the finger upwards.

2.2.1 The Curved Cantilever Case

However, for the cantilevers of this project, the effect of such fringing field effect will be smaller due to the curvature. The reason is that this curvature will render majority of the cantilever away from the bottom electrode. Consequently, some field lines will now start landing on the lower surface of the cantilever; hence, resists/weakens the levitation force (caused by the field lines on the top surface of the cantilever). The more the curvature, the more field lines go to the lower surface of the cantilever up. This will continue up to a certain threshold where the field lines on the *upper* surface of the cantilever equals that on the *lower* surface: at which point, there will be an equilibrium where the cantilever does not move with an applied voltage. More curvature means passing such threshold, which implies majority of field lines would be on the *lower* surface of the cantilever; hence, switching the repulsive force to be attractive.

The above explanation is analogous to the case described by Daeichin et al [44] which was for straight cantilevers as shown in Figure 33. In their case, the switch/flip was done by increasing the gap between bottom electrode and the movable finger (cantilever), which gradually reduces field lines on the cantilever's top surface until reaching the threshold. Since their cantilever is straight (not curved), the cantilever length does not play a role in the repulsive-attractive switch. In our case, however, the curvature does the exact same flip effect except that the cantilever length is the control factor in our case (which implicitly includes steeper vertical gap change as the gap in our case is increasing across the beam length). Therefore, the longer the cantilever, the bigger the curvature radius, the less field lines on the top surface, and hence, the weaker the repulsive force. This will continue for longer cantilever up to a threshold length. In other words, the threshold in our case is a function of the cantilever's length.

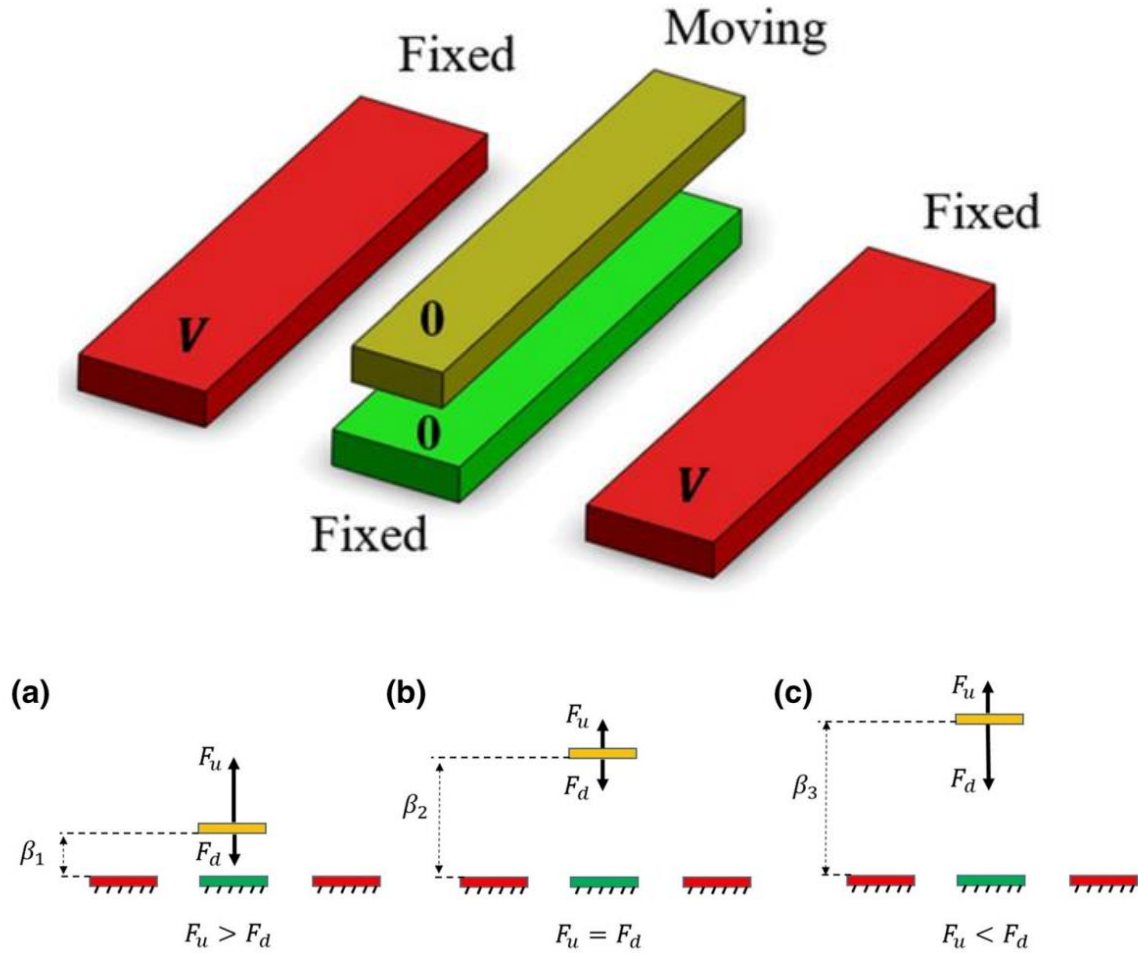


Figure 33: (Top) The type of force acting on a movable finger between two side electrodes and a fixed bottom electrode. (Bottom) The force passes from being repulsive (a) to attractive (c) through a threshold point (b). Used with permission from [44].

Consequently, the short cantilever is better suited as an AFM probe since it experiences a levitation force, which will eliminate the risk of pull-in (rather than the long cantilever that approaches the bottom electrode with higher voltage; hence, higher pull-in risk). Moreover, for the short cantilever, the higher the voltage the further away the tip from the side electrode, which is a desirable feature for such AFM probe (avoiding cantilever-electrode interaction). Therefore, the curvature equation for the short cantilever $w_0(x)_{short} = 129.21 x^2$ (equation (2)) will be the used one and will be denoted as $w_0(x) = 129.21 x^2$.

2.3 Fringing Field Forcing Equations

2.3.1 Existing Literature Force Equations

There are several works that modeled the fringing field force. *Osterberg and Senturia* [45] (it will be called Senturia force for short) have analytically defined the fringing field force in terms of the electrostatic force $f(t)_{ES}$ as

$$f(t)_{Senturia} = 0.65 \frac{d}{w} f(t)_{ES} \text{ (N)} \quad (3)$$

where d is the gap between the two parallel plates, w is the deflection.

The electrostatic force is defined as

$$f(t)_{ES} = \frac{1}{2} \epsilon A \frac{V(t)^2}{(d-w)^2} \text{ (N)} \quad (4)$$

where V is the voltage. Therefore, the fringing field force becomes

$$\boxed{f(t)_{Senturia} = \frac{0.65\epsilon A d}{2 w} \frac{V(t)^2}{(d-w)^2}} \text{ (N)} \quad (5)$$

where A is the area of the plate, ϵ is the permittivity of the capacitor medium (usually air), and V is the voltage applied across the plates. Figure 34 depicts the structure of the actuator.

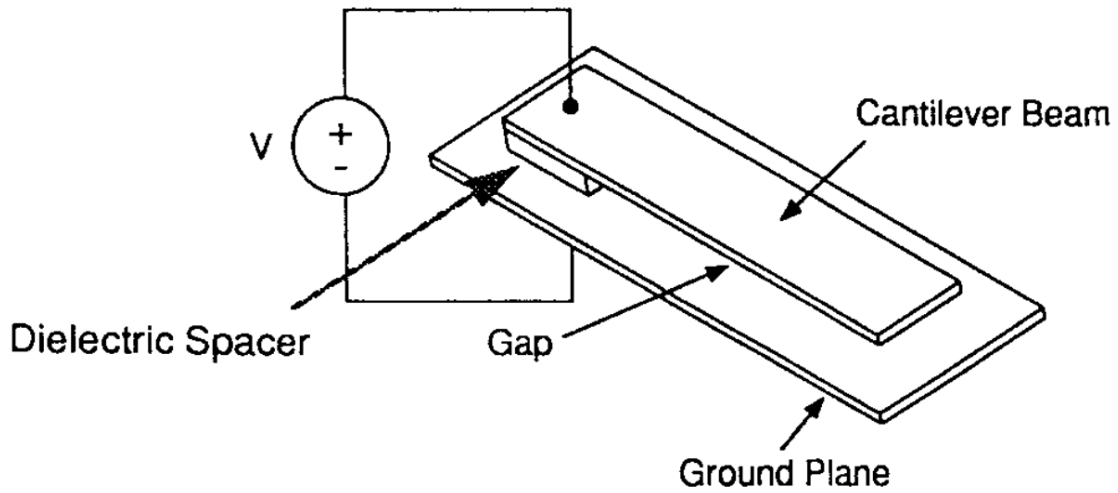


Figure 34: The parallel plate actuator modeled by Osterberg and Senturia. Used with permission from [45].

Kambali *et al* [46] have derived an effective fringing field forcing equation numerically using both COMSOL and Intellisuite softwares. They have found the forcing for various electrodes configurations as shown in Figure 35.

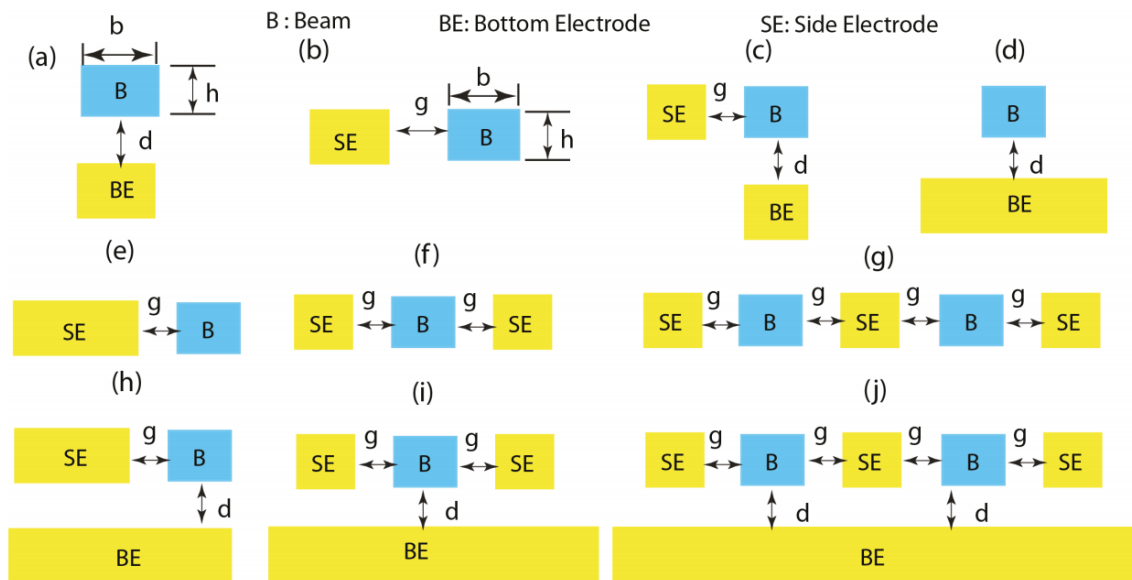


Figure 35: Different configurations studied by Kambali *et al* [46]. The configuration of interest to us is (i) as it closely resembles ours. Used with permission from [46].

The configuration of interest to us is (i), which closely resembles our actuator configuration. Figure 36 is a closer look into the field lines for such configuration.

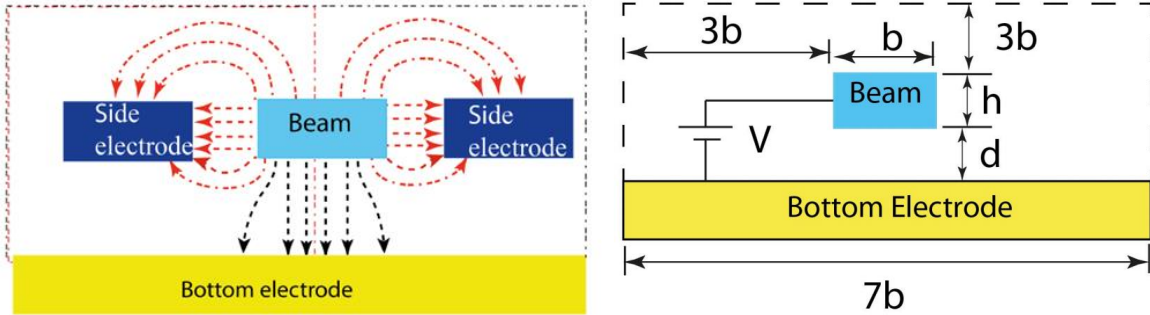


Figure 36: The beam configuration corresponding to our actuator [46]. Note that the bias between cantilever and bottom electrode, which is absent in our case: due changes in the forcing equation to count for that. Used with permission from [46].

The general equation for effective force for all configurations is

$$F_{eff} = p \left(\frac{F_1}{2} + F_2 \right) (1 - \zeta) + q \left(\frac{F_1}{2} + F_2 \right) (1 - \xi) + r \frac{F_1}{2} \quad (6)$$

where p , q , and r are factors with values of 0, 1, or 2 depending on the actuator configuration and voltage distribution. For our configuration (Figure 36), the values are $p = 2, q = 0, r = 0$.

This renders the equation to be

$$F_{eff} = 2 \left(\frac{F_1}{2} + F_2 \right) (1 - \zeta) \quad (7)$$

where F_2 is the force between cantilever and side electrode. F_1 represents the force between the cantilever and the bottom electrode due to the bias between them (dotted downward black arrows in Figure 36). Since both bottom electrode and beam are grounded in our case, this force does not exist for us; hence, equals zero. As per the correction factor ζ , it can be described as the effect of

the bias between cantilever and bottom electrode on F_2 . Similar to F_1 , this bias does not exist; ζ equals zero too. Therefore, the effective force equation renders to

$$F_{eff} = 2 F_2 \quad (8)$$

The factor of 2 represents twice the numerical results since the authors [46] have put the air box in COMSOL covering only half of the structure, then multiplied the results by 2, due to the symmetry of the structure; hence, reduce the computational time.

Depending on the beam-electrodes configurations, F_2 was divided into three cases depending of the value of the ratio $\frac{d}{b}$ as shown in Table 5.

Table 5: Different forms of F_2 and their corresponding applicable ranges. Note that g is the side gap between the cantilever and the side electrode, while d is the gap between the cantilever and the bottom electrode.

The force between cantilever and side electrode (F_2)	Applicable Range
$F_2 = \frac{1}{2} \frac{\epsilon V^2 h}{(g-w)^5} \left -4.52 \times 10^{-6} b^3 + 5.7 \times 10^{-4} b^2 (g-w) - 0.026 b (g-w)^2 - 1.638 (g-w)^3 \right $	$2 \leq \frac{b}{g} \leq 70$ $d = 0$
$F_2 = \frac{1}{2} \frac{\epsilon V^2 h}{(g-w)^2} \left -100 \left(\frac{d}{b}\right)^3 + 57 \left(\frac{d}{b}\right)^2 - 11 \left(\frac{d}{b}\right) - 2.145 \right $	$0 \leq \frac{d}{b} \leq 0.25$
$F_2 = \frac{1}{2} \frac{\epsilon V^2 h}{(g-w)^2} \left 0.00316 \left(\frac{d}{b}\right)^4 - 0.043 \left(\frac{d}{b}\right)^3 + 0.21 \left(\frac{d}{b}\right)^2 - 0.44 \left(\frac{d}{b}\right) - 2.83 \right $	$0.25 \leq \frac{d}{b} \leq 5$

The third (last) case of F_2 in Table 5 corresponds to our configuration since $\frac{d}{b} = \frac{3.25 \mu m}{11 \mu m} = 0.295$, which is within the range of $0.25 \leq \frac{d}{b} \leq 5$.

Now multiplying the corresponding F_2 by 2 (the symmetry factor) results in

$$f(t)_{Kambali} = \frac{\epsilon V^2 h}{(g-w)^2} \left| 0.00316 \left(\frac{d}{b}\right)^4 - 0.043 \left(\frac{d}{b}\right)^3 + 0.21 \left(\frac{d}{b}\right)^2 - 0.44 \left(\frac{d}{b}\right) - 2.83 \right|$$

(9)

2.3.2 The Approach to Find the New Forcing Equation

In this project, a simpler method for extracting the electrostatic force for any structure has been devised using COMSOL only. This is based upon the definition of potential energy which is

$$U = \frac{1}{2} c V^2 \text{ (J)}$$

(10)

where c is the capacitance, and V is the voltage.

Now the relation of electric force to potential energy is known to be

$$f(t) = \frac{\partial U}{\partial w} \text{ (J/m)}$$

$$f(t) = \frac{\partial U}{\partial w} \text{ (N)}$$

(11)

where w stands for the axial position. In our case, w is the tip height.

Substituting U into $f(t)$ gives

$$f(t) = \frac{\partial}{\partial w} \left(\frac{1}{2} c V^2 \right) \text{ (F V}^2\text{/m)}$$

$$f(t) = \frac{\partial}{\partial w} \left(\frac{1}{2} c V^2 \right) \text{ (N)}$$

(12)

The only term that is a function of w is the capacitance

$$f(t) = \frac{\partial}{\partial w} \left(\frac{1}{2} c(w) V(t)^2 \right)$$

(13)

Therefore, the capacitance equation as a function of tip height has to be found (to solve the differentiation equation). It was found using COMSOL. The side electrode was set as *Terminal 1* with a voltage V_{act} (actuation voltage), the cantilever as *Terminal 2* with $V = 0$, and the bottom electrode as *Terminal 3* with $V = 0$.

The following steps were applied in COMSOL to get the representative capacitance equation for our structure.

- 1- Define the cantilever's tip as a *Point Probe* in COMSOL (to track its values).
- 2- Create a plot of V_{act} vs the w *Point Probe* (aka tip deflection vs. applied voltage).
- 3- Define then apply a DC voltage sweep by defining V_{act} range from 1 to 190 Volts.
- 4- Run the model.

The resultant plot (as defined in step 2) will be generated as shown in Figure 37.

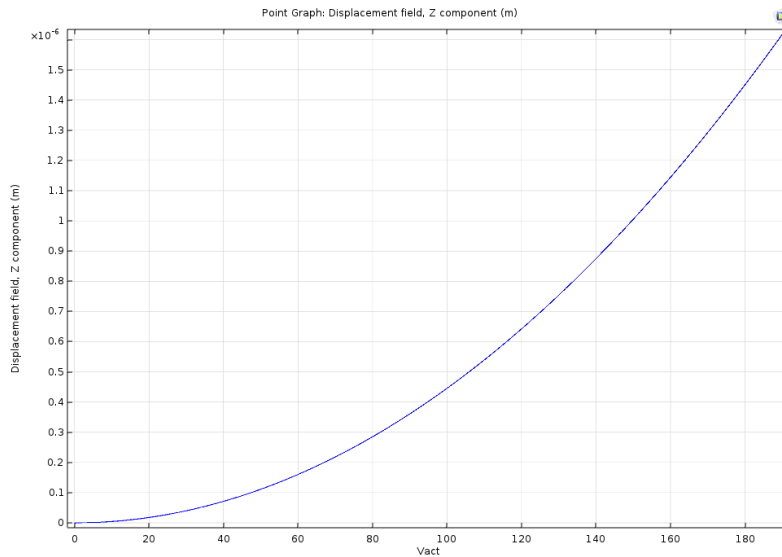


Figure 37: Actuation Voltage (X axis) vs Tip Displacement in μm (Y axis) for the short cantilever. The voltage was applied to the side electrode, with a sweep range from 0-190 V.

- Now define another plot of overall capacitance vs. V_{act} . In COMSOL terminologies, it will be C_{11} vs. V_{act} . Note that C_{11} is the COMSOL terminology for the overall capacitance inside the whole air box.

The resultant plot will be generated as shown in Figure 38.

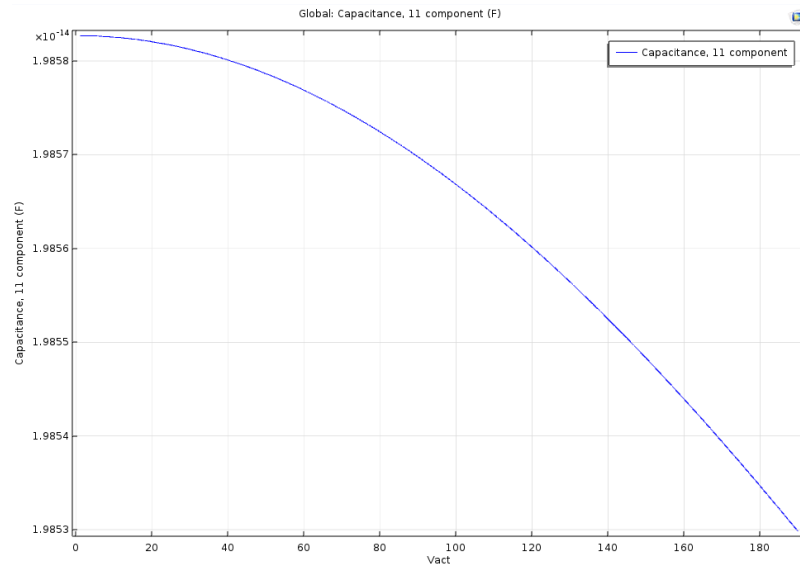


Figure 38: The overall capacitance (Y axis) vs applied actuation voltage (X axis).

- Now we take the voltage out of the scene, and only export the data points of C_{11} and their corresponding values of w into Microsoft Excel (or similar software).
- Create a fitting function for capacitance as a function of deflection (aka $C_{11}(w)$) as shown in Figure 39. The generated fitting function (capacitance function) can be plugged into the above our forcing equation above.

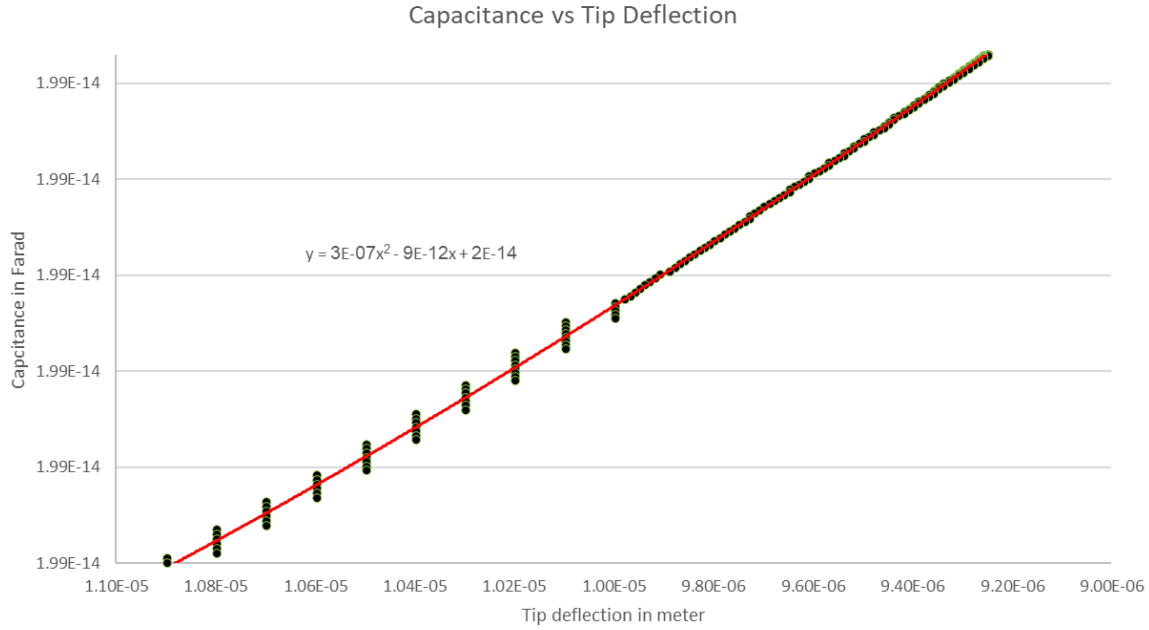


Figure 39: The combined chart of capacitance values (y axis) and their corresponding tip deflection (x axis). Note the fitting function y in the middle of the chart. The black dots (with green borders) represents the COMSOL data points, while the red line is the trend line which is represented by the fitting function y (at the middle of the chart).

The resultant capacitance equation is

$$c(w) = 3 * 10^{-7} w^2 - 9 * 10^{-12} w + 2 * 10^{-14} \text{ (F)}$$

(14)

Back substituting in the derived forcing equation (13),

$$\begin{aligned} f(t) &= \frac{\partial}{\partial w} \left(\frac{1}{2} c(w) V(t)^2 \right) \\ &= \frac{V(t)^2}{2} \frac{\partial}{\partial w} (3 * 10^{-7} w^2 - 9 * 10^{-12} w + 2 * 10^{-14}) \\ &= \frac{V(t)^2}{2} (6 * 10^{-7} w - 9 * 10^{-12}) \end{aligned}$$

Therefore,

$$f(t)_{New} = \frac{V(t)^2}{2} (6 * 10^{-7} \text{ w} - 9 * 10^{-12}) \quad (V^2 \text{ F} \rightarrow \text{N})$$

(15)

Chapter 3: Dynamics Modeling with

Related Experiment

The behavior of the curved cantilever in response to external AC excitations (coupled with DC) has been modeled using Distributed Parameter Modeling, also known as Distributed Coordinate Method. It is one of the approximate solutions of otherwise unsolvable differential equations. Such approximations can be classified as such:

- 1- Discrete Coordinate Method.
 - a. Finite Difference Methods.
 - b. Stepwise Integration Methods.
 - i. Euler method.
 - ii. Runge-Kutta method.
 - iii. Runge–Kutta–Simpson method.
 - iv. etc.
- 2- Distributed Coordinate Method.
 - a. Stationary Functional Methods.
 - i. Rayleigh-Ritz method.
 - ii. Finite Element Method.
 - b. Weighted Residual Methods.
 - i. Boundary residual
 1. Boundary Element Method
 - ii. Interior residual

1. Collocation.
2. Finite Element Method.
3. Galerkin.

From the above approximation methods, the Galerkin method has been applied to generate a Reduced Order Model (ROM) for the Euler-Bernoulli equation of motion, considering the bending elements throughout the cantilever with respect to position. The model was built using Wolfram *Mathematica* software.



First, the model parameters have to be defined. Table 6 shows the parameters used in the model and their corresponding values.

Table 6: Parameters used in the dynamics modelling and their values.

Variable	Description	Design Value	PolyMUMPS Range due to Fabrication Uncertainties [39]			Model Value	Note
			Min.	Typ.	Max.		
h_s (μm)	Poly2 thickness	1.5	1.4	1.5	1.6	1.23	Potential over etching
h_g (μm)	Gold thickness	0.52	0.46	0.52	0.58	0.58	
E_s (GPa)	Poly2 Young's modulus		148	-	168	148	
E_g (GPa)	Gold Young's modulus	70	-			70	

ϵ (F/m)	Permittivity of air			8.854×10^{-12}	
L (μm), short	Length of cantilever	245		246	
g (μm)	Gap between cantilever and side electrode			3.5	Measured by SEM
d	Gap between cantilever and bottom electrode			3.25	

3.1 Equation of Motion

Now the parameters have to be incorporated into the Euler-Bernoulli equation of motion (EOM) of cantilevers [47] (also called thin-beam theory) [1]. The equation of motion is as follows

$$\rho A \ddot{w}(x, t) + c \dot{w}(x, t) + EI w^{iv}(x, t) = f(t) \quad (16)$$

where ρ is the beam material(s) density, A is the cross-sectional area, c is the viscous damping coefficient, E is the Young's modulus of the beam material(s), I is the area moment of inertia, $f(t)$ is the fringing force, and $w(x, t)$ stands for the height or deflection of the beam along the x axis. Note that since the cantilever is composed of two materials, E and I will be calculated as EI_{eff} which is the beam's effective rigidity which will be calculated later.

According to Galerkin method, the EOM has to be non-dimensionalized as follows:

First, we start by dividing by ρA we get

$$\ddot{w}(x, t) + \frac{c}{\rho A} \dot{w}(x, t) + \frac{EI}{\rho A} w^{iv}(x, t) = \frac{1}{\rho A} f(t)$$

(17)

For simplicity, x and t will be removed in later formulations. Converting the equation of motion to its non-dimensional counterpart has to be preceded by the following assumptions:

$\bar{w} = \frac{w}{d}$ where d is the gap between the cantilever and the bottom electrode.

$\bar{x} = \frac{x}{L}$ where L is the length of the cantilever.

$\bar{t} = \frac{t}{T}$ where T is some specific time.

Using the above assumptions, we have to find the following non-dimensional terms:

$$\dot{w} = \frac{dw}{dt} = \frac{d(d\bar{w})}{d(\bar{t}T)} = \frac{d}{T} \frac{d\bar{w}}{d\bar{t}}$$

$$\ddot{w} = \frac{d}{dt} \left(\frac{dw}{dt} \right) = \frac{d}{d(\bar{t}T)} \frac{d}{T} \frac{d\bar{w}}{d\bar{t}} = \frac{d}{T^2} \frac{d^2\bar{w}}{d\bar{t}^2}$$

$$w^i = \frac{dw}{dx} = \frac{d(g\bar{w})}{d(L\bar{x})} = \frac{d}{L} \frac{d\bar{w}}{d\bar{x}}$$

$$w^{iv} = \frac{d^4w}{dx^4} = \frac{d}{L^4} \frac{d^4\bar{w}}{d\bar{x}^4}$$

Substituting back in the equation of motion

$$\rho A \frac{d}{T^2} \frac{d^2\bar{w}}{d\bar{t}^2} + c \frac{d}{T} \frac{d\bar{w}}{d\bar{t}} + EI \frac{d}{L^4} \frac{d^4\bar{w}}{d\bar{x}^4} = f(t)$$

Now dividing by $\rho A \frac{d}{T^2}$

$$\frac{d^2\bar{w}}{d\bar{t}^2} + \frac{cT}{\rho A} \frac{d\bar{w}}{d\bar{t}} + \frac{EI}{\rho AL^4} T^2 \frac{d^4\bar{w}}{d\bar{t}^4} = \frac{T^2}{\rho Ad} f(t)$$

To find the value of T and the damping coefficient c, we will set $\frac{EI}{\rho AL^4} T^2 = 1$. Therefore, $T =$

$$\sqrt{\frac{\rho AL^4}{EI}} \text{ seconds.}$$

Now, we will find an equivalent damping coefficient term $(\frac{cT}{\rho A})$ by substituting the value of T, the call it \bar{c} for simplicity.

$$\bar{c} = \frac{cT}{\rho A} = \frac{c}{\rho A} \sqrt{\frac{\rho AL^4}{EI}}$$

Re-writing the equation of motion using the above derived terms, it will be in the following simple form

$$\frac{d^2\bar{w}}{d\bar{t}^2} + \bar{c} \frac{d\bar{w}}{d\bar{t}} + \frac{d^4\bar{w}}{d\bar{t}^4} = \frac{T^2}{\rho Ad} f(t)$$

(18)

which can be written in yet simpler form

$$\boxed{\ddot{\bar{w}} + \bar{c} \dot{\bar{w}} + \bar{w}^{iv} = \bar{f}(t)}$$

(19)

where $\bar{f}(t) = \frac{T^2}{\rho Ad} f(t)$.

3.1.1 The Deflection Revisited

Deflection, w , in regular Euler-Bernoulli equation assumes a straight cantilever, unlike our curved one. Therefore, the curvature has to be incorporated to the model.

The total cantilever deflection, w , is the sum of the initial curvature of the cantilever w_0 (due to the bi-material induced stresses), plus the deflection due to voltage, w_V , as shown in Figure 40.

Hence

$$\bar{w}(x, t) = \bar{w}_0(x) + \bar{w}_V(x, t) \quad (20)$$

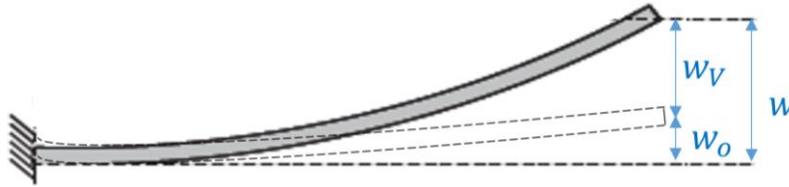


Figure 40: Total beam deflection $w(x,t)$ including the initial curvature due to stress gradient.

The response of the cantilever will be assessed at the point of interest to an AFM: the cantilever tip. The tip lies at $x = L$, where L is the cantilever length. However, since we have non-dimensional modeling, the length at $x = L$ is $\bar{x} = \frac{x}{L} = 1 = \bar{x}^2$. Therefore, the total deflection will be assessed at the tip only. Therefore, the deflection in the model is composed of the $w(x, t)$ at the tip (viz. $w(1, t)$) found from solving the Euler-Bernoulli equation, then the height of the tip due to initial curvature, $w_0(1)$, will be added.

Re-writing the equation of initial curvature $w_0(x) = 129.21 x^2$ (equation (2) for the short cantilever) in the non-dimensional form gives

$$\bar{w}_0(\bar{x}) = 129.21 \bar{x}^2 L^2 \quad (21)$$

where $\bar{w}_0(x) = d w_0(x)$ as previously shown.

3.1.2 Forcing Equations Revisited $f(t)$

There are different fringing field forcing equations that could be applied to our curved cantilever discussed above. Here we are going to non-dimensionalize them as follows

- 1- For Osterberg and Senturia [45], same rule applies: $\bar{f}(t)_{Senturia} = \frac{T^2}{\rho A d} f(t)_{Senturia}$

which renders

$$\bar{f}(t)_{Senturia} = \frac{T^2}{\rho A d} \frac{0.65 \in A d}{2 w} \frac{V(t)^2}{(d - w)^2}$$

The final form of the non-dimensional force including initial curvature is as follows

$$\bar{f}(t)_{Senturia} = \frac{0.65 \in L^4}{2 E I_{eff} d^2} \frac{V(t)^2}{1 - (w_0 + w)}$$

(22)

- 2- Similarly for Kambali et al forcing [46], $\bar{f}(t)_{Kambali} = \frac{T^2}{\rho A d} f(t)_{Kambali}$. Therefore, the

non-dimensional form including curvature is as follows

$$f(t)_{Kambali} = \frac{T^2}{\rho A d} \frac{\in V^2 h}{(g - (w_0 + w))^2} \left| 0.00316 \left(\frac{d}{b}\right)^4 - 0.043 \left(\frac{d}{b}\right)^3 + 0.21 \left(\frac{d}{b}\right)^2 \right. \\ \left. - 0.44 \left(\frac{d}{b}\right) - 2.83 \right|$$

(23)

- 3- For our new force formula $f(t)_{New} = \frac{V(t)^2}{2} (6 * 10^{-7} w - 9 * 10^{-12})$, and from the non-dimensional equation of motion above, the force could be transformed to it non-

dimensional form as $\bar{f}(t)_{New} = \frac{T^2}{\rho A g} f(t)_{New}$. Moreover, w in $f(t)_{New}$ has to be converted to its non-dimensional equivalent $\bar{w} d$

$$\begin{aligned} \bar{f}(t)_{New} &= \frac{T^2}{\rho A d} f(t)_{New} = \left(\frac{T^2}{\rho A d} \right) \left(\frac{V(t)^2}{2} (6 * 10^{-7} \bar{w} d - 9 * 10^{-12}) \right) \\ &= \frac{L^4}{2 E I_{eff} d} V^2 (6 * 10^{-7} \bar{w} d - 9 * 10^{-12}) \end{aligned}$$

(24)

It can be seen from all above three non-dimensional equations that all parameters of $\bar{f}(t)$ s are known by now, except the effective rigidity $E I_{eff}$ (embedded in $T = \sqrt{\frac{\rho A L^4}{E I_{eff}}}$).

3.1.3 The effective rigidity $E I_{eff}$

The rigidity here is an effective one due to the fact of the beam/cantilever is being made of two materials: composite beam or bilayer beam. Therefore, we will implement the classical *Equivalent Cross Section* method (also called *Transformed Cross Section*) of composite beams made of two dissimilar materials [1, 48] which finds a new cross section with different widths while maintaining the same thicknesses of the original cross section. This new equivalent cross section will be treated as being made of either one of the two materials. Figure 41 shows the schematics of the cross-section transformation into a new equivalent cross section made of polysilicon.

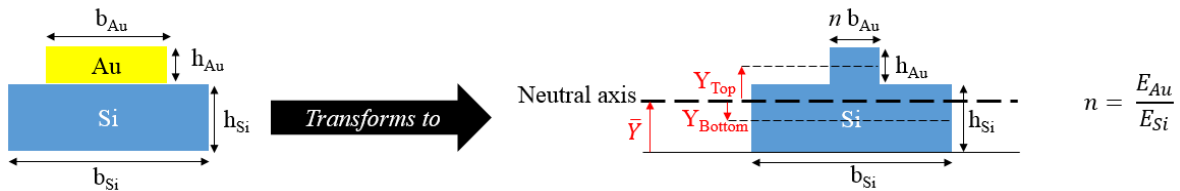


Figure 41: The original cross section of the beam (left) transformed into a new equivalent cross section (right) made of polysilicon only.

The area moment of inertia has to be found around the neutral axis. This axis passes through the centroid of the new or equivalent cross section. The centroid of the new cross section is as follows

$$\bar{Y} = \frac{\sum YA}{\sum A} = \frac{Y_{Top}A_{Top} + Y_{Bottom}A_{Bottom}}{A_{Top} + A_{Bottom}} \quad (25)$$

where Y_{Top} is the distance from the centroid to the center of the top layer (gold), Y_{Bottom} is the distance from the centroid to the center of the bottom layer (polysilicon), A_{Top} is the cross sectional area of the top layer (gold), and A_{Bottom} is the cross sectional area of the bottom layer (polysilicon). Table 7 shows the different values of Y_s and A_s .

Table 7: The components needed to calculate the height of the neutral axis.

	Centre Line (Y)	Area (A)
Top rectangular cross section	$h_{Si} + \frac{h_{Au}}{2}$	$n b_{Au} h_{Au}$
Bottom rectangular cross section	$\frac{h_{Si}}{2}$	$b_{Si} h_{Si}$

where h_{Au} is gold's thickness, b_{Au} is gold's width, h_{Si} is polysilicon's thickness, b_{Si} is polysilicon's width, and n is the ration of gold's Young's modulus to polysilicon's ($\frac{E_{Au}}{E_{Si}}$).

Now the effective area moment of inertia is the sum of the two moments of inertia as follows

$$I_{eff} = I_{Top} + I_{Bottom}$$

$$= \left[\frac{1}{12} (n b_{Au} h_{Au}^3) + A_{Top} Y_{Top}^2 \right] + \left[\frac{1}{12} (b_{Si} h_{Si}^3) + A_{Bottom} Y_{Bottom}^2 \right] (m^4)$$

which turns to be

$$I_{eff} = \left[\frac{1}{12} (n b_{Au} h_{Au}^3) + n b_{Au} h_{Au} \left(h_{Si} + \frac{h_{Au}}{2} - \bar{Y} \right)^2 \right] + \left[\frac{1}{12} (b_{Si} h_{Si}^3) + b_{Si} h_{Si} \left(\bar{Y} - \frac{h_{Si}}{2} \right)^2 \right] (\text{m}^4)$$

(26)

The effective rigidity the is then

$$\text{Effective Rigidity} = EI_{eff} = E_{Si} I_{eff} (\text{N.m}^2)$$

As for the density ρA , it represents the density of the original cross section (having both materials) [1], which means

$$\rho A = \rho_{Si} A_{Si} + \rho_{Au} A_{Au} (\text{kg/m})$$

(27)

Therefore,

$$T = \sqrt{\frac{(\rho_{Si} A_{Si} + \rho_{Au} A_{Au}) L^4}{E_{Si} I_{eff}}} (\text{kg.m/N})$$

(28)

3.2 Solving the Equation of Motion by Galerkin's Weighted Residual Method

The equation of motion discussed above is a partial differential equation in x and t , and can never be solved analytically except if we eliminate either terms. However, the approximation method of Galerkin's assumes $w(x,t)$ as the multiplication of two functions, one in x and the other in t , as follows

$$w = u_1(t)\phi_1(x) + u_2(t)\phi_2(x) + u_3(t)\phi_3(x) + \dots$$

$$= \sum_{i=1}^N u_i(t)\phi_i(x)$$

(29)

Re-writing the equation of motion to be in similar form to the Galerkin's assumption:

$$\sum_{i=1}^N \left(\ddot{u}_i(t) \phi_i(x) + c \dot{u}_i(t) \phi_i(x) + u_i(t) \phi_i^{iv}(x) \right) = \bar{W}$$

(30)

Comparing the equation of motion and \bar{W} , we can say that

$$\bar{W} \approx \frac{T^2}{\rho A g} f(t)$$

(31)

Now if we call the difference between the actual value of $\frac{1}{\rho A} f(t)$ and \bar{W} as the Residual (R),

then it is equal to

$$R = \bar{W} - \frac{T^2}{\rho A g} f(t)$$

(32)

Now if we can find a function ϕ so that $\int R_i \phi_i = 0$ or $\sum R_i \Phi_i = 0$, then as per Galerkin's method we can eliminate the dependence on x if we assume that ϕ is the mode shape of the beam/cantilever under investigation.

3.2.1 Finding the mode shape

First, we find the mode shape $\phi_i(x)$ by solving the unforced, un-damped linear problem. This approximation will render the equation of motion to be in the following Eigen-value problem form

$$\ddot{w}(x, t) + w^{iv}(x, t) = 0$$

(33)

To make solution in the following form (described above) $u(t)\phi(x)$, assume $w(x, t) = \phi(x)e^{i\omega t}$, where $u(t) = e^{i\omega t}$.

Taking the second derivative with respect to t , and the fifth with respect to x result in

$$-\omega^2\phi(x)e^{i\omega t} + \phi^{iv}(x)e^{i\omega t} = 0$$

$$e^{i\omega t}(-\omega^2\phi(x) + \phi^{iv}(x)) = 0$$

Since $e^{i\omega t} \neq 0$, then

$$-\omega^2\phi(x) + \phi^{iv}(x) = 0$$

To solve this equation, assume $\phi(x) = Ae^{sx}$

Therefore,

$$-\omega^2 Ae^{sx} + As^4 e^{sx} = 0$$

$$e^{sx}(-\omega^2 A + As^4) = 0$$

Since $e^{sx} \neq 0$, then $s^2 = \pm\omega \rightarrow s^2 = +\omega$ and $s^2 = -\omega$. This renders four roots as follows: $s_1 = \sqrt{\omega}$, $s_2 = -\sqrt{\omega}$, $s_3 = \sqrt{-\omega} = i\sqrt{\omega}$, $s_4 = -i\sqrt{\omega}$.

This results in $\phi(x)$ being

$$\phi(x) = A_1 e^{\sqrt{\omega}x} + A_2 e^{-\sqrt{\omega}x} + A_3 e^{i\sqrt{\omega}x} + A_4 e^{-i\sqrt{\omega}x}$$

which also can be written as

$$\phi(x) = c_1 \sin(\sqrt{\omega}x) + c_2 \cos(\sqrt{\omega}x) + c_3 \sinh(\sqrt{\omega}x) + c_4 \cosh(\sqrt{\omega}x)$$

where constants can be found by the boundary conditions.

The equations of the first three mode shapes are

$$\phi_1(x) = c_1 \sin(\sqrt{\omega_1}x) + c_2 \cos(\sqrt{\omega_1}x) + c_3 \sinh(\sqrt{\omega_1}x) + c_4 \cosh(\sqrt{\omega_1}x) \quad (34)$$

$$\phi_2(x) = c_1 \sin(\sqrt{\omega_2}x) + c_2 \cos(\sqrt{\omega_2}x) + c_3 \sinh(\sqrt{\omega_2}x) + c_4 \cosh(\sqrt{\omega_2}x) \quad (35)$$

$$\phi_3(x) = c_1 \sin(\sqrt{\omega_3}x) + c_2 \cos(\sqrt{\omega_3}x) + c_3 \sinh(\sqrt{\omega_3}x) + c_4 \cosh(\sqrt{\omega_3}x) \quad (36)$$

The model above was plugged into Mathematica software, which provided a great insight about the dynamics of the beams. The model predictions will be mapped with their experimental counterparts in the coming chapter.

Chapter 4: Experimental Results vs Related Models

The chip was mounted to a custom designed Printed Circuit Board (PCB), which has easy connectable pins at which the wire clips are hooked as shown in Figure 42.

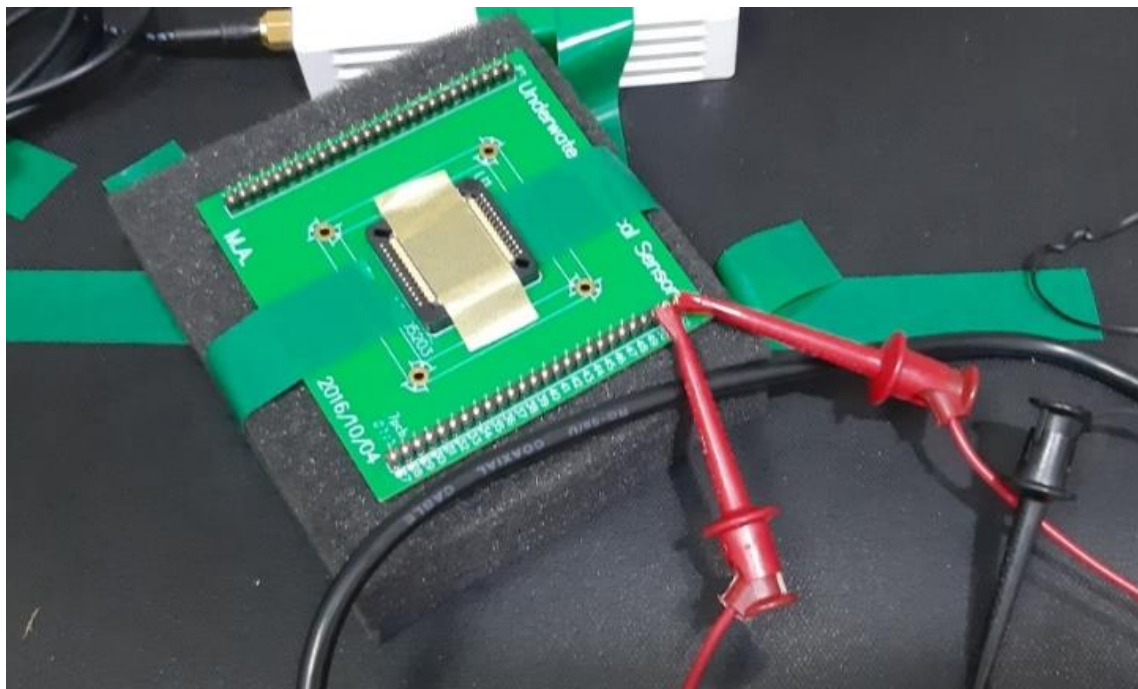


Figure 42: Wire clips (red) as they are connected to the PCB connectable pins. One pin connects the side electrode to the voltage source, the other connects the cantilever and bottom electrode to external grounding. The chip was covered with glass lid, mounted by the golden tape for protection.

The chip layout, dimensions, and numbering identification are shown in Figure 43.

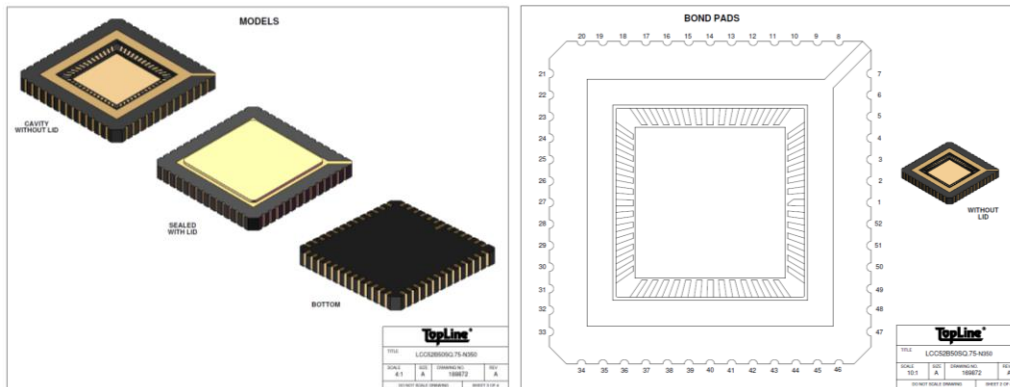
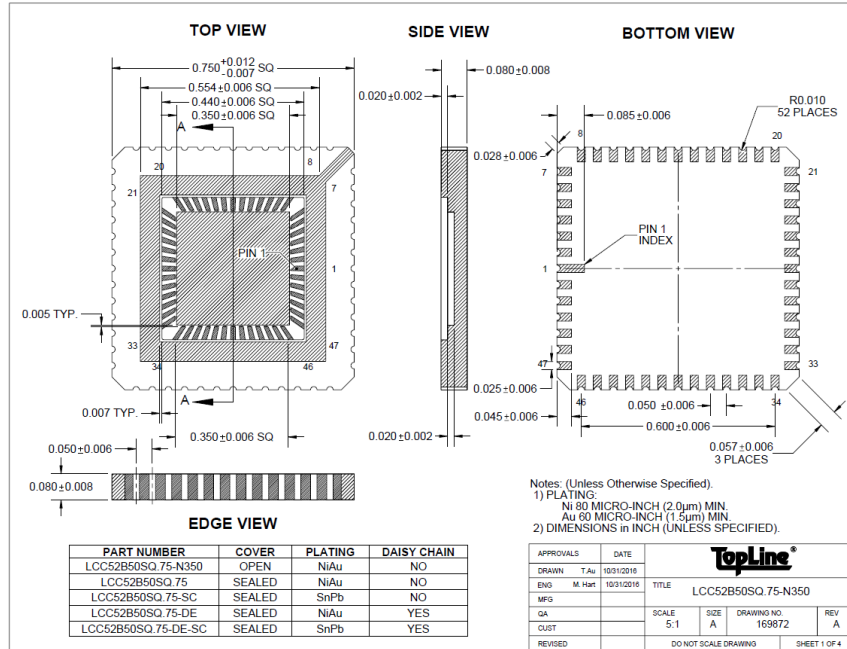


Figure 43: The drawing and dimensions of the chip on which the device was fabricated (top), a closer view showing the bond pads their numbering for cantilever identification (bottom right), and a 3D view showing the cavity inside which the cantilevers are protected with the lid (bottom left). Used with permission from [49].

The actuator was first studied by Lock-in amplifier, however, due to some technical difficulties due to high parasitic capacitance, the actuator dynamics was better to be studied by *Polytec* vibrometer shown in Figure 44.

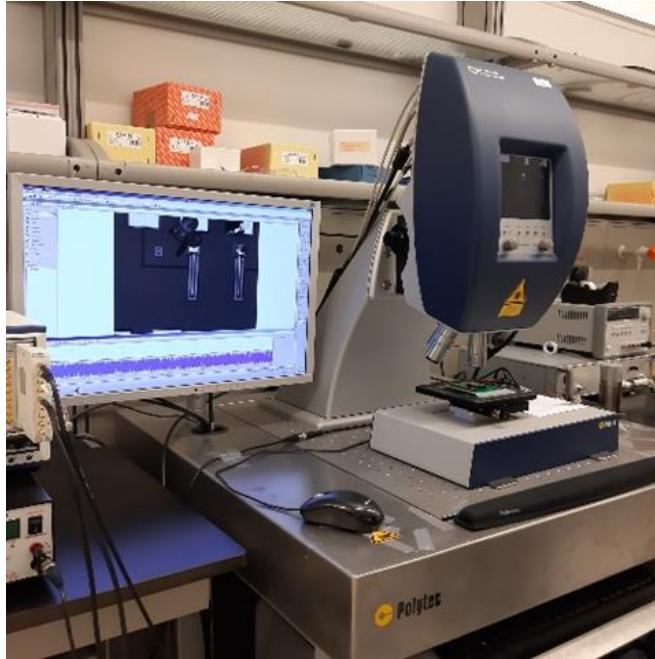


Figure 44: The Polytec vibrometer. The photos show the device and its computer interface.

The voltage source was connected to the side electrode via the PCB pin, so does the grounding of the cantilever and bottom electrode. The laser pointer was directed to the cantilever tip as shown in Figure 45.

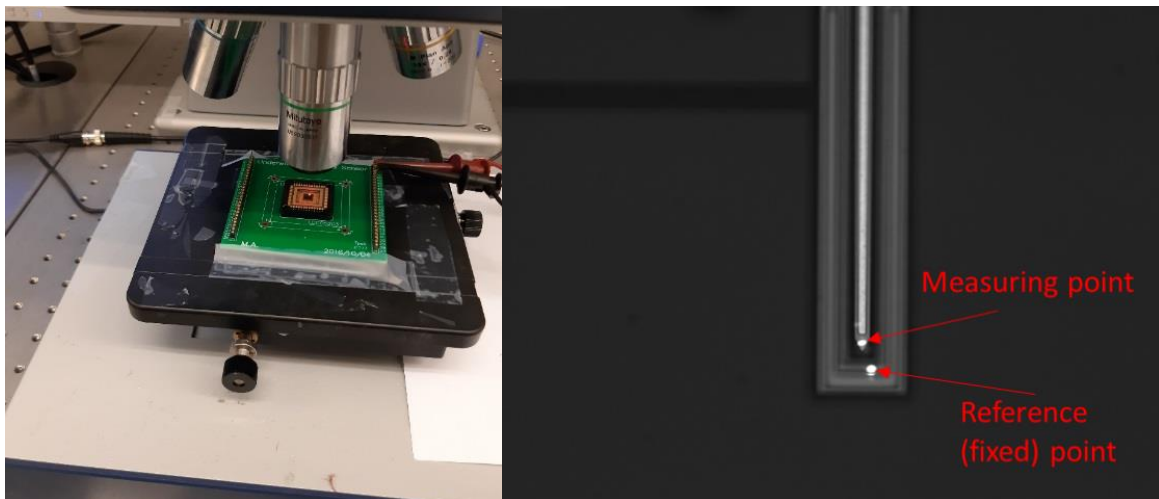


Figure 45: (Left) The chip as mounted on the PCB and subjected to the laser beam. (Right) The laser beam pointer directed to the cantilever's tip as observed under the vibrometer's optical microscope.

The natural frequencies have been obtained through a hammering pulse as shown in Figure 46.

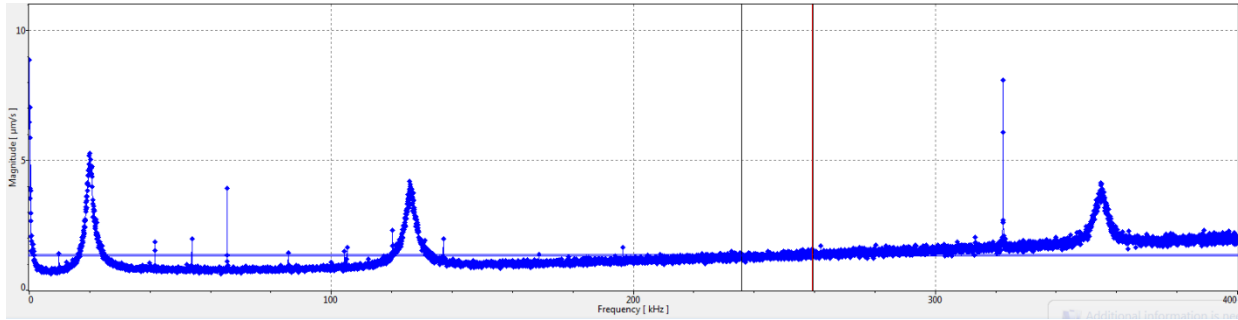


Figure 46: First three natural frequencies experimentally obtained in air medium. The image was co-published by the student in [41] and was reused here with permission.

The natural frequencies obtained by the model and the experiment were closely matching as depicted in Table 8. Note that the model natural frequencies were obtained by a code in Mathematica that solves for the three natural frequencies (ω_1, ω_2 & ω_3) in the mode shapes equations above (ϕ_1, ϕ_2 & ϕ_3) (equations (34) (35) (36)).

Table 8: Comparative table of natural frequencies of the cantilever as obtained experimentally and analytically.

	Experiment	Model
1 st natural frequency (kHz)	20.125	20.116
2 nd natural frequency (kHz)	125.81	126.066
3 rd natural frequency (kHz)	354.750	352.988

The quality factor is 10.7 which was calculated at the half power bandwidth, or 0.707 of the maximum amplitude for the first natural frequency.

The side electrode was then subjected to the AC/DC voltage source, while the cantilever and bottom electrode were grounded. Frequency response curves for deflection were taken for the

cantilever experimentally and compared to all three forces used in the model: Osterberg and Senturia force [45], and Kambali et al force [46], and our new force. As per the model, and for each excitation frequency, the deflection amplitude was measured post the transient response (at the steady state). Figure 47 shows the transient response.

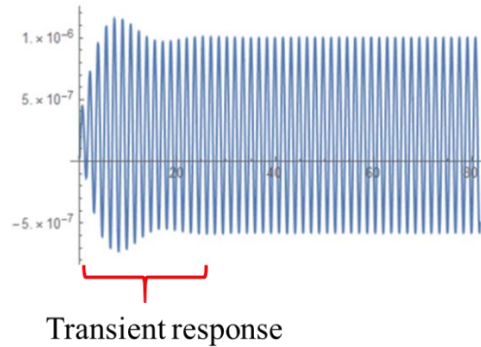


Figure 47: An example of time history response for the cantilever at excitation frequency of 22 kHz using 10 AC-10 DC forcing (on Mathematica) showing the transient response in nondimensional time units (x-axis). Note that the deflection amplitude was taken for the last three periods.

To match the model with the experiment, different correction factors were needed to be introduced for different DC voltages. This was expected, since different DC voltages mean different curvatures, which implies different field line distributions between top and bottom surfaces of the cantilever (as described in details in previous chapters); hence, different correction factors are needed for different DC voltages. Figure 48 shows COMSOL depiction of different curvatures with different DC voltages from 0-190 V sweep. The curved lines represent the cantilever's different curvatures as DC voltage increase.

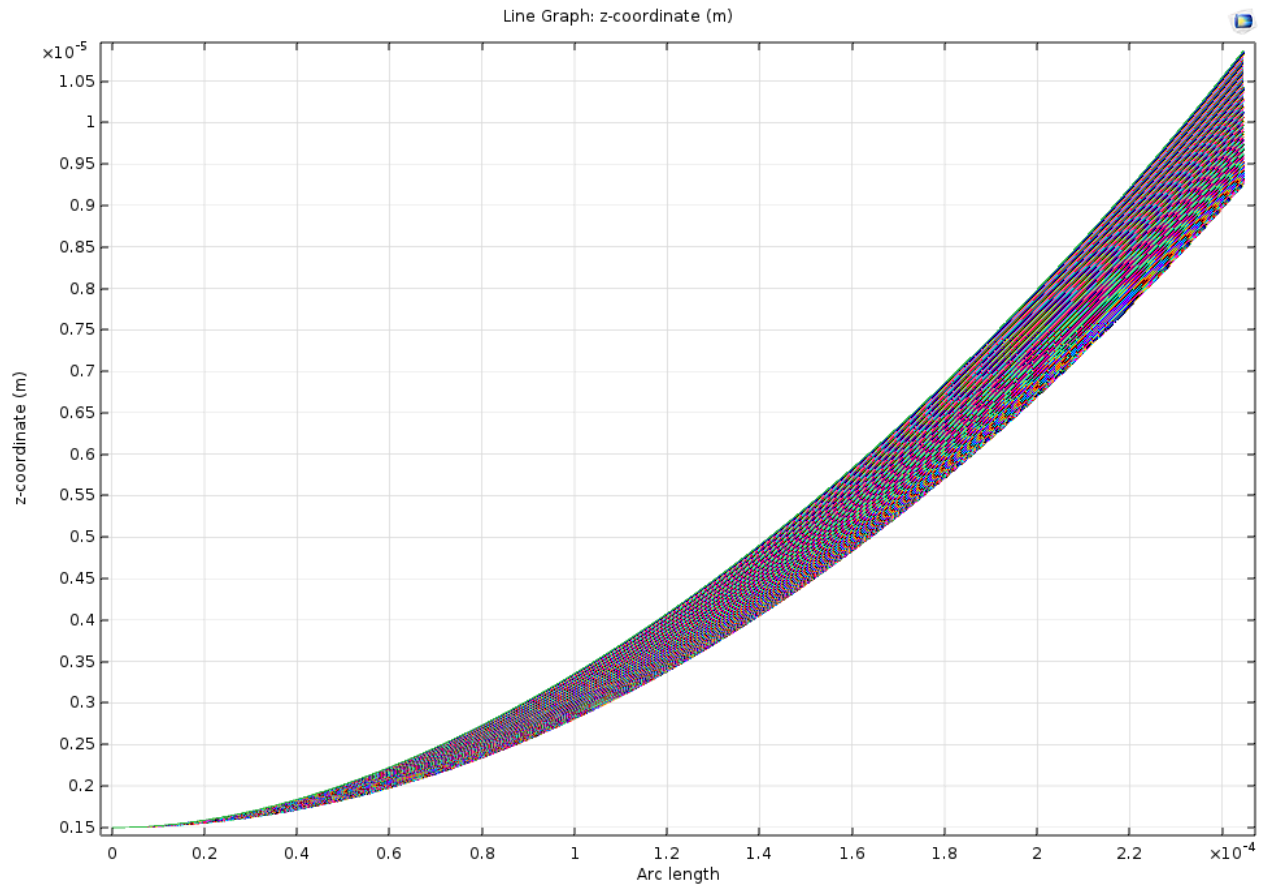


Figure 48: Different curvatures for different DC voltages in a sweep from 0-190 Volts using COMSOL. Different lines here represent cantilevers with different curvatures.

The model was first adjusted to match the 10 AC 7 DC frequency sweep, and the correction factor was found to be 1.95 for Osterberg and Senturia force [45] and 1.66 for Kambali et al force [46], and 0.14×10^6 for our force. The large order of 10^6 of the factor of our force was due to some impeded issue within COMSOL that could not be identified. One issue with FEM softwares (known to be called "black box") is the inability to track the derivation of equations used to be able to debug the model.

However, when we tried different AC-DC combinations, a dramatic shift in model amplitudes occurred that made impossible to match with experiment. Therefore, several investigations were conducted to explain such dramatic decrease in amplitude compared to experiment. To our

surprise, this discrepancy was overcome when the equation of initial curvature was simply removed from the model; hence, the model was simply that of a straight, non-curved cantilever. It seems that the curvature equation introduced a geometric nonlinearity in the model, with which a small change in voltage caused a big shift in amplitude. However, we still needed the correction factors to correct for the curvature-induced weakening of the effective levitation force felt by the cantilever top surface. The correction factors were 0.88 for Osterberg and Senturia force [45] and 0.179×10^6 for our new force. However, the Kambali et al force [46] showed a singularity point when the correction factor was reduced to further below 0.29, where the displacement was dropped from the micrometer regime at a correction factor ≥ 0.29 , to the 10^{-13} order of magnitude at correction factor < 0.29 . This is due to the equation's high order (4th order), which makes it very sensitive to such perturbation. Therefore, the Kambali et al force [46] could not be matched with the experiment. Figure 49 shows experimental frequency sweep curves as matching with the Osterberg and Senturia force [45] and our new force.

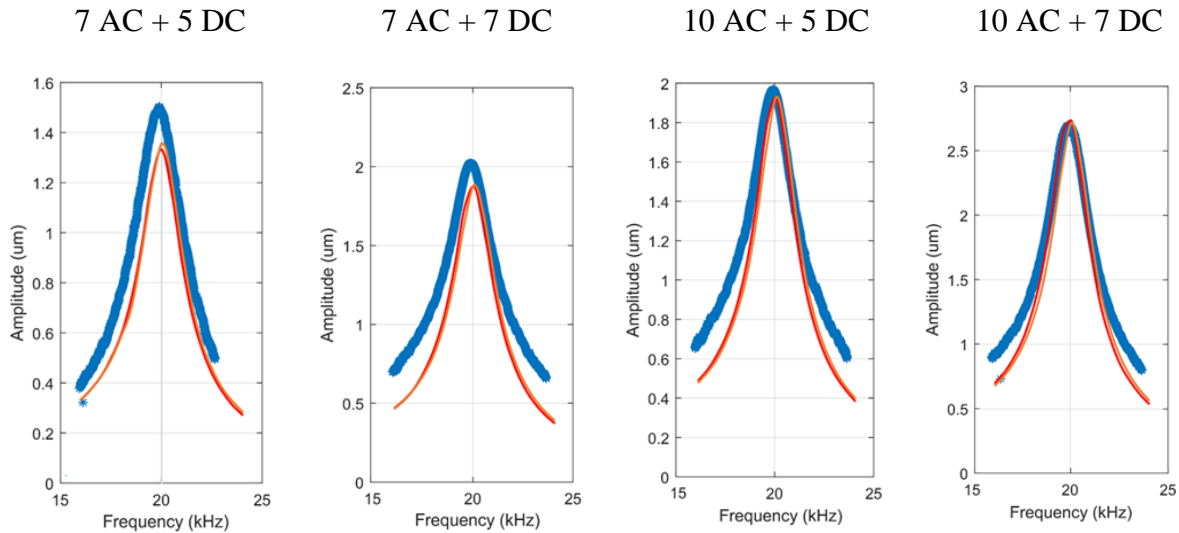


Figure 49: Experimental frequency sweeps (blue) as compared with the theoretical ones: Osterberg and Senturia (red) and our new force (brown).

Such factors as our correction factor are known in theoretical physics as “free parameters” which are unknown parameters the theory needs to make predictions while the theory itself does not constrain nor predict the value of these free parameters [50]. The exact reason or physical phenomenon for the existence of this correction factor could be the topic for future studies as will described in next chapter.

Chapter 5: Conclusion and Recommendations for Project 1

This work provided a simpler numerical forcing equation approach to model electrostatic force, other than the analytical approach by Osterberg and Senturia force [45], or the complicated numerical approach by Kambali et al [46] that required two numerical softwares and lengthy equations (to the fourth order) that are different for different actuator configuration. This work also shows that the curvature equation may not be needed to model the dynamics of curved AFM probes (and other MEMS structures) electrostatically actuated. Intuitively speaking, this could be true for other actuation types, and future studies could investigate this. However, the relation between curvature and the correction factor need to be further investigated and more precisely modeled as a function of curvature, actuation electrode-cantilever distance, relative axial/longitudinal cantilever-electrode orientation, etc. One way is an experimental one where different beam lengths (viz. different curvatures) can be studied and an overall governing equation can be extrapolated. This is very tedious and inefficient way since any sound fitting function should stem from around 100 or more points. However, another method can be applied if the correction factor is to be omitted: the gap between cantilever and bottom electrode (d) needs to be replaced by the curvature equation. If we do that for Kambali et al force [46] and Osterberg and Senturia force [45], the Mathematica model needs to be completely upgraded to account for way higher order calculus the model needs to solve. In the case of our COMSOL derived force, the equation of capacitance, $c(w)$, needs to be a function of actual curvature, not for tip deflection as per this study. We have tried doing so by slicing the airbox into strips so we can measure the capacitance variance through

different strips across the curvature. We could not do that due to COMSOL limitation: COMSOL only measures the capacitance for the whole airbox. We have tried a simple curved structure and sliced it into few slices and put a capacitance probe per slice (that measures capacitance per that slice only); COMSOL only calculated same capacitance for all strips, which is the total capacitance as shown in Figure 50. This slice-probe technique could be tried using different software (e.g. Ansys) which might have such segmentation capabilities.

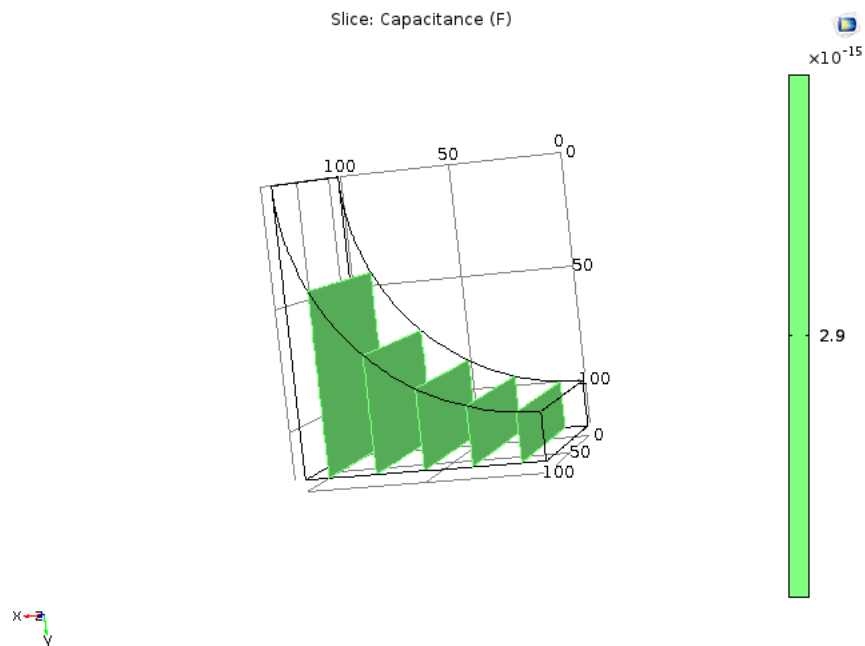


Figure 50: Capacitance for curved structure turned into slices. Note how COMSOL only measures one capacitance per whole structure despite the defined slices and defined corresponding probes.

We strongly expect that this is the best way to eliminate the need for correction factor, since the curvature will be embedded in the forcing equation. Moreover, the factor order for our force (10^6) should be further investigated and identify the root cause of it. We suspect that such high order was due to an impeded issue within COMSOL. COMSOL Middle East customer help could not identify the problem, which confirms that FEM is indeed a black box.

We also recommend that future work should include the wire bonding in the original design (instead done post fabrication as was done here and shown in Figure 51) since the thick wire bonding between connecting pads is expected to produce stronger field; hence, stronger force.

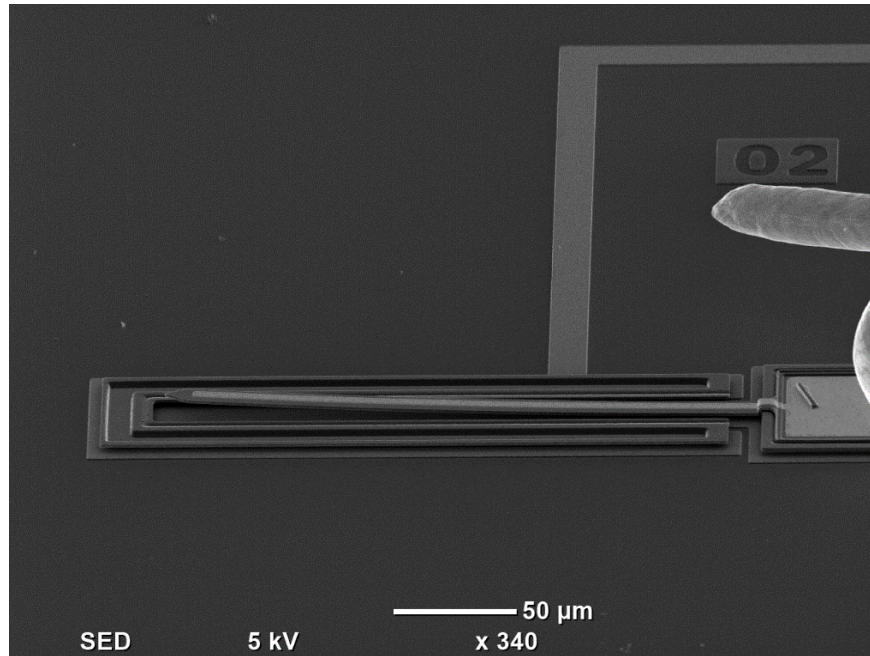


Figure 51: The thick wire bonding (right of the image) which might have produced more field onto the cantilever.

Moreover, further work may also compare the curved cantilever dynamics under vibrometer to that under lock-in amplifier. In such case, the design should connect both the cantilever and bottom electrode to two separate grounding pads, even if they are both grounded and can be connected to the same grounding pad. This will enable getting an independent signal from the cantilever, and another independent one from the bottom electrode. This recommendation is based on months of investigations conducted at the onset of this project, which led us to shift to the vibrometer since it directly measures the probe vibration optically using laser, instead of transduced from electrical signal like the lock-in amplifier. The lock-in used was of model HF2LI, equipped with transimpedance current amplifier of model HF2TA. The device is operated with *LabOne* online

software provided by *Zurich Instruments Inc.* Figure 52 shows the user interface and the initial parameters used. Note that since the device was newly bought, the device has been setup by us in coordination with Zurich Instrument live support.

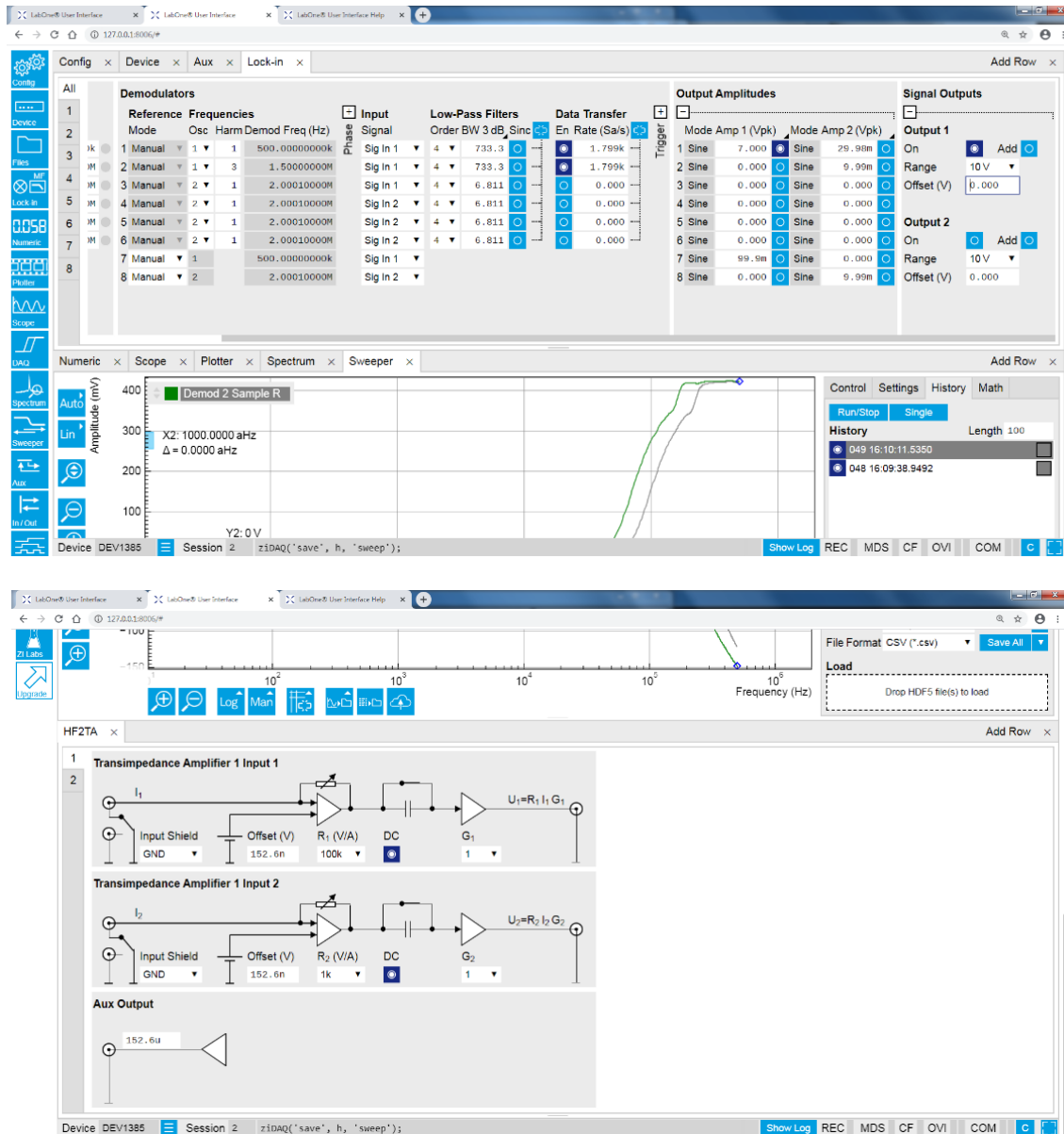


Figure 52: The lock-in amplifier user interface (LabOne) for 10 DC - 7 AC (top) and the transimpedance amplifier (bottom).

As per the wire connection used, it is shown in Figure 53. Note the existence of only two clamps connected to the pins through the red wire. One alligator clamp is for connecting the side electrode,

and the other is for connecting both the probe and bottom electrode to ground since the cantilever/probe and the bottom electrode are grouped to one connection pad in the design. Note that this should be adjusted to two separate grounding pins as described above.

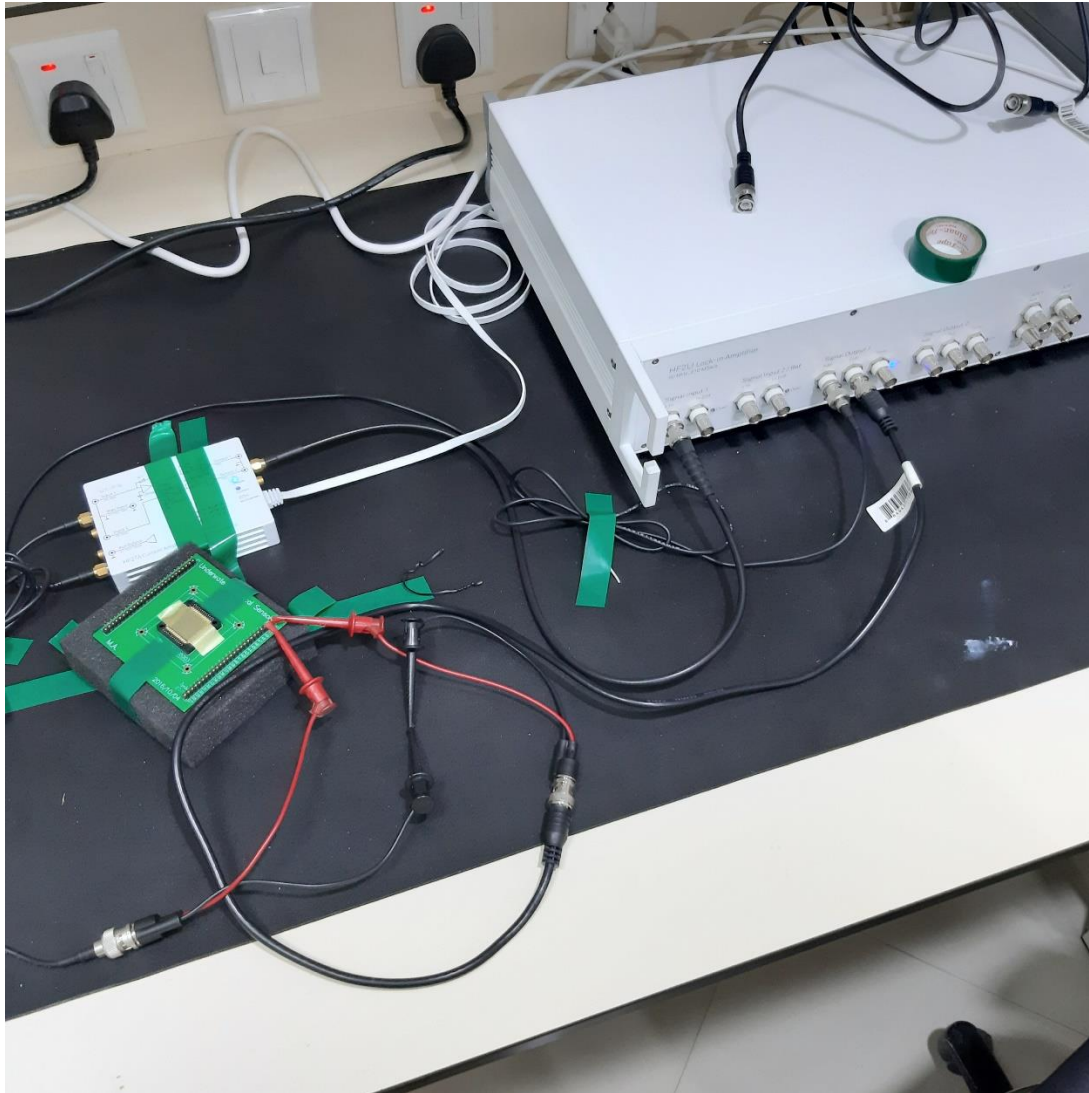


Figure 53: The probe connections to the lock-in amplifier via the chip carrier pins. Note that there exist only two clamps connected to the pins (red wire): one is for connecting the side electrode, and the other is for connecting both the probe and bottom electrode to ground.

The sequential operation mechanism of the lock-in amplifier is illustrated in Figure 54, and is as follows:

- 1- The DC signal (as entered to the *LabOne* software) will be generated by the current amplifier, then fed into the lock-in device.
- 2- The lock-in amplifier will generate an AC signal then group it with the DC signal. This signal will then be fed into the side electrode trough the BNC connector and coaxial cable.
- 3- The cantilever will vibrate; hence, generate a voltage signal that will be transferred by the coaxial cable into the transimpedance amplifier (note that having the new proposed connection to two separate groundings, the signal will be purely from the cantilever, unlike the existing signal which represents both cantilever and bottom electrode).
- 4- The transimpedance amplifier will convert the voltage signal into current, then feed it to the lock-in amplifier.
- 5- The lock-in amplifier will readout the results through *LabOne* as per the desired setup/parameters.

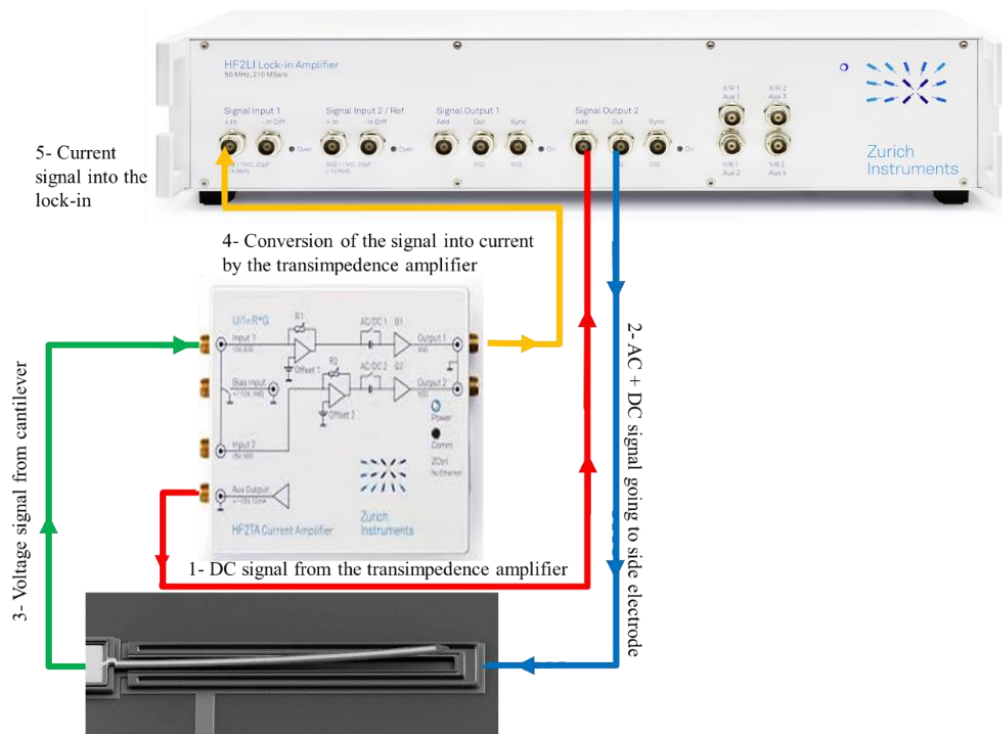


Figure 54: The proposed lock-in amplifier connection and the description of its mechanism with numbered steps.

The capacitance can be calculated using the following formula

$$c = \frac{1}{\Omega Z} \text{ (F)}$$

(37)

where Ω is the excitation frequency in radian, and Z is the impedance. The impedance, Z , can be found from the following formula

$$Z = \frac{V}{I/\text{gain}} \text{ (\Omega)}$$

(38)

where V is voltage (2nd harmonic), and I is current (3rd harmonic), and the gain is 100k.

We have found that the lock-in obtained capacitance of the actuator is in 10^{-12} Farad, while COMSOL model shows a capacitance in the 10^{-14} regime, which means that the parasitic capacitance is at least two orders of magnitudes higher than the real signal; hence, dominate the response.

We also recommend that further AFM tip improvements should involve a cantilever of length less than 250 μm for higher field reach. An initial recommendation is 100 μm . Also, further tip sharpness might be induced as shown in Figure 55 where the edge of the beam (i.e. the tip) will suffer a shear stress caused by the peeling force at the bottom of the cantilever. This could be enabled by waiting for some time before removing the sacrificial layer which could be communicated with CMC Microsystems. The reason is that the sacrificial layer is preventing the cantilever from bending upwards, and will consequently cause a peel force that will curl up the upper corner of the cantilever (i.e. its tip)

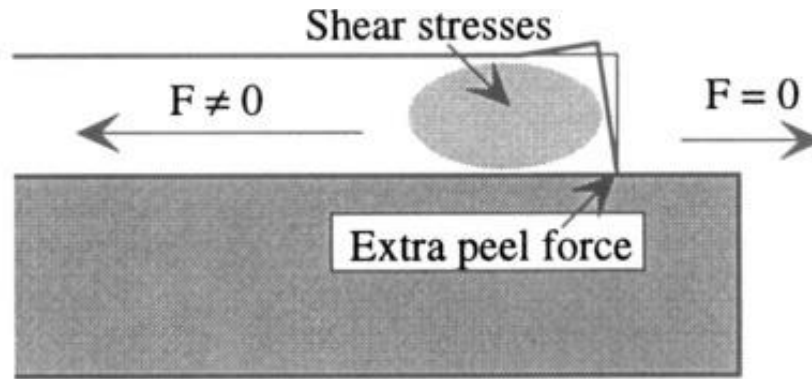


Figure 55: The peel force acting on the cantilever's tip due to the shear stress induced force imbalance caused by the sacrificial layer below it. Used with permission from [16].

This holds true given that both the sacrificial layer and the cantilever are isotropic materials. Such curl up will be of the interest to future work as it will further sharpen the AFM tip. Moreover, the gold layer could be made into a heater for further control of the curvature. This is attainable by making the gold layer as a U-shaped loop on top of polysilicon in order to form a circuit, where one could pass current through the loop to heat up the structure; hence, induce more curvature.

**Project 2: Light-Matter Interaction Using
1D Mirror Inscribed in a 2D Photonic
Crystal Fiber**

Chapter 1: Introduction

1.1 Light-Matter Interactions

Increasing the interaction between light and matter is usually explored to unravel more understanding about the nature of both interacting entities: light and matter. This basic research is enabled by engineering platforms with which such maximally interacting light and matter can be realized.

Moreover, once such platforms are constructed, the optical fields have to be strong enough to change the material properties so that they emit more signals with which the properties can surface. This strong optical field induces a non-linear interaction. This can be modeled in bulk materials. However, there are some applications where we need a single photon-single atom regime such as a quantum bit. Moving to a single atom to few atoms' regime, the light has to move down to a single to few photons in order to make a trackable interaction; hence, a better understood qubit behavior. In such few atoms-few photons system, the interaction will be linear; hence, reveals less signals. A non-linear interaction at this scale is hard to induce (without high intensities). Therefore, it is one of the longstanding challenges in non-linear optics. The second project of this dissertation addresses such challenge by providing a device/platform with which this non-linear interaction can be intensified yet with low intensities.

Before describing the proposed platform, it is worth elaborating the parameters contributing to the interaction probability. Knowing such parameters will help make a system that addresses increasing their occurrence chance. The interaction probability, P , between light and matter at this nanoscale can be roughly thought of as the following

$$P \approx \frac{\sigma_0}{A_{Beam}} \approx \frac{\lambda^2}{A_{Beam}} \approx \mu^2 E^2 t \tag{39}$$

where σ_0 is the effective cross section of these few atoms (the atomic gas) as seen by the few photons beam (also called scattering cross section which can be approximated by the square of wavelength λ^2), A_{Beam} is the light (laser) beam area, μ is the dipole moment, E is the electric field, and t is interaction time. There are four possible ways to increase such interaction probability:

- 1- **Increase the number of atoms**, hence, give the photon a bigger chance to hit an atom, as shown in Figure 56. This increases the probability of interaction on the expense of reducing non-linearity.



Figure 56: Single photon-multi atoms interaction.

However, in order to increase the probability of the single photon hitting only one single atom out of the atomic cloud, one must increase the system cooperativity which will add to the difficulty of achieving the goal (cooperativity is the ability of one photon to interact with a single atom in an atomic cloud).

- 2- **Increase transverse confinement**. This option can be visualized by the schematics in
- 3- Figure 57.



Figure 57: Schematic of a cross section of a fiber core confining one photon and one atom.

Such system can be implemented in the hollow core of a photonic crystal fiber (PCF) which will allow the photon to propagate only in the longitudinal direction (along the waveguide axis) while blocking the transverse propagation.

The problem with this system is that the photon will hit the atom in one pass only; after that, the photon will leave from the other side of the fiber.

- 4- **Increase the interaction time.** Interaction time can be done by increasing the number of passes, which can be enabled by two mirrors in a cavity, as shown in Figure 58.

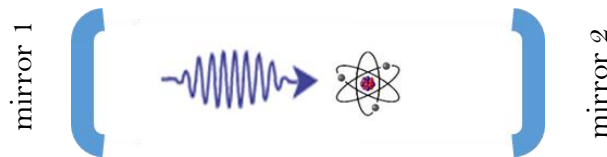


Figure 58: Schematic of a cavity confining one photon and one atom allowing the photon to go through multiple passes.

While this system provides multiple passes with which the interaction time increases, the problem is that it does not prevent/confine the photon from leaking from upward transverse direction.

- 5- It seems natural to propose a system which combines the above systems (2 and 3) as shown in Figure 59.

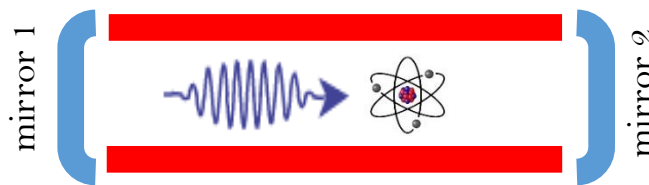


Figure 59: Schematic of a cavity cross section confining one photon and one atom both longitudinally and transversally.

The problem with such a system is that there is no way to inject/insert the atom into the system.

1.1.1 The Proposed Platform

Here, we propose a novel system which combines both longitudinal and transverse confinement yet allow for atoms insertion into the system. Such system can be realized using a Bragg mirror inscribed at the hollow core of a photonic crystal fiber (HC-PCF) as shown in Figure 60. So instead of a vertical mirror, Bragg reflection concept is employed here. Note that it is called “mirror” while it is just an inscription on the fiber wall; not a real physical orthogonal mirror to the light; it just gives a “mirror effect” by having the ability to bounce the light back and forth.

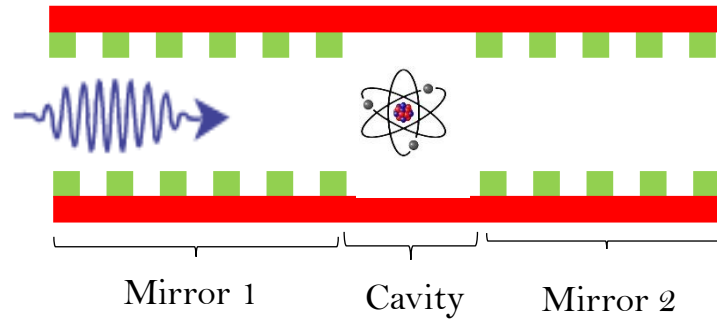


Figure 60: Schematic of fiber cross section confining one photon and one atom with an impeded cavity of two Bragg mirrors inscribed on the core's wall. Hence, it allows the photon to go through multiple passes while keeping the core unobstructed.

Such fiber is shown in Figure 61.

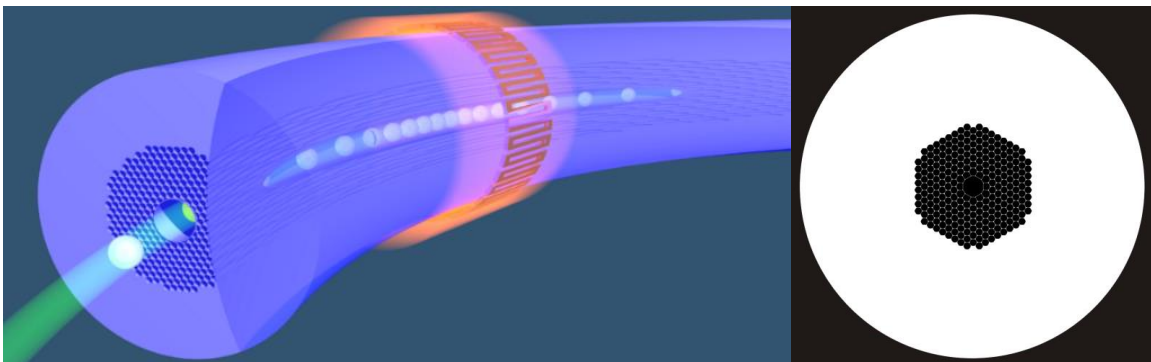


Figure 61: Cartoon visualization of the HC-PCF (left) [51] and an optical microscope image of the HC-PCF used in this project (right) [52]. Used with permission from [51] and [52].

The numerical and experiential procedures to realize such platform will be discussed in later chapters. It is worth describing the concept behind the enablement of such system: Photonic Crystals and Bragg reflections.

1.2 Photonic Bandgap Effect and the Light Matter Similarities

Light is guided inside the normal telecom fiber with no limitation except to the light power which should not exceed the melting point of the fiber material. However, the photonic crystal inscribed across the fiber length limits the range of the light frequencies that can propagate through. This is due to the photonic bandgap effect. The photonic bandgap is a phenomenon with which there will be some forbidden band (bandgap) or a range of wavelengths that will be “forbidden” from propagating; hence, create a mirror by reflecting back the resonant light. This was known in solid state physics with the electronic bandgap, but to see it happens with light was a shock to the scientific community since light was shown to behave like matter where some calls it the semiconductor of light [53]; a shock to which the nature magazine editor at the time, John Maddox, commented “*If only it were possible to make dielectric materials in which electromagnetic waves cannot propagate at certain frequencies, all kinds of almost-magical things would be possible*” [54]. Note that the 2D photonic crystal discovery was motivated by the quest to find a device/system to keep the atoms in the excited state upon population inversion in lasers; hence, suppress the spontaneous emission [55].

NEWS AND VIEWS

Photonic band-gaps bite the dust

Hopes that dielectric materials in which the transmission of certain frequencies would be forbidden seem to have been disappointed by the difficulty of realizing expectation and, now, by calculation.

<small>If only it were possible to make dielectric materials in which electromagnetic waves cannot propagate at certain frequencies, all kinds of almost-magical things would be possible. For example, it would be possible to embed in such a material atoms or molecules in excited states that would literally be incapable of getting rid of their excess energy by radiation if its frequency were in the forbidden range; the result might be a novel state of matter in which atoms or molecules are forever bound to the photons they would emit if their surroundings would accommodate</small>	<small>dently important prize. More surprising was the prediction that the properties of many molecular systems, when embedded in such materials, would be modified radically; dissociation energies of homonuclear diatomic molecules, for example, might be substantially reduced. The explanation is that interatomic interactions entailing the interatomic transfer of even virtual photons in the forbidden ranges of frequency will no longer occur.</small>	<small>appear not to have inhibited microwave transmission, but Yablonovitch was able to report that, provided that the two refractive indices of the dielectric components stand in the ratio of at least 3.5 to 1, a photonic band-gap does indeed appear. The most successful of his crystals consisted of spheres filled with air machined into a proprietary dielectric material with a refractive index of 3.5 in the frequency range between 1 and 20 GHz. Only 14 percent of the crystal volume was made of dielectric, so that the structure was more closely packed than expected for a face-</small>
---	---	---

However, it is hard to fathom why this was a surprise since light and matter has been showing some similarities in behaviors since the 1800s. The first to investigate extending matter behavior to light was the British physicist John Henry Poynting in 1884 CE, when he proposed that light may have orbital angular momentum just like matter [56]. Beth [57] proved it experimentally. Now we know that when you run light through a spirally twisted fiber, the light exits from the other end of the fiber with a spin [58]: the very same way that matter acquire spin upon going through a similar route! So, light behaves like matter. However, in 1924 Louis de Broglie formulated the exact opposite phenomenon, where matter behaves like light, which became known as Wave-Particle duality [59]. Four years later, this duality was experimentally proven by Clinton Davisson and Lester Germer [60] where electrons displayed a diffraction pattern (just like light) when scattered by a nickel crystal. As time progressed, this light-matter similarity continued to be manifested in other discoveries. The atomic fountain is one of such discoveries where light tosses an atom exactly like how water fountain tosses to a ball [61]! The optical tweezers are another example where we could hold matter using light, the same as we use regular tweezers to hold macro matter [62]. Moreover, the Bose-Einstein condensate is another example where matter flows coherently, the very same way light photons flow in lasers. Also, quantum computation could be carried out by either matter or light qubits [63], and most recently scientists started exploring the dark photons, as opposed to dark matter [64]. Last but not least the capillary force, the smaller the trench the faster the liquid propagates. Similarly, light travels faster in smaller diameter fiber (Single Mode) than in bigger diameter fiber (Multi Mode). Therefore, the 2D photonic bandgap (like in HC-PCF) should have not been as shocking as it was for two reasons: firstly the above light-matter similarities was already known, and secondly the 1D photonic bandgap crystal was already discovered in 1887 by Lord Rayleigh [65]! Despite these two facts, it took one hundred

years just to simply extend the 1D photonic crystal to its 2D form by Eli Yablonovitch [66] and Sajeev John [67] in 1987. Not only that, the 2D photonic crystal was rejected at first by the prestigious *Physical Review Letters*! However, Yablonovitch paper was later accepted after some attempts with the editor, and the paper became one of the most highly cited papers in the journal's history [68]!

The lesson here is that light has been consistent in showing us that it could behave like matter since the advent of the twentieth century, and in my opinion this trend is crying out for more extensions where current light-only behavior could be explored in matter and vice versa. Such unexplored trend extensions will create a vast number of venues to explore potential inventions and discoveries given the matter-to-light extensions that could be made. Nevertheless, the phenomenon of two separate paradigms behaving similarly is not something novel to science. When Newton found that the force between two masses is a function of the inverse squared of the distance between them, Coulomb found it to be same between two charges! Then, while still an undergrad at Cambridge, William Thompson discovered that the equations for the strength and direction of the electrostatic force and those describing rate and direction of the steady flow of heat through a solid material were sharing the same mathematical form [69]. Similarly, the equivalent circuits in Micro Electro Mechanical Systems (MEMS) is another example where the mechanical system can be modeled by creating and solving an equivalent electrical circuit, and vice versa. The mass in the mechanical system is represented by an inductance in the electrical equivalent circuit, mechanical damping is represented by electrical resistance, mechanical force is represented by voltage, and so forth [70]. Therefore, some scientists are now trying to learn lessons from nature to invent new technologies inspired by biology. This is known as *Biomimetics* or *Biomimicry* [71] where scientists and engineers are borrowing from nature some clues to solve technical and scientific problems. The

photonic crystals could have been discovered via biomimetics since it already existed in nature as will be seen below. Pushing the light-matter similarities should follow suit: *photonomimics*².

1.2.1 Photonic Crystals and Photonic Bandgap

Photonic crystals are commonly found in nature. All three types of photonic crystals are found in nature: 1D, 2D, and 3D. An example of which is the 3D photonic crystal found in some beetles which is of a diamond like crystal shape [72]. See Figure 62.

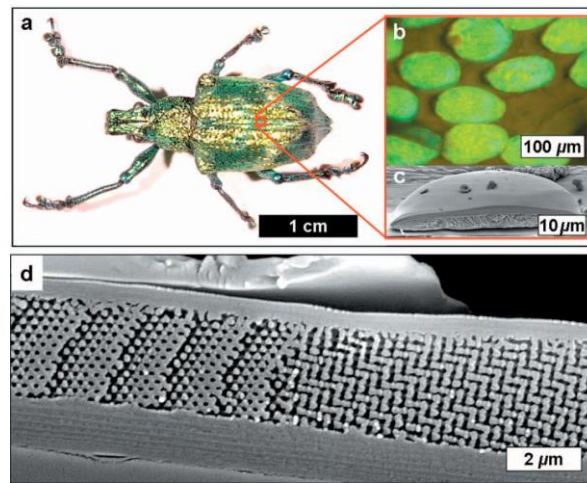


Figure 62: a) Photograph of the beetle. b) Optical micrograph of few scales. c) Cross section SEM image of a single scale. d) Higher magnification of SEM image of a region of a scale. Used with permission from [72].

The photonic bandgap can also be synthetic via fabricating a photonic crystal: a periodic structure of two alternating materials with sufficient refractive index contrast. It could be a one-dimensional bandgap (induced from structures that varies along one direction), two dimensional (induced by 2D structures), and a three-dimensional bandgap (induced by 3D structures) as shown in Figure

² For example, similar to the electronic solenoid, we can ask if it is possible to make an optical solenoid into a generator of some sort where something will be generated in its core like some form of matter!

63.

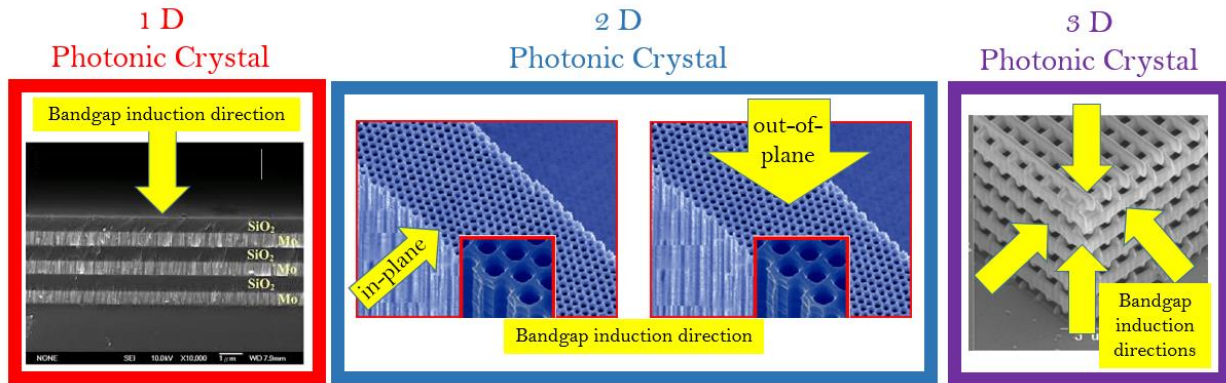


Figure 63: 1D PBG crystal [73], 2D PBG crystal [74], and 3D PBG crystal [75], respectively. Modified and reused with permission from [74] and Fair Use Doctrine.

For 1D photonic bandgap, an infinitesimal refractive index (n) contrast is sufficient to induce a bandgap [65]. However, for 2D and 3D cases, a substantially larger index contrast is needed to open up a bandgap. For the HC-PCF, the case is a two-dimensional photonic bandgap and is made of glass and air that satisfy such substantial index contrast: $n_{air} = 1.000293$ & $n_{glass} = 1.458$ [76].

The physical explanation of these low or no transmission intervals (viz. the bandgaps) along the transverse direction of the fiber is a combination of light scattering, reflection and interference phenomena across the multiple dissimilar layers with different thicknesses and/or refractive indices [77]. Such mechanism can be described in the 1D (called Bragg mirror) and 2D case, respectively.

1.2.1.1 The Mechanism of 1D Photonic Bandgap: Bragg Reflection

The Bragg mirror is composed of two alternating layers of dissimilar materials with different refractive indices, which is essentially a one-dimensional photonic crystal as shown above. For a

given light wavelength propagating through these layers, there is a specific Bragg layer thickness that will cause destructive interference for forward propagation (no transmission \rightarrow bandgap) but a constructive interference for the backward propagation (hence, reflection) as illustrated in Figure 64. Such wavelength is called resonant wavelength.

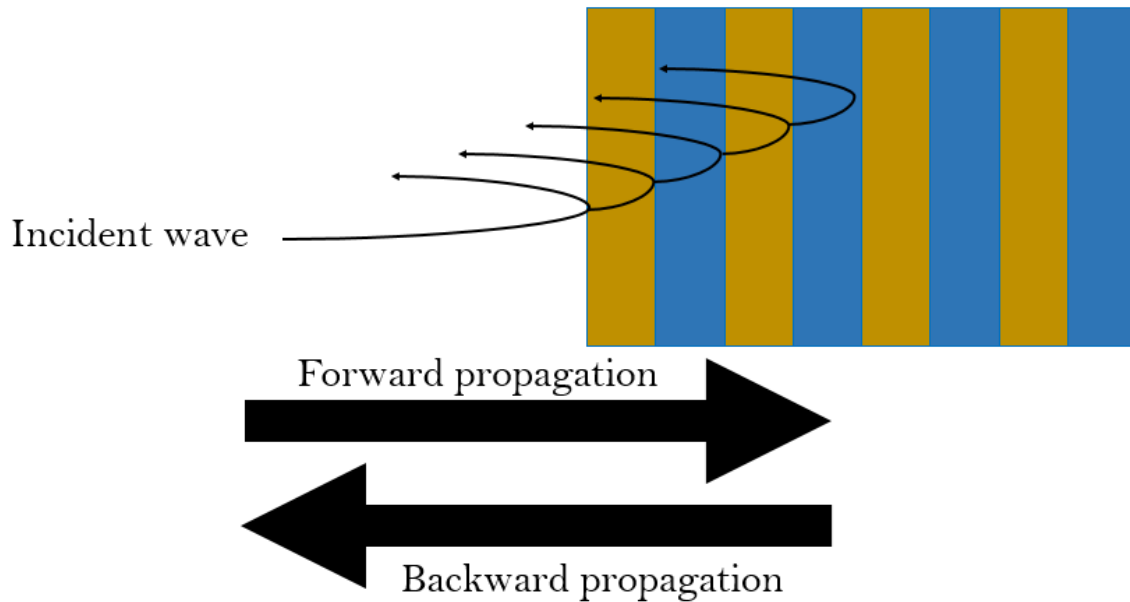


Figure 64: Schematic showing the mechanism of Bragg reflection: no forward propagation, and only backward reflection for the resonant wavelength. The rest of wavelengths will cause both forward and backward propagations.

1.3 Modified Optical Fibers (MOFs)

Optical fibers are just one case of 2D photonic crystals which can be either planar/slab shape or fiber shape. The first stage that led to the invention of PCF was when researchers started playing with the structure at the end face of the telecom fiber. The first of which was a work in 1974 by Kaiser and Astle [78] in which they altered the end face of the fiber as shown in Figure 65.

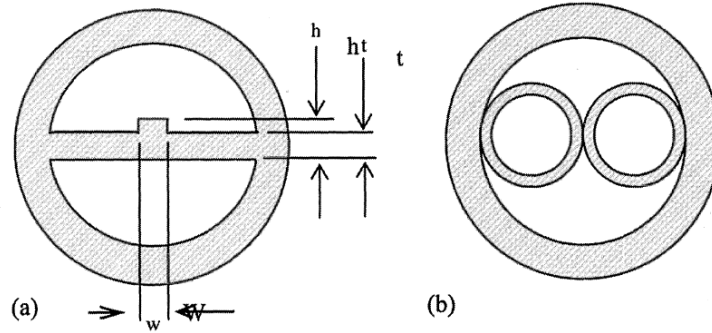


Figure 65: The first two proposed MOF as shown in [77] which were slightly modified from [78]. Used with permission from [78].

Much later (1996), Knight et al [48] made a crystal shaped hole pattern in the cladding. Though it is a crystal-like shape, it is not a photonic crystal fiber. The reason why is because it guides light by modified total internal reflection (TIR) and the structure does not induce a photonic bandgap. So, for a crystal shaped hole pattern in a fiber to be called a photonic crystal, it should induce a photonic bandgap. In 1998, Broeng et al [79] *numerically* proved the possibility of photonic bandgap guidance in MOF which was *experimentally* produced by Knight et al [80] and Broeng et al [81] at the same year (1998). This, however, was solid core PCF. The first HC-PCF was fabricated by Cregan et al [82] in 1999, then further investigated *analytically* by Broeng et al [83] and Naumov and Zheltikov [84].

The first HC-PCF is shown in Figure 66 which was first named “air guiding” fiber.

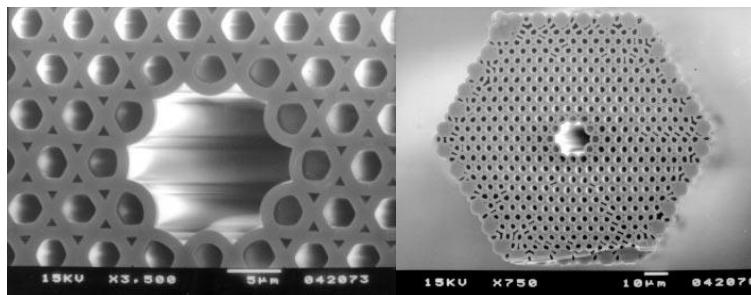


Figure 66: The first HC-PCF demonstrated experimentally [82]. No reuse permission was required from [82].

Figure 67 shows different kinds of MOF and how they relate to other kinds of fibers.

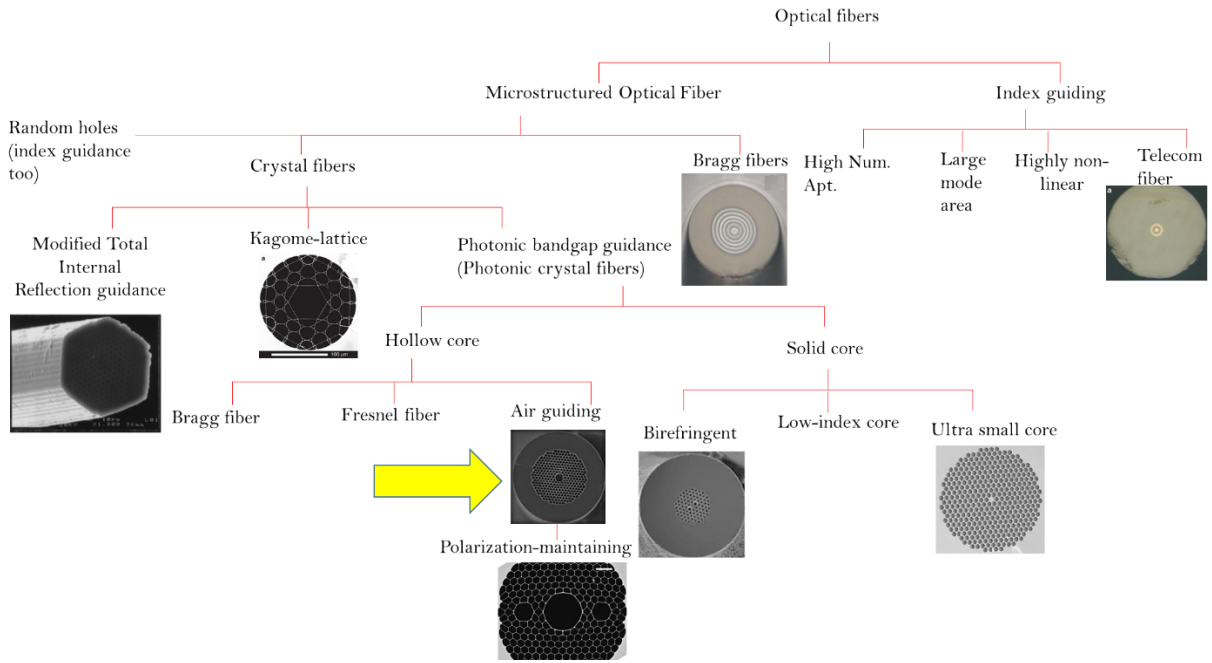


Figure 67: A tree showing different kinds of fibers and how it relates to HC-PCF.

1.3.1 The Bandgap Mechanism of 2D Photonic Crystal Fiber

Similar to the 1D crystal, the 2D crystal around the fiber core will block certain light frequencies propagating transversely; hence, will result in confining light longitudinally inside the core. Figure 68 illustrates such guidance mechanism.

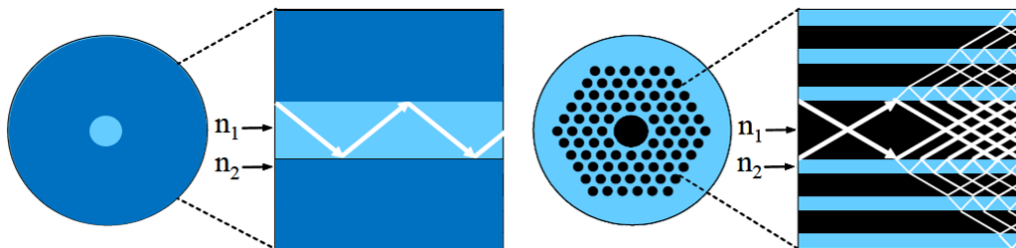


Figure 68: Guidance by TIR between two glasses with different refractive indices (left). Guidance by TIR coupled with PBG caused by transversely destructive interference of certain light frequencies, allowing light to confine and propagate

longitudinally along the core. Note that the core here is shown as hollow, though the same mechanism applies for solid core also (right). Adopted and modified with permission from [85].

An example of such induced 2D bandgap diagram is shown Figure 69.

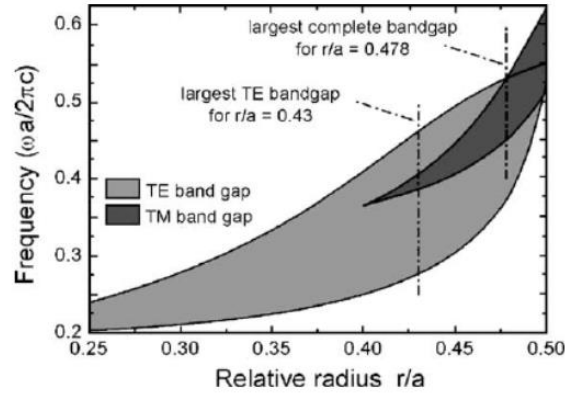


Figure 69: The band diagram of the out of plane light propagation into a 2D photonic crystal fiber (PCF) showing the bandgaps. Used with permission from [86].

For our project, the choice of the best fiber means the choice of the best hollow core size which can be difficult: choosing large core size is motivated by the need to reduce atom-wall collisions [87] while choosing smaller core is motivated by the need to increase light-matter interaction. For our experiment, our choice was the commercially available HC-800-02 NKT Photonics (already shown in Figure 61). This particular fiber was chosen because it can guide wavelengths that correspond to transitions of alkali atoms (e.g. rubidium and cesium) whose vapors are commonly used to study the non-linearities and quantum optics of low light levels. Moreover, lasers were shown to be able to hold cesium atoms (largest known atom of diameter of 0.53 nm [88]) in place in a five-by-five grid as a part of a neutral-atom quantum-computer prototype [89] as shown in Figure 70. Cesium overall proves to be good information carrier in optical traps at the single atom level [90].

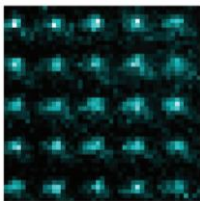


Figure 70: Five-by-Five grid for a neutral cesium atom-based quantum-computer prototype built at Penn State University. Used with permission from [89].

The specification of such fiber is listed in Table 9 below.

Table 9: Physical and optical properties of the hollow core fiber we are using [52].

Physical properties	
Core diameter	$7.5 \pm 1 \mu\text{m}$
Cladding pitch	$2.3 \pm 0.1 \mu\text{m}$
Diameter of PCF region	$45 \pm 5 \mu\text{m}$
Cladding diameter	$130 \pm 5 \mu\text{m}$
Coating diameter	$220 \pm 50 \mu\text{m}$
Coating material	Single layer acrylate
Optical properties	
Design wavelength	800 nm
Attenuation @ 820 nm	< 250 dB/km
Typical GVD @ 820 nm	100 ps/nm/km
Operating wavelength (over which the attenuation is < 250 dB/km)	770-870 nm
Mode field diameter @ 850 nm (full $1/e^2$ width of the near field intensity distribution)	$5.5 \pm 1 \mu\text{m}$

The typical near field intensity profile for the fiber is shown in Figure 71. Note that majority of the field highest intensity is centered within the core that is of $7.5 \pm 1 \mu\text{m}$ diameter, which indicates light confinement to the core.

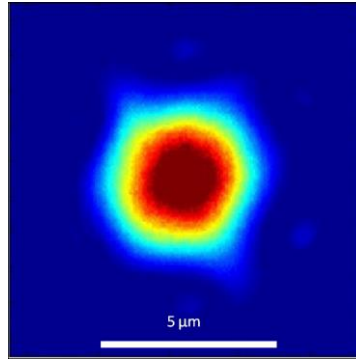


Figure 71: Near field intensity profile at the core of the HC-PCF with $7.5 \pm 1 \mu\text{m}$ hollow core diameter. Used with permission from [52].

1.3.2 Fabrication of HC-PCF

The fabrication process of the HC-PCF is a true visualization of top-down fabrication method, yet in a very simple straight forward way. The process is illustrated in Figure 72.

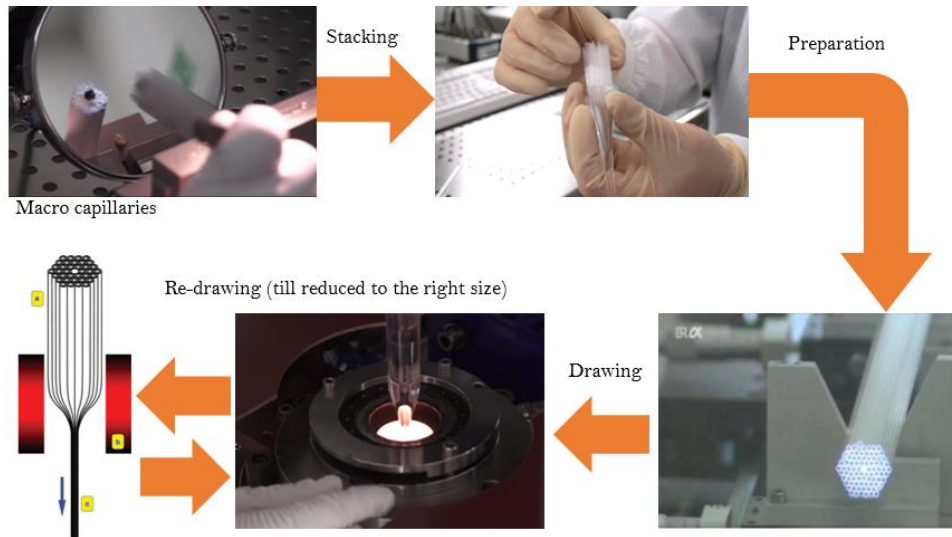


Figure 72: Fabrication process of HC-PCF. Compiled from references. Figure composed from [91] and [92]. Used with permission from [91] (no permission was required from [92]).

Macro-sized capillaries are first assembled in the way that the PCF is supposed to look like. After that the capillary stack will be tightened together into a glass cone, then drawn inside a drawing furnace into thinner/smaller dimensions. The drawing process will be repeated until reaching the desired photonic crystal dimensions (while preserving the original capillaries structural order). The drawing temperature is always above 150 °C [93] in a clean room environment. Different fibers have different drawing parameters, an example of such can be found in Ghosh et al [94].

Chapter 2: Experimental

2.1 Inscribing 1D PC into 2D PC

One of the main contributions of this project is to merge the aforementioned 1D PC (Bragg mirror) into the hollow core of the 2D PCF (HC-PCF). This can be done by inscribing the Bragg mirror inside the fiber's hollow core as can be visualized in Figure 73. The alternating strips constitute the Bragg reflective mirror.

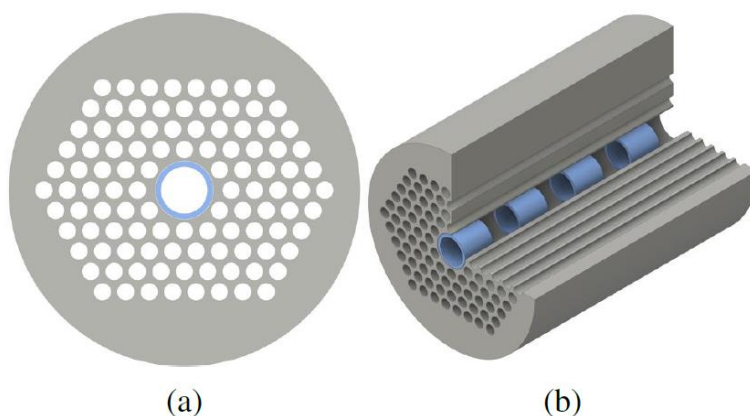


Figure 73: The FBG as should look inside the hollow core from front (a) and cross sectional (b) views (not to scale). The image was co-published by the student in [95] and no reuse permission was required.

Therefore, when the light propagates through the hollow core, only the tails of the beam will interact with the Bragg mirror, and the majority of the beam will not interact with the mirror; instead, with the cesium atoms as shown in Figure 74. For the fiber used for this project, only less than 5% of the optical power of the guided light is located in the silica: the rest of the light power lay within the core [52].

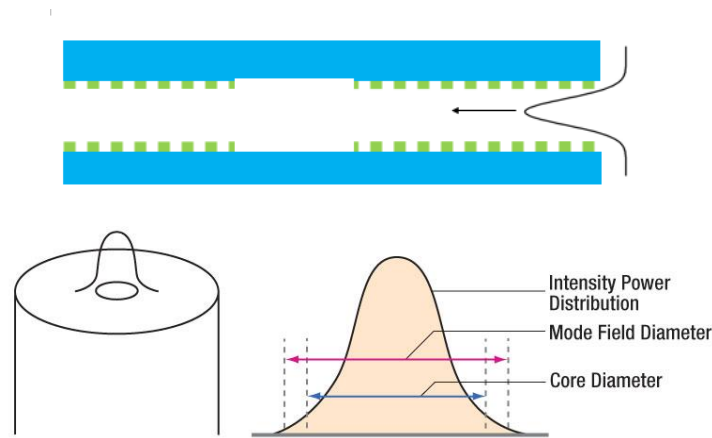


Figure 74: Schematic showing the small portion of the propagating light that interacts with the grating (top). The light mode field diameter compared to the fiber core's diameter (bottom). Bottom image was reused with permission from [96].

Here, with such setup, the light will propagate back and forth caused by the Bragg mirror back and forth reflections. This is part of what is known as dispersion engineering. The dispersion relation in the modulated section of the waveguide is designed such that at the wavelength of interest the group velocity v_g becomes significantly less than the speed of light c , before it gets totally reflected. This lower light speed will increase the time of interaction, in addition to the multiple passes the Bragg mirror will cause. So, instead of two-mirror cavity, the Bragg mirror inscribed at the fiber core will do the two aforementioned functions:

- 1- slowing light (viz. more interaction time).
- 2- bouncing it back and forth (viz. more interaction chances).

However, since the light beam is not totally interacting with the Bragg mirror, the length of the mirror needed to cause 100% a reflection will be longer than those needed for *regular* 1D Bragg mirror that is perpendicular to the beam. This will affect the confinement of light to a smaller space, a confinement needed to have more chance for the light to interact with the atom(s). A way around this large modal volume associated with thin mirrors is to increase the refractive index

difference between the two alternating layers (composing the Bragg mirror). The greater the refractive index difference between the materials of the layers, the fewer layers will be needed to cause 100% reflection. See Figure 75.

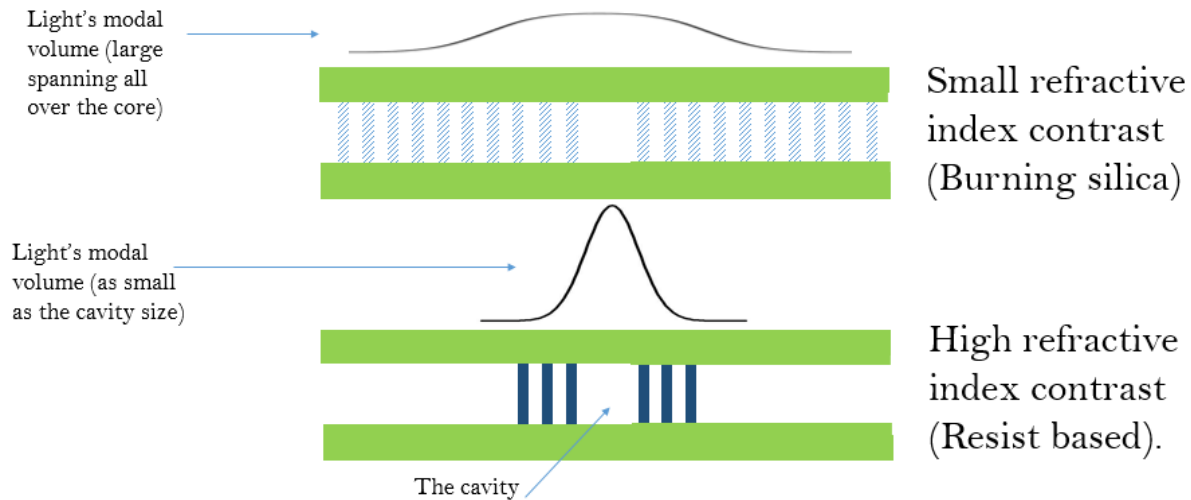


Figure 75: For the same amount of light incident into both cavities (top and bottom) and a given reflectivity, the lower index contrast mirror (top) requires more layers to achieve the given reflectivity; hence, longer penetration depth which in turn distributes the light volume over larger area as seen by the intensity distribution curve above. The higher index contrast mirror (bottom) requires less layers; hence, shorter penetration depth which in turn allows for a tighter confinement of the light in the cavity and can thus lead to stronger light-matter interactions.

Looking at current ways to induce Bragg mirrors in solid core fibers, the index contrast is about 10^{-4} [97] which is very small (hence requires longer mirrors). Such small contrast/difference is due to the fact that the fabrication process of such gratings is done by modulating the refractive index of the glass itself (the fiber material) using a laser interference pattern in which the high intensity bright fringes will “burn” the corresponding fiber fringes. This will in turn make the burnt strips have slightly different refractive index than the fiber fringes/strips that have not been exposed or “burnt” (since they reside at the dark fringes of the laser interference pattern). Bragg grating formation is, however, more challenging for a hollow-core waveguide, as the core is empty and,

furthermore, the waveguide is designed with an effort to minimize the overlap between the propagating light and the material of the cladding. The only part that could be modulated to interact with the propagating light is the walls of the hollow core: this will further reduce the index contrast modulation which is already small for solid cores (10^{-4}).

2.1.1 The Proposed Platform

Therefore, we propose an alternative way to make a higher index contrast fiber core mirror by having alternating layers of two different materials attached to the wall of the fiber (instead of modulating the hollow core glass surface). Due to the extremely small size of the fiber core (around 10 microns), the selection of materials that can be introduced to form the layers (and hence increase the contrast) is limited. For these reasons, it was perceived in the literature that introducing any kind of material to these small cores is technologically difficult [98]. However, we are reporting here a method in which only one material can be introduced into the core yet producing two alternating layers with dissimilar refractive indices while keeping the hollow core hollow (not block it).

The method is as follows: injecting a photoresist liquid into the core of the fiber, then blow filtered purified Nitrogen gas after. The photoresist will not be blown out completely: a thin layer will stick to the wall of the hollow core. After that the fiber will be exposed to a UV laser interference pattern (alternating bright and dark fringes). Such interference patterned will imprint itself into the photoresist layer attached to the wall: the bright strips of the pattern will develop the photoresist while the dark strips will keep the photoresist undeveloped. A compatible developer will then be injected into the core which will remove the developed sections of the photoresist; hence, forming a Bragg grating/mirror with a high index contrast between the fiber glass (absence of PR: material

1) and the photoresist (material 2). We can say that this is an incorporation of 1D photonic crystal (Bragg grating) into 2D photonic crystal (HC-PCF).

Note that the real resist structure will not be like a step function, but a sinusoidally varying function of the resist layer thickness as a result of the interference lithography process. However, it was found to give negligible corrections to the reflectivity value in our simulations as will be shown in a later section. With this structure, light will experience “effective” refractive index modulation which will act as a reflective mirror for the corresponding wavelength as shown in Figure 76.

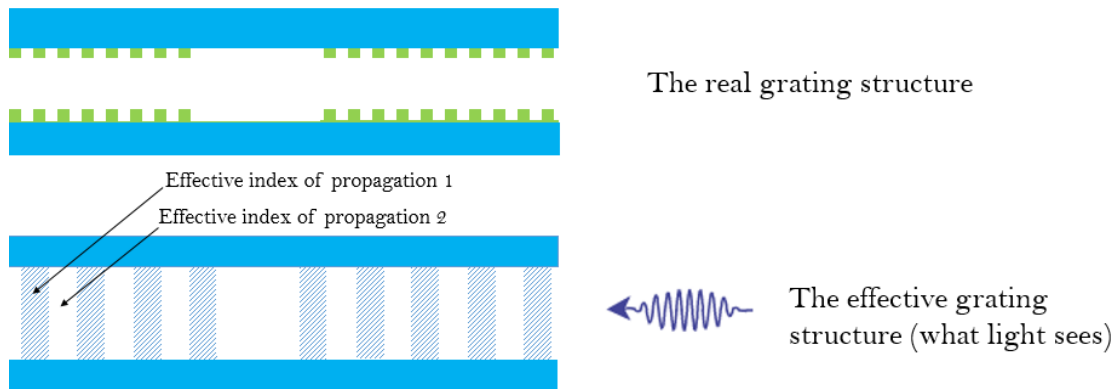


Figure 76: The index modulation as it appears in a cross section of the fiber (top) and the “effective” index modulation as experienced by the propagating light (bottom).

2.2 Experimental Procedures

2.2.1 Blocking the Cladding Photonic Crystal

Here, we want to block out all of the photonic crystal holes and only keep the central hollow core open for resist injection. There are few methods to do so, which are as follows:

- a) *Femtosecond laser drilling [99].*

In this method, the HC-PCF is spliced to a single mode fiber (SMF) which is a solid core one. After that a cap on top of the PCF is created by cleaving the SMF few microns

above the tip of PCF. Next step will be to drill a hole into the middle of the cap, which will cut-it through. This drilled hole will be parallel to the central hollow core of the HC-PCF; hence, a channel will be created from the top of the cap selectively only to the hollow core of HC-PCF. Figure 77 is a schematic of such process.

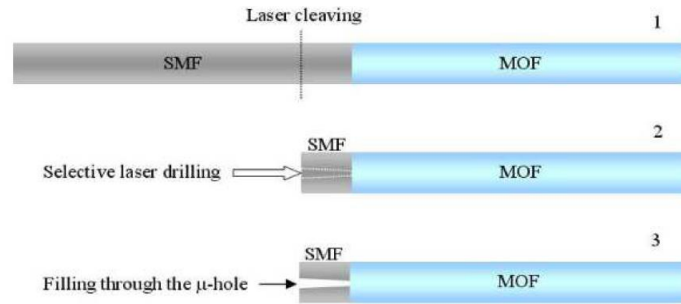


Figure 77: Sequential steps from top to bottom of creating a cap for selective injection using femtosecond laser cleaving. No reuse permission is required from [99].

This method gives a great flexibility of choosing any hole from the photonic crystal holes (not only the central hole), a flexibility that comes with a price of needing high tech expensive apparatus (femtolasers). However, for our project we don't need such flexibility as we are only interested in selecting only the relatively large central hole (hollow core).

b) *UV-assisted cleaving* [100].


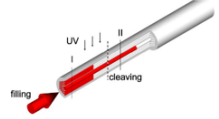
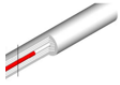
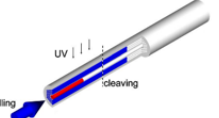
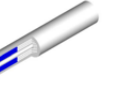
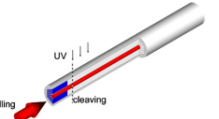
Here, a four-step UV-assisted filling technique can be employed to selectively fill the central hole. It utilizes a property of certain polymers that propagate with different rates depending on different hole diameters. Moreover, they can be solidified by UV exposure once reaching the desired depth.

As the viscosity of the UV curable polymer (e.g. NOA73) is high (130 cps at room temperature), the capillary force is insignificant. Hence, the injection is modeled not as

a capillary flow, but as laminar flow where liquid fills larger holes (i.e. central hole) faster than smaller ones (i.e. photonic crystal holes) [101, 102]. Therefore, the injection must be done by an external pressure applied to a syringe pump.

Table 10 describes the steps done in this process.

Table 10: Different steps of introducing a cap on the fiber end-face by UV glue in preparation for selective injection (modified from [100]).

	Step	Schematics
	<p>The polymer is injected, then UV cured to solidify.</p>	
	<p>Fiber cleaving (from a point that keeps the hollow core filled only). This will create a cap on the hollow core.</p>	
	<p>The polymer is injected again, then UV cured again (to solidify).</p>	
	<p>Fiber cleaving gain (from a point that keeps the small holes filled only). This will create a cap on the photonic crystal.</p>	
	<p>Now the hollow core is ready to be injected with the desired resist.</p>	

This method was firstly tried in this project but turns out to produce highly non-repeatable results with a lot of fiber waste in turn (HC-PCF is expensive).

c) *Lateral access filling* [103, 104].

In this method, a hole is drilled on to the side wall of the fiber and from which the liquid transports to the core. This lateral hole could be drilled either by a fusion splicer and air pressure [103] or by FIB milling [104]. See Figure 78.

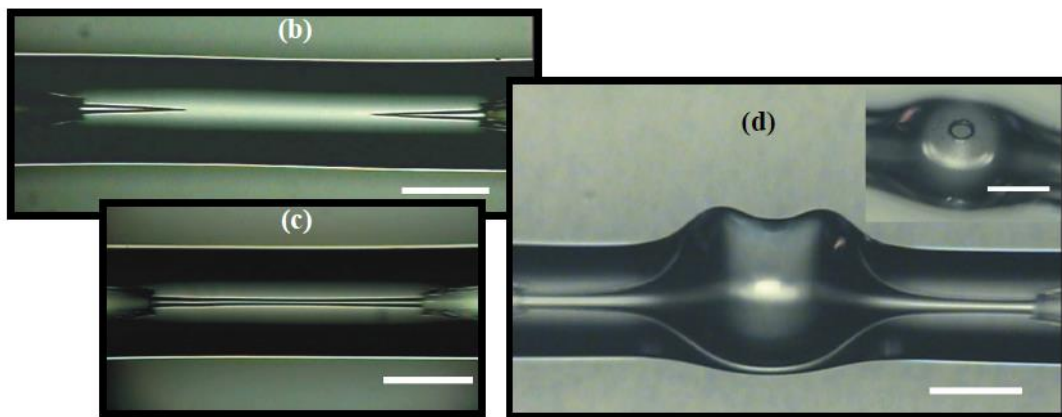


Figure 78: Optical microscope images of the different steps towards opening the lateral hole in the wall of the fiber. No reuse permission was required [103].

Note also that the lateral hole could be drilled by FIB milling [104] as shown in Figure 79.

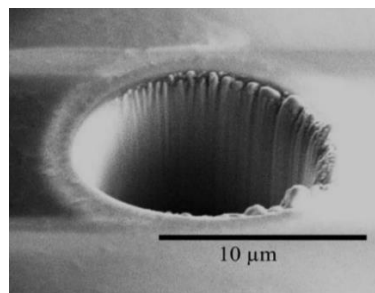


Figure 79: A hole drilled on the fiber side wall by FIB drilling. No reuse permission was required from [105].

The problem with this technique is that an accurate selective filling for one hole only might not be possible due to the difficulty of filling only one hole because other holes might suck the liquid/resist by capillary forces while on its way to the desired hole (the central hollow core in our case).

d) Manual gluing [106, 107]

This method uses a glass tip (under a microscope) to place a drop of a UV glue on the desired holes to be blocked which is then followed by UV curing [107, 108] as shown in Figure 80. Note that with this method, the glass tip size has to vary according to the holes to be blocked; hence, needing more than one glass tip [99]. The main problem with this problem the very long time it requires to individually block the many holes a photonic crystal has.

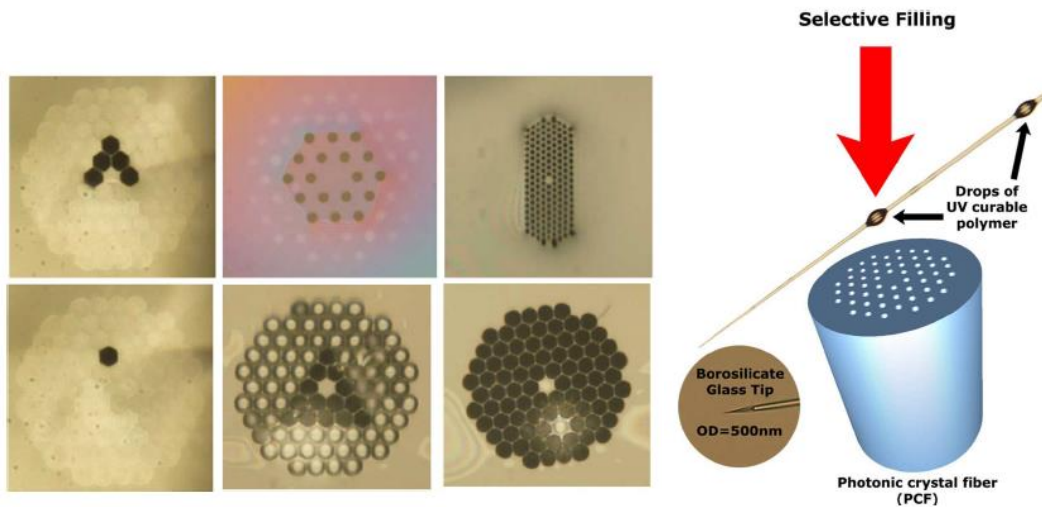


Figure 80: PC-holes manual blocking using a UV-curable glue. Used with permission from [107].

Note also that the glue could be carried by another fiber [106] as shown in Figure 81, which is not as individual as the above tip-based method, but not as accurate.

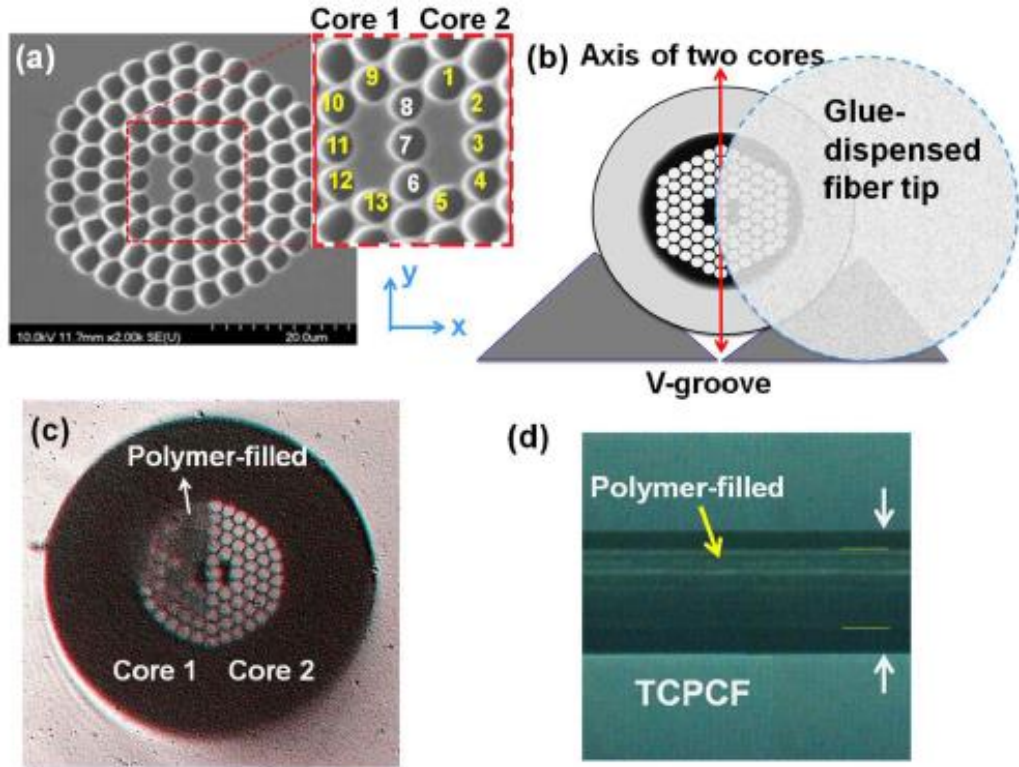


Figure 81: Blocking photonic crystal holes using a glue carried on another fiber. Used with permission from [106].

e) Air-holes collapse [102].

Here, an electric arc of short duration and weak discharge current is used to collapse the cladding small holes while keeping the central hole open. The method is done by bringing single mode fiber (SMF) in close proximity (around 50 micron) to the HC-PCF and then remove the SMF just before the beginning of the arc discharge; hence, the end face of the HC-PCF will not be spliced to the SMF and it will just be heated up causing the collapse the photonic crystal holes depending on the parametric values used [102]. The process is shown in Figure 82.

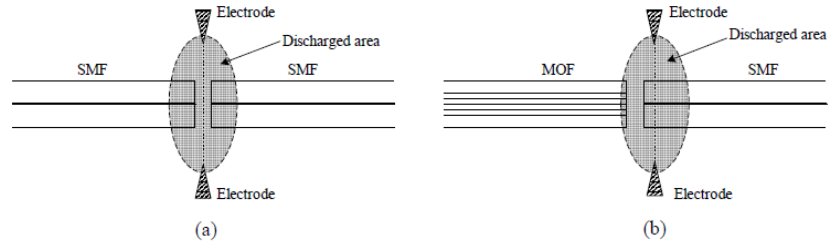


Figure 82: Air holes' collapse by splicing arc-induced heating. No reuse permission is required from [102].

Note that the reason for the central hole not collapsing is that the central hole of the HC-PCF has large air content of the core versus silica; hence, very weak heat transfer take place. This is unlike the HC-PCF cladding holes/rings which have more silica that when heated to above the softening point (around 1670 C°) will causes the surface tension to overcome the viscosity which will cause the HC-PCF's air holes to begin collapsing [102]. It should be mentioned that closer holes to the hollow core collapse less than those farther. Also note that the central hole will not be completely intact: it will experience some shrinkage depending on the current and duration of fusion [102]. Careful choice of parameters is crucial for the desired fusion to happen.

After that the fiber is to be dipped into the desired PR. Figure 83 shows a cleaved cross section of a HC-PCF filled with NOA74.

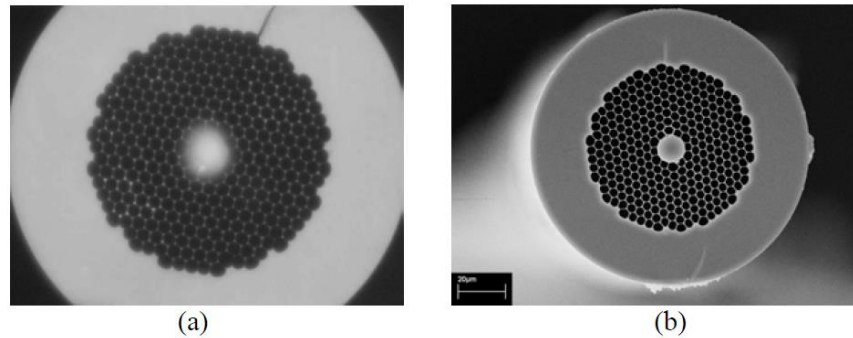


Figure 83: Optical microscope image (a) and SEM image (b) of NOA74-filled central hole PCF. No reuse permission is required from [102].

f) 4.1.7 Capillary splicing [109, 110].

This method is one used in this project. It is the simplest conceptually and instrumentally out of the six methods listed above: a capillary (basically a single-hole fiber) is spliced to the HC-PCF where the capillary hole is placed on top of the hole that needs to be filled: the hollow core [109, 110]. After splicing, the capillary will be cleaved few microns away from the spliced interface [110]. Now the fiber end face is capped with the short-lengthed capillary, and consequently any injection will only go through the central hole (core) selectively. See Figure 84.

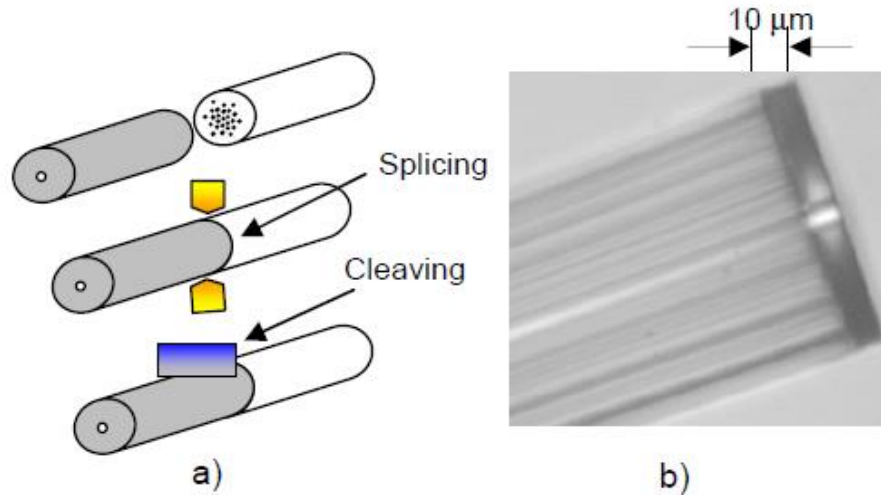


Figure 84: Capillary splicing assisted infiltration. a) The steps to make the infiltration cap. b) optical microscope image of the infiltration cap. Used with permission from author of [110].

This process can be done with a conventional table-top fusion splicer. The splicer used was ORIENTEK T40 model, and the automatic splicing option was disabled, and a manual splicing was done with the splicing parameters shown in Table 11. Note that these parameters were selected after careful try and error.

Table 11: HC-PCF to capillary splicing parameters. Note that the offset is the distance between the arc and the center of the gap between the fibers.

Pre-fusion time	200 ms
Pre-fusion current	8 mA
Fusion time	300 ms
Fusion current	14 mA
Offset	50 μm
Overlap	0 μm
Gap between HC-PCF and capillary tube	50 μm

After mounting the fiber, the fiber-capillary interface could be seen by a magnifying camera as shown in Figure 85.



Figure 85: The splicer screen showing a top view of the HC-PCF & capillary interface (left of the screen) and a side view of the interface (right of the screen).

The spliced joint is shown in Figure 86.

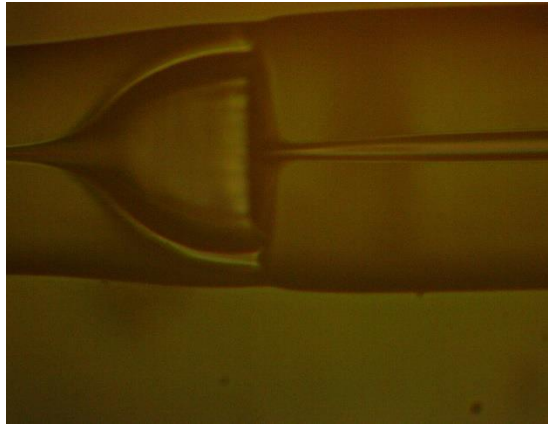
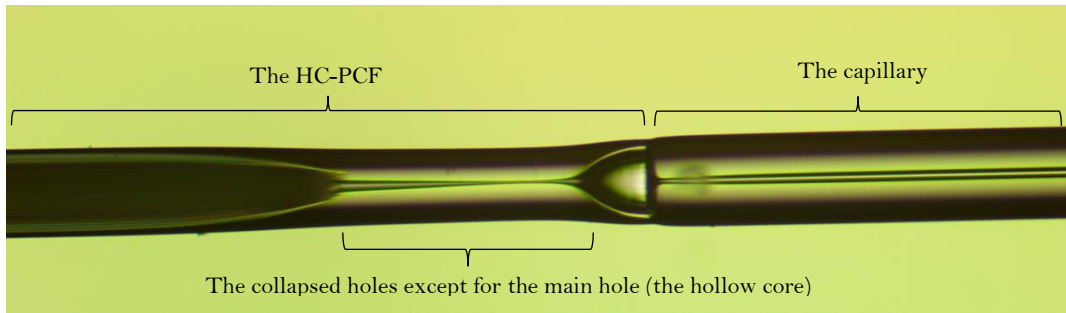


Figure 86: The HC-PCF as spliced to a capillary of the same diameter (top) and a closer image (bottom). Fiber diameter is 120 microns, hole diameter is 7 ± 2 microns. The central hole can still be seen continuous across the cap.

The capillary now has to be cleaved using a cleaver rig (shown in Figure 87).

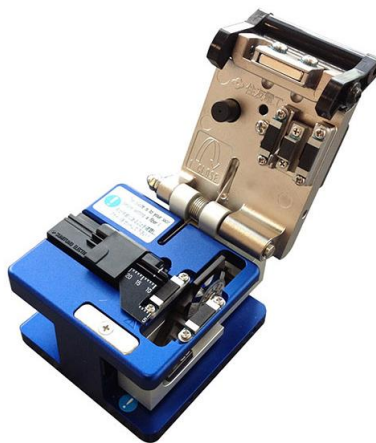


Figure 87: The cleaver used.

First, the V groove fiber holder has to be brush cleaned the with alcohol-soaked cotton in one direction (away from the blade direction). The reason is to remove any small particle that will obstruct the fiber from perfectly laying on the V groove. Then both fibers to be spliced has to be cleaved was cleaned with alcohol-wet kimwipes. The fiber coating was stripped for 10-16 mm. The clamp should close onto the fiber coating, but the part from clamp till the blade should be the bare fiber, as shown in Figure 88.

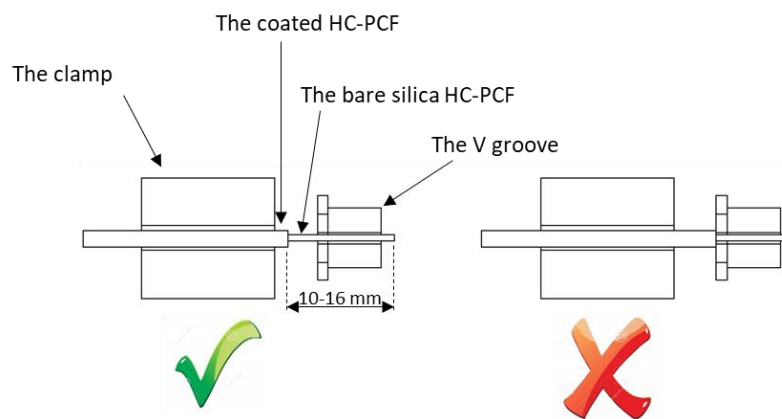


Figure 88: Schematics of the proper HC-PCF loading onto the V groove holder.

Cleaving procedures were as follow:

- 1- Open the cleaver shield.
- 2- Open the clamp
- 3- Clean the V groove as described above.
- 4- Slide the blade carrier out.
- 5- Place the *prepared* fiber on the proper groove (250 or 900 grooves).
- 6- Close the fiber clamp.
- 7- Close the cleaver shield.
- 8- Gently slide the blade carrier back into the cleaver body.
- 9- Pull the fiber out.

10- Dispose the scrap end finally.

11- Always close the cleaver shield when you are done (to prevent dust particles accumulation).

After cleaving the capillary, and leaving only some part of it as a face cap to the HC-PCF, the capped HC-PCF was illuminated and indeed light was blocked by the cap except at the hollow core as shown in Figure 89.

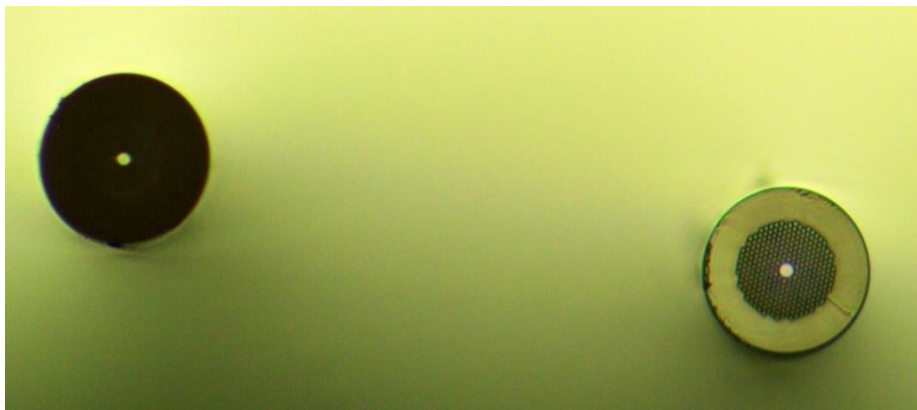


Figure 89: The capped HC-PCF (left) and the bare HC-PCF (right). The cap successfully blocked fiber outgoing light except at the hollow core, as intended.

2.2.2 Resist Injection

The fiber at this stage is capped and should be ready for injection. The injection can take place by one of the following methods:

a) Drop held on Single Mode Fiber.

The first method is to hold a drop on the top of Single Mode Fiber (SMF) and bring it close to the fiber end face so the drop gets absorbed by the hollow core through capillary force as shown in Figure 90. The problem with this method is that it applies only to liquids/photoresists thin enough to be acted upon by capillary forces; otherwise, syringe-

assisted method must be applied instead to force high viscosity liquids inside the hole(s). Also, this method cannot be used to inject air into the core (to flush out photoresist).

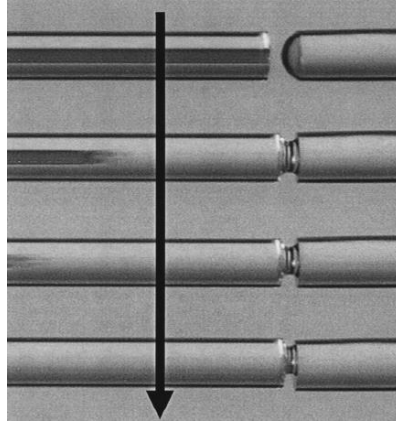


Figure 90: SMF-based fluid delivery system. Used with permission from [111].

b) Syringe.

A syringe filled with the photoresist is used to inject the resist into the photonic crystal fiber using a syringe pump. An epoxy is used to glue and seal the PCF to the syringe needle as shown in Figure 91.

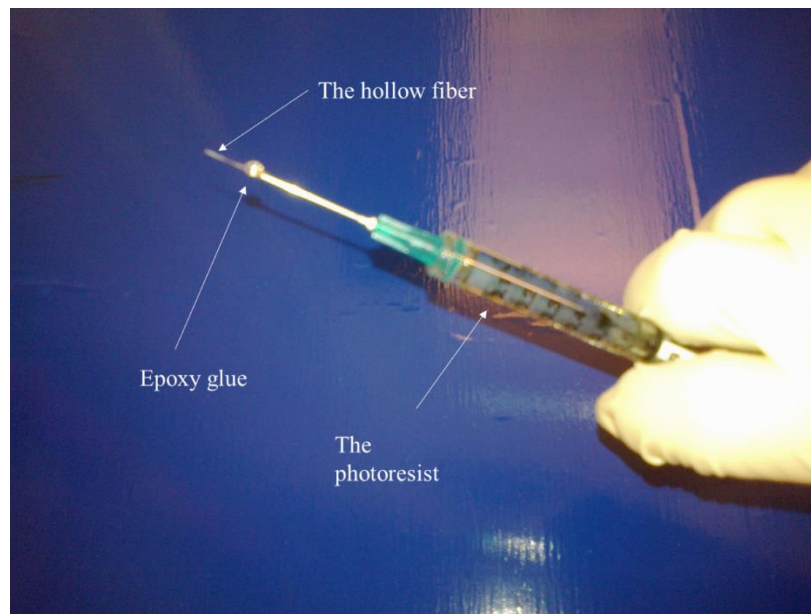


Figure 91: Injection of photoresist inside the fiber hollow core using an epoxy-sealed syringe.

The problem with this method is the loss of fiber after each consecutive injection (to break the epoxy seal) which is not the best economical choice given the high price of the fiber used.

c) *Custom-Made Injection Port*

For the above reasons, we have designed and assembled an injection port that is based on vacuum technology in which the photoresist is inserted from one side of the port, then a nitrogen gas flow from another side pushes/injects the resist into the fiber. Once injected, further blowing of nitrogen gas is expected to spit out the resist. A schematic of the setup is shown in Figure 92.

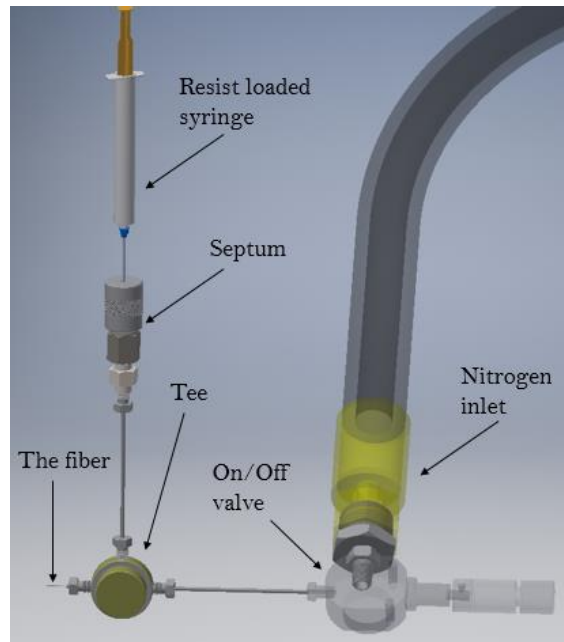


Figure 92: Schematic of the designed injection port.

Different design parts were bought from Valco, Swagelok and ThorLabs companies and were assembled as shown in Figure 93.

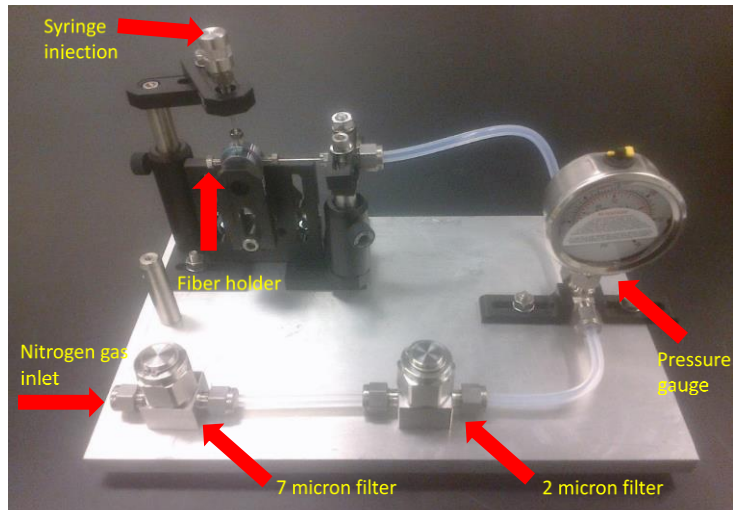


Figure 93: The injection port we designed and assembled.

Instead of sealing the fiber to the syringe by epoxy (causing fiber loss), the HC-PCF is sealed by the vacuum seal shown in Figure 93 (the fiber holder). Note that the photoresist gets injected from the top of the injection port, then gets pushed by the incoming nitrogen gas into the fiber core. After injecting and blowing out the photoresist using the injection port above, a successful SU-8 photoresist inner layer was formed as can be seen in Figure 94. SU-8 photoresist was used as a proof of concept, where if successful the desired photoresist will be bought (AZ-701 photoresists).

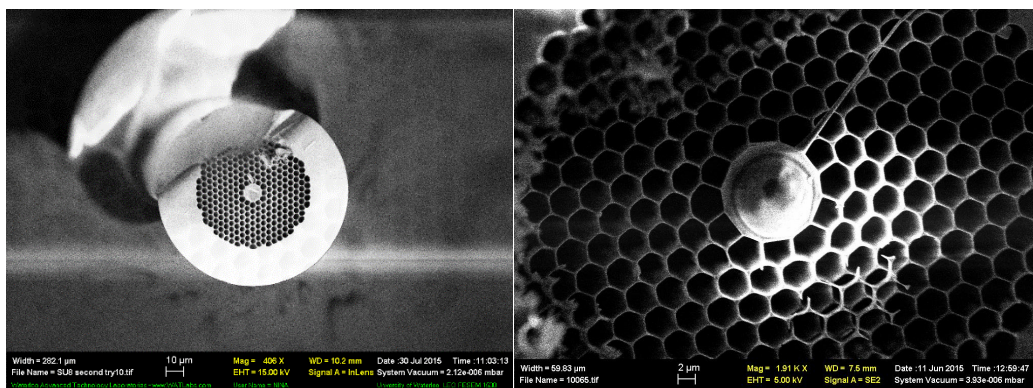


Figure 94: SEM image of the SU-8 fully blocked core (left) and the post nitrogen blow ring formed by the high viscosity SU-8 photoresist (right).

2.2.3 Laser Interference Pattern Inscription

Now after the hollow core has been selectively filled with the resist, the fiber will be exposed to a UV laser interference pattern to imprint the interference fringes on the photoresist-coated hollow core. Generally speaking, there are four ways of writing Fiber Bragg Grating (FBG) with or without resist:

a) *Direct ablation/burning (also called point by point) [112].*

Bragg grating in HC-PCF has been done using this method but as long period grating (LPG) (few micron) by Iadicicco et al [113]. This was done by periodically burning the fiber using arc discharge while moving the fiber using a micro-stepper as shown in Figure 95.

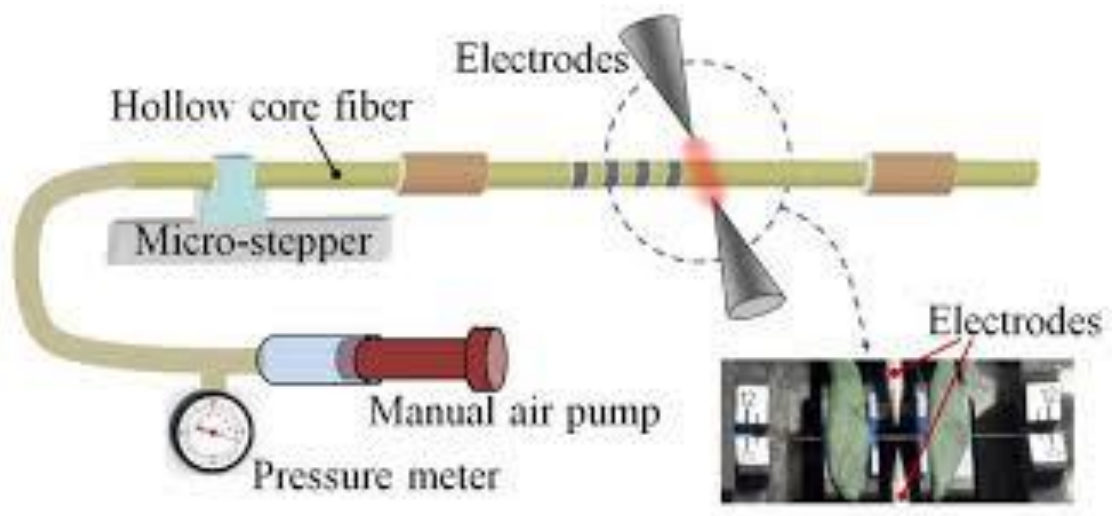


Figure 95: Long Period Grating made into HC-PCF by splicing arc, air pump, and a micro-stepper. The air pump is used to prevent hole's collapse by the arc partially maintaining the hollow structure. Used with permission from [114].

There are few issues with such method. First, it is LPG, which induces only higher order bandgaps; hence, cannot have smaller mode volume. Second, it modifies the cladding due to

the air pressure [114]; hence, perturb the photonic crystal structure which in turn affects its designed bandgap properties which means light leakage.

b) Interferometer-mask coupling [115].

Here, the laser beam goes through a hard mask followed by the regular two mirrors of an interferometer as shown in Figure 96. The Bragg wavelength is controlled either by adjusting the spacing length between diffraction slits or adjusting the wavelength of the writing source. The problem with this method is that it requires both highly technically sophisticated apparatus in addition to an expensive custom-made hard mask.

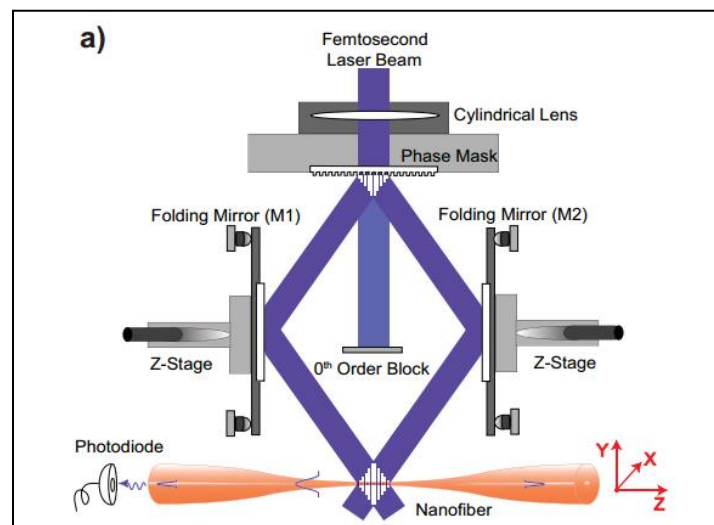


Figure 96: Mirror inscription into the nanofiber by both a phase mask and an interferometer (dual beam interferometer here).

No reuse permission is required from [116].

c) Bare phase mask [117].

This method uses only a phase mask that is brought to a close proximity with the fiber to inscribe the pattern needed (the mirror). The problem again with this technique is the need of a high expensive mask for each interference pattern inscribed.

d) *Bare interferometer* [118, 119].

Here an interferometer is used to inscribe the pattern. In interferometer-based writing, the Bragg wavelength is controlled either by adjusting the angle of intersection between the two writing beams or adjusting the wavelength of the writing source (the laser).

Note that in all of these methods above, the grating could be written by a single shot [115, 120], multi-pulses, or continues wave.

The best method in terms of simplicity is the point by point. In terms of stability and repeatability, the phase mask technique is the best as it is less sensitive to environmental disturbances and also produces gratings with highly repeatable characteristics [115]. Flexibility wise, **interferometer**-based writing is the most flexible [115].

Among these methods, we have chosen the bare interferometer method which can be manifested instrumentally through two setups: Lloyd Interferometer (for high resolution), and Dual Beam Interferometer (for large areas) [121]. The reason we chose the Interferometer option is because it gives the most accurate and flexible outputs [115], and in particular, Lloyd Interferometer offers also a more feasible option economically, which in turn made it our choice. Figure 97 is a schematic illustrating the working concept of Lloyd Interferometer.

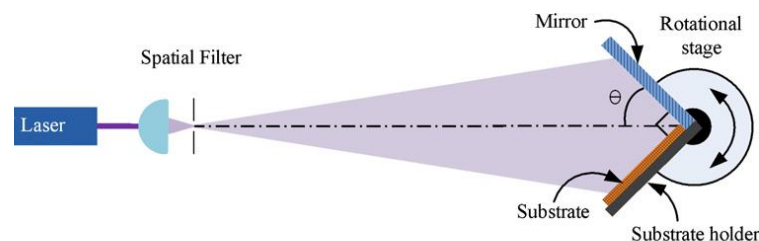


Figure 97: A schematic showing the full light beam where the lower half of the beam is directly projected onto the substrate, while the upper half reaches the substrate reflected from the mirror; hence forming the interference pattern when interfering with the directly projected light. Used with permission from [122].

The Lloyd Interferometer has been assembled in a rotatable mirror and fiber holder. See Figure 98. Note that the interferometer is enclosed in a box to minimize airflow avoiding optical path differences [121].



Figure 98: The assembled Lloyd Interferometer. The holder on the right is covered with partially sticking tape for easier loading and unloading of samples (the setup is enclosed in a box to minimize airflow avoiding optical path differences).

2.2.4 Bragg Grating Material and Parameters

The interference pattern employing such Lloyd interferometer was first tried on a silicon wafer coated with photoresist. The reason why is that we can easily optimize/tune and characterize the different parameters so once we get the desired grating period on the wafer then same parameters can be applied to the fiber. The laser used to inscribe the pattern is a diode laser of of 405 nm. Note that the best lasers for inscribing gratings are the gas lasers such as He-Ne [123] or He-Cd due to their long coherence length. The problem is that such lasers are expensive. However, we don't need large grating areas: we need a grating length of about 100 μm as shown by the simulations

(will be discussed in details later). Hence, the diode laser serves the purpose economically and practically. Careful choice of proper parameters combination is vital for imprinting the grating onto the wafer and subsequently onto the fibre hollow core photoresist layer.

As per the selection of the proper photoresist, we have chosen AZ 1512. According to *Integrated Micro Materials Inc.*, one of the largest photoresist distributors in North America, this photoresist is the best in terms of adherence to silica glass. It also has an absorption spectrum from 365-450nm, which includes the wavelength of our diode laser (405 nm). The coated film thickness range it gives is from 1-2 microns [124].

Now the grating period, g , must be identified. It can be tuned as a function of the stage rotation angle as in the following equation

$$g_{Lloyd} = \frac{\lambda_{Lloyd}}{2 \sin\theta} \text{ (m)}$$

(40)

where λ_{Lloyd} is the laser wavelength (405 nm) and θ is the stage rotation angle (the angle between incident laser's beam axis and the mirror axis [125]), which are shown in Figure 99.

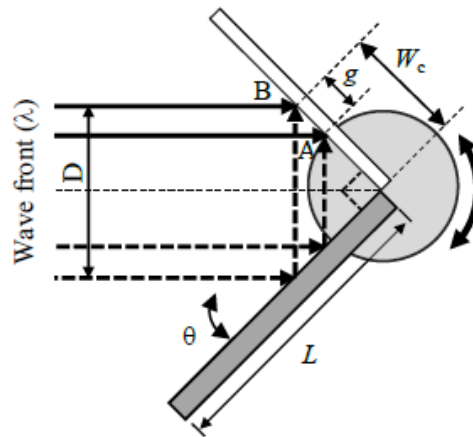


Figure 99: Parameters for Lloyd interference lithography. Used with permission from [125].

The period in the Lloyd interferometry must match the Bragg period for the corresponding resonant light we are interested in: 852nm (which corresponds to the atomic transition of Cs atom from S to P). Note that the laser used in Cs atoms trapping is different that the diode laser used to inscribe the grating. Such Bragg period is given by

$$g_{Bragg} = \frac{\lambda_{Bragg}}{4 n_{eff}} \text{ (m)} \quad (41)$$

where λ_{Bragg} is the wavelength of the incident laser in the cavity (852 nm) and n_{eff} is the effective refractive index of Bragg period, which was found by using a commercially available software, *Lumerical*, which equals to 0.992 for 700nm resist film thickness of 1.61 photoresist refractive index (numerical simulations will be discussed in a later chapter). Now equating the Bragg condition period length (equation (40)) to that of Lloyd condition (equation (41)) gives the angle at which the rotation stage should be rotated.

$$g_{Bragg} = \frac{\lambda_{Bragg}}{4 n_{eff}} = \frac{852}{4*0.992} = 214.7nm = \frac{405}{2 \sin\theta} \text{ (m)}$$

Now, equating g_{Bragg} with g_{Lloyd} results in

$$g_{Bragg} = g_{Lloyd}$$

$$214.7nm = \frac{405}{2 \sin\theta}$$

Solving for θ , the Lloyd stage rotation angle becomes 70.58 degrees giving a resultant grating period of 214.7 nm.

Another important parameter is the continuous grating width, W_c , (shown in Figure 99) which is given by the minimum of three values as follows [125]

$$W_c = \min \left\{ 2 \frac{L_c}{\lambda} \cdot g, \frac{D}{2 \cos \theta}, L \cdot \tan \left(\arcsin \frac{\lambda}{2g} \right) \right\} \text{ (m)} \quad (42)$$

where L is the effective mirror length, and L_c is the coherence length of the laser which is 0.68 mm for the 405nm laser diode [76, 125].

As per the beam quality, it is very important to have a clean beam to form the grating. The beam can be cleaned by a special filter. At the beginning of the project, we have tried to use a polarizing maintaining fiber (PM fiber) to act as a spatial filter. In this way, the small diameter of the fiber will act as a filter for the exiting laser beam. However, it was technically difficult to obtain a good coupling of the diode laser into the PM fiber. Therefore, another method of beam cleaning was tried: pinholes as shown in Figure 100.

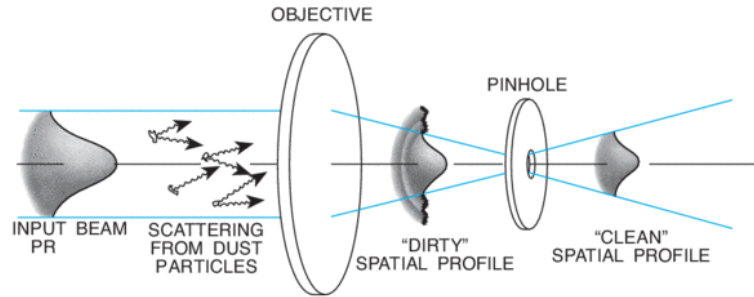


Figure 100: Beam cleanliness enhancement as a result of the pinhole. Used with permission from [126].

The use of a pinhole to clean the beam greatly enhance the value of W_c by enhancing the coherence length, as in Li et al [125] in which the use of a pinhole increased the value of W_c substantially from 1.92 mm to 16 mm. The pinhole diameter can be determined from the following equation [122]

$$d = 8 \frac{\lambda f}{\pi D_i} \text{ (m)} \quad (43)$$

where f is the focal length of the focusing lens, D_i is the incident beam diameter and λ is the incident light's wavelength. For our laser, the pinhole diameter should be roughly around 11.2 microns. The closest commercial pinhole diameters are 10 and 15 microns. Both pinholes were used.

2.2.5 Grating Characterization

Once the laser interference pattern is replicated onto the photoresist film on the core's wall, the developer 300MIF will be injected into the core using the same injection port. The fiber will be ready for characterization to check if the grating was formed.

There are two grating characterization methods:

a) *SEM imaging.*

This can be done by slicing the fiber by FIB to have a cross section of the core that can be SEM imaged. An example of an SEM image of the grating is shown in Figure 101 which is a Bragg mirror but engraved into a solid core fiber.

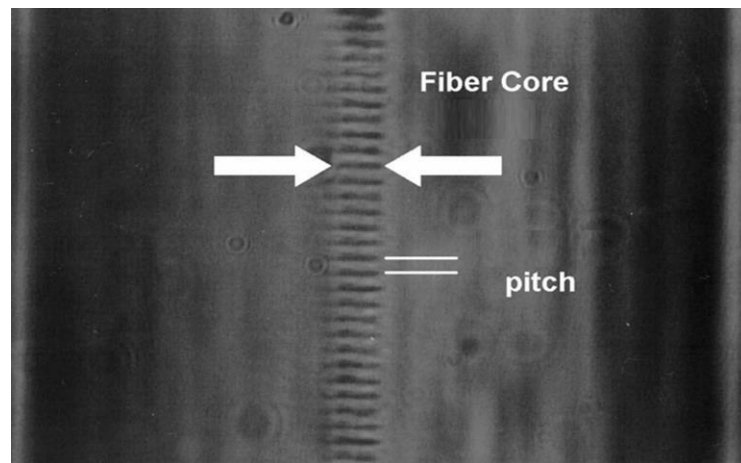


Figure 101: Cross section of a solid core fiber with FBG inscribed on its core. Used and modified from [97]. No reuse permission was required [97].

b) Custom Built Optics Table Setup.

The actual experimental setup should look like the setup shown in Figure 102.

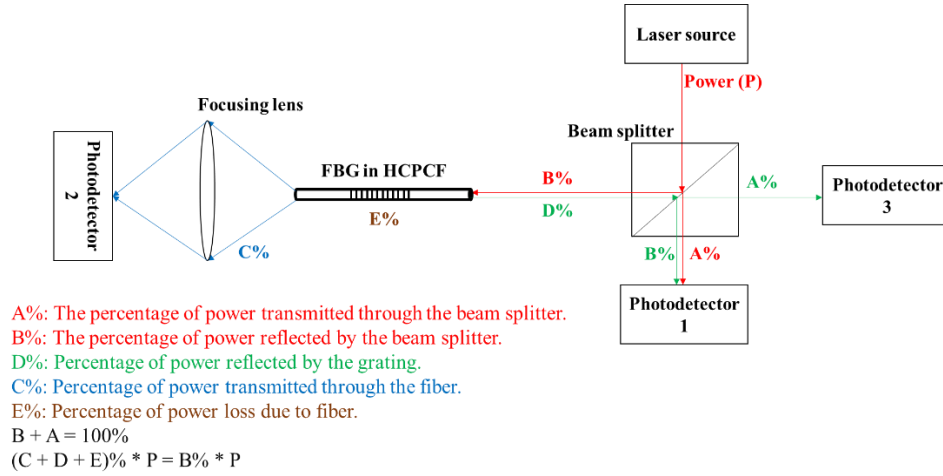


Figure 102: Experimental setup for characterizing the FBG formation showing light power distribution due to transmission, reflection, and refraction due to beam sampler and the fiber.

The ideal case will be if there is zero power detected by the photodetector 2 (PD 2), which means that all of the B% light power was reflected by the FBG. However, experimental and instrumental imperfections (in addition to fiber fabrication imperfections) dictate some non-zero value. Therefore, PD 3 can be used to determine how strong the reflection was: the higher the power detected the stronger the reflection. Note that the transmitted power percentage (A%) and the reflected (B%) are known properties of the beam splitter. The percentage of the power reflected by the FBG could be calculated as follows

$$\% \text{ of power reflected by FBG} = \frac{\text{Power reflected}}{\text{Power in}}$$

which in turns equals to

$$\% \text{ of power reflected by FBG} = \frac{\text{PD 3 reading} + (\text{PD 1 reading} - \text{A}\% * \text{Laser Source Power})}{\text{B}\% * \text{laser power}}$$

where PD stands for Photodetector.

Alternatively, the reflectivity percentage also could be calculated as follows

$$\begin{aligned} \% \text{ of power reflected by FBG} &= 1 - \frac{PD2 \text{ reading} + \text{fiber loss}}{B\% * \text{Laser power}} \\ &= 1 - \frac{PD2 \text{ reading} + E\% * B\% * \text{Laser power}}{B\% * \text{Laser power}} \end{aligned}$$

The exact FBG reflectivity and other properties of the mirror will be modeled in the numerical simulation chapter below.

Chapter 3: Numerical Simulations

We have implemented a fiber model by using the *Lumerical* MODE Solutions software in which the eigenmodes of the field of the structure are solved to find its attenuation coefficient and effective index. The HC-PCF shape was selected to resemble the SEM image of the real fiber as shown in Figure 103.

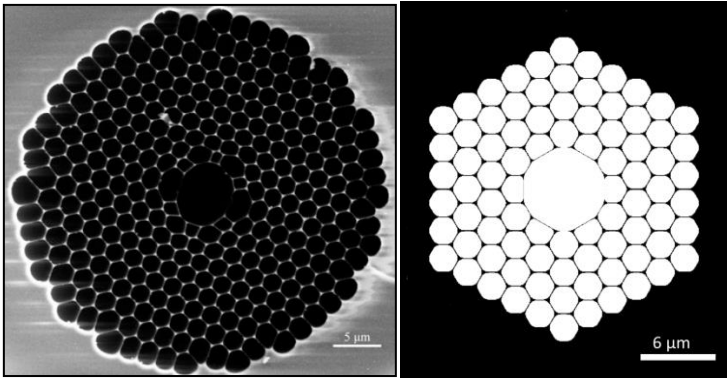


Figure 103: SEM image of the HC-PCF (left) and the imported image to Lumerical (right).

Note that circular holes were tried first (see Figure 104) then replaced with hexagonal holes for better accuracy (in comparison with experimental data).

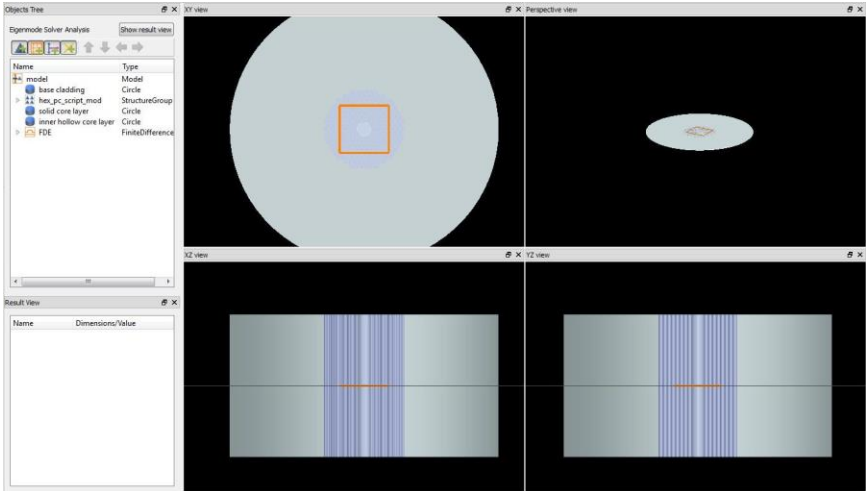


Figure 104: The Lumerical software interface showing the initial model built with circular holes.

The Lumerical MODE Solutions is a finite-difference eigen-mode solver, which works on the eigenmode expansion (EME) method.

The HC-PCF initial parameters fed to the model are shown in Table 12.

Table 12: Fiber dimensions fed to the Lumerical model.

Hollow-Core Diameter	6 μm
Distance between the edge of the hollow core and the surrounding photonic crystal small lattice holes	0.109 μm
Lattice Pitch	2.1 μm
Lattice holes' diameter	2 μm
Gap between lattice holes	0.126 μm
Cladding Diameter	130 μm

Minimum attenuation in such a model occurred at a wavelength of 851 nm and all subsequent simulations for the fiber model are performed at this wavelength unless stated otherwise. This minimum attenuation agrees with the manufacturer's specification sheet which states that the minimum attenuation falls in the interval 770-870 nm as shown in Figure 105.

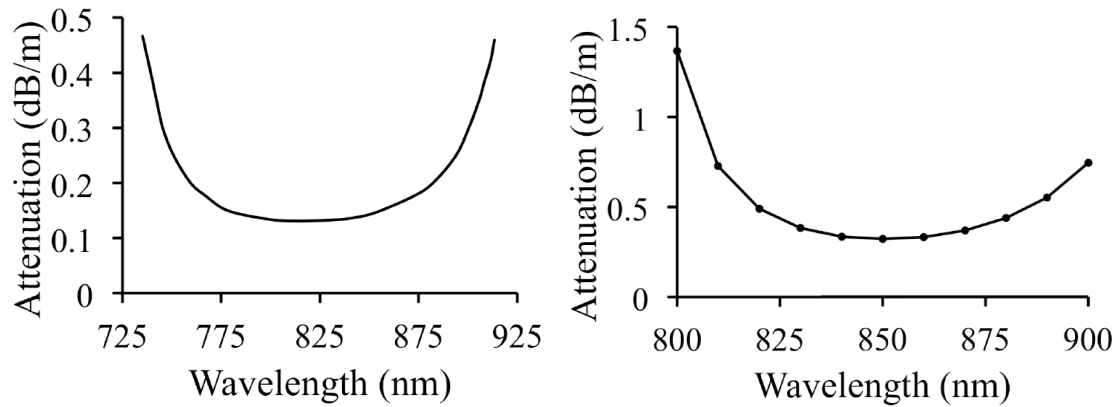


Figure 105: The light attenuation curve as a function of the propagating wavelength into the HC-800-02 HC-PCF as provided by the manufacturer (left) and as simulated by Lumerical (right). Used with permission from [52].

Due to lack of access to high computational resources, note that the simulated minimum loss found is ~ 0.330 dB/m which is not quite exact to the manufacturer's measured value of 0.150 dB/m. This increased loss value in the simulated value is due to the lack of computational resources, which dictates choosing only four rings of holes surrounding the hollow core, while the real fiber has nine of them. Such reduction of number of hole rings will surely reflect on the accuracy of the Bragg mirror reflectivity's simulated value to be found below in comparison to the real value to be measured after fabrication. It is only meant to give some guidance of the mirror's reflectivity and the parameters contributing to its increment or decrement.

3.1 Bragg Mirror Reflectivity

The maximum theoretical reflectivity of an infinite period Bragg mirror/grating at the Bragg condition for the photoresist in the hollow core was found by calculating the reflectivity as a function of the average penetration depth of light into the Bragg Mirror (average of $z_1 + z_2$ as shown in Figure 106). The reflectivity will then be reduced (from the 100% maximum value) by the amount of loss which can be found by the following equation [127]

$$R \approx e^{-2(\alpha_1 z_1 + \alpha_2 z_2)} \quad (45)$$

where α_1 and α_2 are the attenuation coefficients of the Bragg layers, and z_1 and z_2 are the total distances the light travels in the two Bragg layers, respectively, as shown in Figure 106.

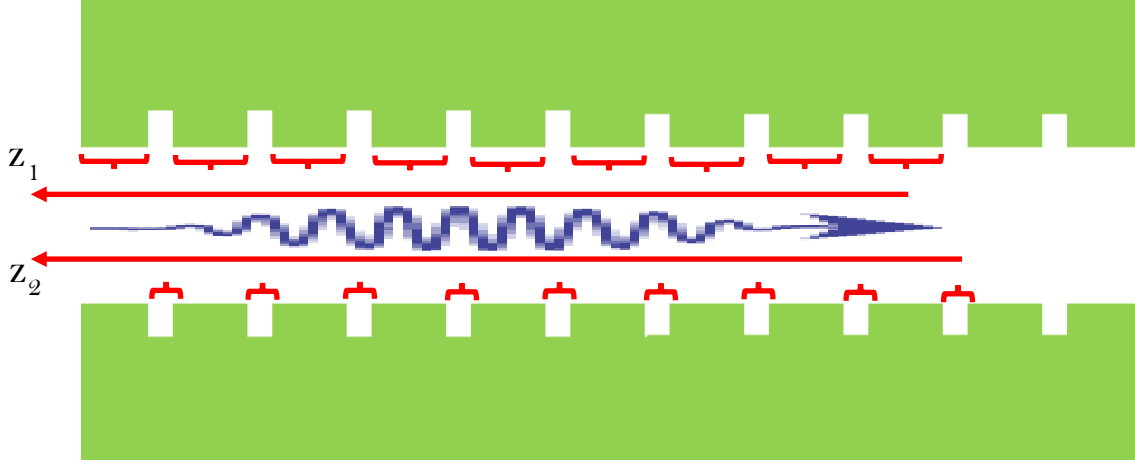


Figure 106: The penetration depth components, z_1 and z_2 , in which the blue arrow represents the light beam/photon penetrating the hollow core. The penetration depth basically is how far this beam/photon “penetrates” the core which is simply the sum of z_1 and z_2 .

The penetration depth, z_p , can then be found can be calculated as follows [128]

$$z_p = z_1 + z_2 \approx \frac{2a}{\pi} \frac{\epsilon_{00}}{|\epsilon_1|} \text{ (m)}$$

(46)

where a is the length of an individual Bragg period, and ϵ_{00} and $|\epsilon_1|$ are the two leading terms of the Fourier expansion of the dielectric constant, ϵ . Both terms are determined by the effective indices of the Bragg layers found by the numerical simulations.

3.1.1 Resist Thickness

The light propagation attenuation in the fiber is greatly dependent on the resist’s film thickness and it has been modeled here. Results are shown below in Figure 107 which shows both the loss and effective propagation refractive index for various film thicknesses. Three photoresists were investigated with their indices as 1.61 (that of AZ 701 photoresist), 1.45 and 1.30 which act to span the region of possible resist indices in the hopes to observe a general trend and a guiding principle for choosing the best resist in different applications.

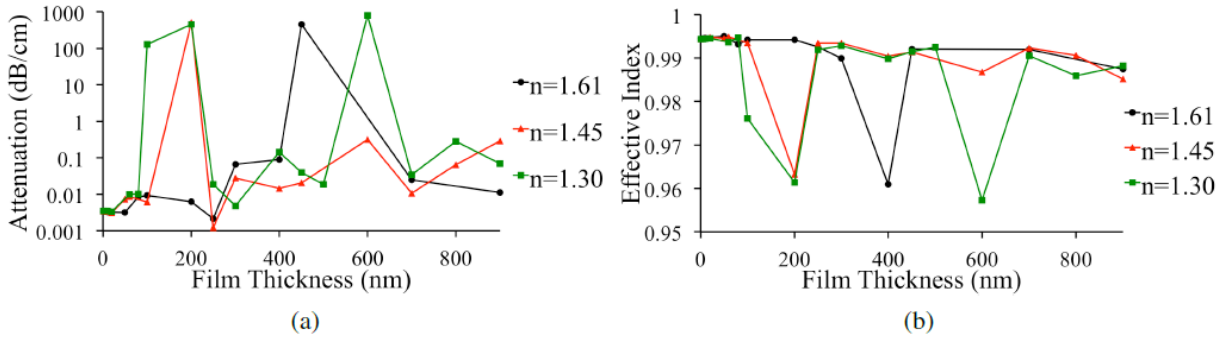


Figure 107: The attenuation as a function of the photoresist film thickness for photoresist indices of 1.61 (black line) 1.45 (red) and 1.3 (green). The image was co-published by the student in [95] and no reuse permission was required.

Plugging the values of α_1, z_1, α_2 & z_2 (air and AZ 701) into the reflectivity formula (equation (45)), the maximum reflectivity was found to occur using the 700 nm thick resist film (at all three resist indices) with a value of $R > 99.99\%$. Figure 109 shows the reflectivity as a function of the resist film thickness. The simulation shows that the number of Bragg periods needed to cause such reflectivity for such thickness is 300, corresponding to $\sim 100 \mu\text{m}$ penetration depth ($z_p = z_1 + z_2 \sim 100 \mu\text{m}$); hence, small modal volume and high light matter interaction probability (see Figure 108).

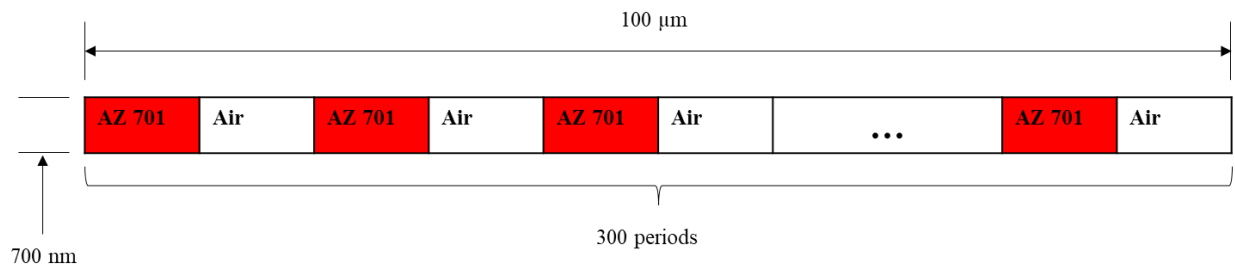


Figure 108: Visualization of the 300 periods made of AZ-701 photoresist and air that spans across 100 μm inside the fiber, in order to cause the 99.99% reflectivity.

Here the reflectivities were calculated using two methods. Method 1 calculates reflectivity by finding the average penetration depth of light into the Bragg Mirror. The reflectivity will then be reduced by the amount of loss caused by the fiber as the light travels this distance, as described in

Figure 106 and its corresponding equation. Method 2 uses the method of single expression (MSE) [129] whereby reflectivity is calculated from the forward and backward propagating field amplitudes at the beginning of the grating (see Figure 109).

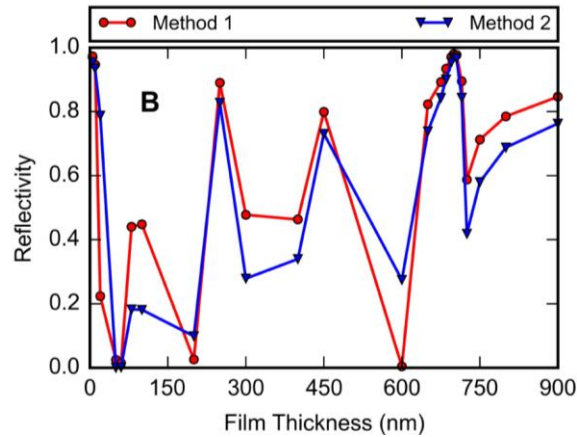


Figure 109: FBG reflectivity as a function of the photoresist film thickness. The image was co-published by the student in [127] and no reuse permission was required.

Note that we have tried a second approach to produce a Bragg grating in HC-PCF using a photoresist which is by introducing a polymer into selected holes of the photonic crystal, as shown in Figure 110.

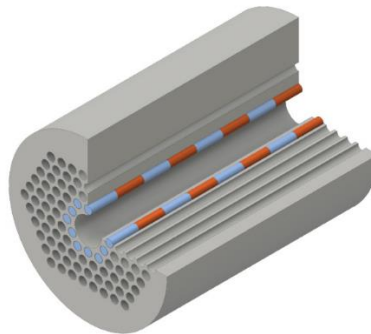


Figure 110: Visualization of the index modulation of the first layer of PCF holes surrounding the hollow core, in which the photonic crystal holes are selectively filled with a polymer then exposed to interference pattern-based index contrast. The image was co-published by the student in both [95] and [127] and no reuse permission was required.

The disadvantage of this method is that because of the small diameter of the photonic crystal holes, the polymer will fill them completely and the holes will not be flushed with a developer after exposure to remove the exposed (or unexposed) sections of the resist. The Bragg grating formed in this approach will then rely on the index contrast between the exposed and unexposed sections of the resist, which is relatively low. Assuming the holes are filled with a UV-curable epoxy (e.g., Norland optical adhesives), the index contrast between the exposed and unexposed sections will be $\sim 10^{-2}$. This method is expected to result in lower reflectivity compared to the first approach because of the significantly lower resulting effective index modulation ($\sim 10^{-4}$). The low effective index modulation will lead to rather long penetration depths into the grating combined with high attenuation due to the partial disruption of the finely tuned photonic-crystal guiding mechanism. The reflectivities obtained by this method did not exceed 40%, which excluded this case from further investigation. See Figure 111.

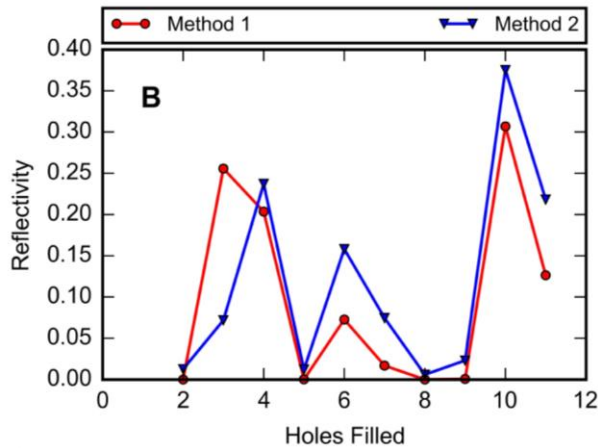


Figure 111: The corresponding maximum reflectivities that can be achieved using a perfect Bragg reflector with optical losses associated with the fiber are shown for polymer in the photonic crystal region (in which the holes in the first layer are filled one at a time in a counter-clockwise direction). The image was co-published by the student in [127] and no reuse permission was required.

3.1.2 Resist-based FBG compared to FBG by bare silica modulation

In contrast to our resist based FBG, we can compare it to reflectivities potentially achievable by another commonly used FBG fabrication method which is to directly modulate the fiber glass by exposing it to the laser interference pattern. In other words, forming FBG by exposing the HC-PCF to the laser interference pattern directly where the index modulation will happen to the bare core wall directly (this has been done for modulating the refractive index of the solid core PCF [130, 131]). Such modulation produced a 10^{-3} index contrast between exposed vs. unexposed silica modulating a solid core, but since we are dealing with a hollow core fiber, only a thin layer of glass (the core wall) will be modulated and we are no longer using index contrast; instead, we are talking about “effective” index contrast which for such thin glass layer on the core wall will be 10^{-5} which will render a maximum reflectivity of $\sim 99.2\%$. However, to obtain such reflectivity based on this very low effective index contrast (10^{-5}), the number of Bragg periods/layers that would be required to cause such 99.2% reflectivity would be $\sim 10^5$ which corresponds to > 5.1 cm penetration depth, which in turn mean a very unwanted large modal volume (interaction area). This would in turn decrease the atom-field coupling strength in cavity quantum electrodynamics (QED) experiments [132] as described before. However, when we plug an extremely thin layer of resist in the hollow core (700 nm for AZ 701 photoresist), we can have high reflectivities up to 99.99% from only about 3×10^2 Bragg periods (shorter mirror) corresponding to only ~ 100 μm penetration depth. Therefore, it is very evident how beneficial the resist based FBG is for HC-PCF.

Although introducing the slightest amount of the photoresist into the fiber gives a significant increase of the propagation loss, it is compensated by the increase in the effective index contrast between the grating layers which greatly enhance the mirror performance.

Chapter 4: Future Work for Project 2

Few recommendations can be given to build on the above findings.

4.1 Selective Injection

The injection port has been assembled and the fiber and the capillaries have been purchased and ready for implementation.

4.2 Laser Interference Inscription

Similarly, the setup needed was partly assembled. The remaining work also contains figuring out the best parameters for exposure, notably the laser exposure time and resist development time. This is needed to be done to a silicon wafer first, and then to be applied to the fiber.

4.3 Characterization

Once the resist has been selectively injected then exposed by the laser interference pattern then developed, the FBG should be successfully fabricated in principle. Characterizing the formed structure can be done either by SEM (after slicing the fiber in two halves by FIB) or by the simple optics table setup described in Figure 102. Practically speaking, perfectly reflecting mirrors/gratings are not achievable due to practical fabrication challenges and losses associated with the fiber itself (in addition to the insertion loss of laser beam inside the fiber). In such projects, power losses are tolerable for the sake of inducing non-linear interactions. However, some work remains in careful choice of photolithographic parameters through trial and error [125]. Eventually, the sample can be handled for loading the Cs cold atoms and observe

nonlinear interactions between the atom(s) and the light going through multiple passes due to Bragg reflections.

تم بحمد الله

References

1. Younis, M.I., *MEMS linear and nonlinear statics and dynamics*. Vol. 20. 2011: Springer Science & Business Media.
2. Bullen, D. and C. Liu, *Electrostatically actuated dip pen nanolithography probe arrays*. *Sensors and Actuators A: Physical*, 2006. **125**(2): p. 504-511.
3. Stuart, H.R., F.H. Baumann, and A. Wong-Foy. *Monolithic integration of optical waveguides and micromechanical switching in silicon-on-insulator*. in *Integrated Photonics Research*. 2003. Optica Publishing Group.
4. Al-Ghamdi, M., et al., *Quasi-Static pull-in: an instability in electrostatic Actuators*. 2020. **10**(1): p. 1-8.
5. Rützel, S., et al., *Nonlinear dynamics of atomic-force-microscope probes driven in Lennard-Jones potentials*. 2003. **459**(2036): p. 1925-1948.
6. Brugger, J., et al., *Microlever with combined integrated sensor/actuator functions for scanning force microscopy*. 1994. **43**(1-3): p. 339-345.
7. Company, B., *Specifications of FASTSCAN-A Atomic Force Microscope Tip*, B. Company, Editor. 2023.
8. Zhou, N., et al., *The Study of Reactive Ion Etching of Heavily Doped Polysilicon Based on HBr/O₂/He Plasmas for Thermopile Devices*. *Materials*, 2020. **13**(19): p. 4278.
9. Siffert, P. and E. Krimmel, *Silicon: evolution and future of a technology*. 2013: Springer Science & Business Media.
10. Laconte, J., et al., *Thin films stress extraction using micromachined structures and wafer curvature measurements*. *Microelectronic engineering*, 2004. **76**(1-4): p. 219-226.

11. *BERKELEY SENSOR & ACTUATOR CENTER*. 1996 [cited 2021; Available from: <https://www-bsac.eecs.berkeley.edu/~pister/245/>].
12. Morrison, J., et al., *Electrothermally actuated tip-tilt-piston micromirror with integrated varifocal capability*. 2015. **23**(7): p. 9555-9566.
13. Legtenberg, R., et al., *Electrostatic curved electrode actuators*. Journal of Microelectromechanical Systems, 1997. **6**(3): p. 257-265.
14. Rosa, M.A., et al., *A novel external electrode configuration for the electrostatic actuation of MEMS based devices*. Journal of Micromechanics and Microengineering, 2004. **14**(4): p. 446.
15. Pinto, R.M., V. Chu, and J.P.J.A.E.M. Conde, *Amorphous Silicon Self-Rolling Micro Electromechanical Systems: From Residual Stress Control to Complex 3D Structures*. 2019. **21**(9): p. 1900663.
16. Senturia, S.D., *Microsystem design*. 2007: Springer Science & Business Media.
17. Li, X., et al., *Process for preparing macroscopic quantities of brightly photoluminescent silicon nanoparticles with emission spanning the visible spectrum*. Langmuir, 2003. **19**(20): p. 8490-8496.
18. Temple-Boyer, P., et al., *Residual stress of silicon films deposited by LPCVD from silane*. MRS Online Proceedings Library Archive, 1998. **518**.
19. Sharma, N., M. Hooda, and S. Sharma, *Synthesis and characterization of LPCVD polysilicon and silicon nitride thin films for MEMS applications*. Journal of Materials, 2014. **2014**.
20. Gaspar, J., et al., *Mechanical properties of thin silicon films deposited at low temperatures by PECVD*. Journal of Micromechanics and Microengineering, 2010. **20**(3): p. 035022.

21. Patel, R. and M. Metzler, *Optimization of Plasma Enhanced Chemical Vapor Deposition (PECVD) of Amorphous Silicon (a-Si) Using Oxford Instruments System 100 with Taguchi L9 Based Design of Experiments (DOE)*. 2017.
22. Gusev, E.Y., J. Jityaeva, and O. Ageev, *EFFECT OF PECVD CONDITIONS ON MECHANICAL STRESS OF SILICON FILMS*. Materials Physics and Mechanics, 2018. **37**: p. 67-72.
23. Michael, A., et al., *Investigation of E-beam evaporated silicon film properties for MEMS applications*. Journal of Microelectromechanical Systems, 2015. **24**(6): p. 1951-1959.
24. Morgan, D.V. and K. Board, *An introduction to semiconductor microtechnology*. 1990: John Wiley & Sons.
25. Yang, J., et al., *A new technique for producing large-area as-deposited zero-stress LPCVD polysilicon films: The multipoly process*. Journal of Microelectromechanical Systems, 2000. **9**(4): p. 485-494.
26. Adams, A. and S. Sze, *VLSI technology*. 1988, McGraw-Hill Book Co., Inc., New York.
27. French, P., *Polysilicon: a versatile material for microsystems*. Sensors and actuators A: Physical, 2002. **99**(1-2): p. 3-12.
28. Kahn, H., *Mechanical Properties of Micromachined Structures*, in *Springer Handbook of Nanotechnology*. 2017, Springer. p. 1459-1479.
29. Krulevitch, K., et al. *Stress in undoped LPCVD polycrystalline silicon*. in *Solid-State Sensors and Actuators, 1991. Digest of Technical Papers, TRANSDUCERS'91., 1991 International Conference on*. 1991. IEEE.
30. Oei, D. and S. McCarthy, *The effect of temperature and pressure on residual stress in LPCVD polysilicon films*. MRS Online Proceedings Library Archive, 1992. **276**.

31. Yu, C.-L., et al., *Stress and microstructural evolution of LPCVD polysilicon thin films during high temperature annealing*. MRS Online Proceedings Library Archive, 1996. **441**.
32. O'Bannon, L., *Dictionary of Ceramic Science and Engineering*. 2012: Springer Science & Business Media.
33. Charles P. Poole, J.a.F.J.O., *Introduction to Nanotechnology*. 2003: John Wiley & Sons, Inc.
34. Eliyahu, D., et al., *Atomic Force Microscope-Based Meniscus-Confined Three-Dimensional Electrodeposition*. Advanced Materials Technologies, 2020. **5**(2): p. 1900827.
35. Zhang, Y., et al., *Nanopore Formation via Tip-Controlled Local Breakdown Using an Atomic Force Microscope*. Small Methods, 2019. **3**(7): p. 1900147.
36. Dietrich, P.I., et al., *3D-printed scanning-probe microscopes with integrated optical actuation and read-out*. Small, 2020. **16**(2): p. 1904695.
37. Sun, L., et al., *3D-printed cellular tips for tuning fork atomic force microscopy in shear mode*. Nature Communications, 2020. **11**(1): p. 5732.
38. Zhang, C., et al., *3D Printing of Functional Magnetic Materials: From Design to Applications*. Advanced Functional Materials, 2021: p. 2102777.
39. Allen Cowen, B.H., Ramaswamy Mahadevan, and Steve Wilcenski. *PolyMUMPs Design Handbook: a MUMPs® process*. 2011; Available from: http://www.memscap.com/_data/assets/pdf_file/0019/1729/PolyMUMPs-DR-13-0.pdf.
40. COMSOL. *Electrostatically Actuated Cantilever Tutorial*. Available from: <https://www.comsol.com/model/electrostatically-actuated-cantilever-444>.

41. Omar Alshehri, M.A.-G., Mahmoud Khater, Mohamed Arabi, Maher Bakri-Kassem, David Yevick, *PROSPECT OF NEW AFM PROBE DESIGN ENABLED BY STRESS GRADIENT*, in *International Conference on Solid-State Sensors, Actuators and Microsystems (Transducers)*. 2021, IEEE.
42. Voldman, J., *Course materials for 6.777J / 2.372J Design and Fabrication of Microelectromechanical Devices, Spring 2007*. MIT OpenCourseWare (<http://ocw.mit.edu/>), Massachusetts Institute of Technology. 2007.
43. Tang, W.C.-K., *Electrostatic comb drive for resonant sensor and actuator applications*. 1990: University Microfilms.
44. Daeichin, M., R. Miles, and S.J.N.D. Towfighian, *Lateral pull-in instability of electrostatic MEMS transducers employing repulsive force*. 2020. **100**(3): p. 1927-1940.
45. Osterberg, P.M. and S.D.J.J.o.M.s. Senturia, *M-TEST: a test chip for MEMS material property measurement using electrostatically actuated test structures*. 1997. **6**(2): p. 107-118.
46. Kambali, P.N. and A.K.J.I.S.J. Pandey, *Capacitance and force computation due to direct and fringing effects in MEMS/NEMS arrays*. 2015. **16**(2): p. 375-382.
47. Rao, S.S., *Mechanical Vibrations [SI]*. 2011, Pearson education.
48. Crandall, S., et al., *An introduction to the mechanics of solids; with SI units, ser.* 1978.
49. TopLine.tv. *LCC52B50SQ.75-N350*. 2023; Technical Drawing].
50. Humphrey, M., P.V. Pancella, and N. Berrah, *Quantum Physics*. 2015: DK Publishing.
51. Dholakia, K. and T. Čižmár, *Light and heat in a balancing act*. Physics, 2012. **5**: p. 76.
52. NKTPhotonics, *HC-800-02 Hollow Core Photonic Bandgap Fiber*, NKTPhotonics, Editor. 2015, NKTPhotonics.

53. Sargent, E.H., *Dance Of Molecules*. 2005: Penguin Canada.
54. Maddox, J., *Photonic band-gaps bite the dust*. Nature, 1990. **348**(6301): p. 481-481.
55. Yablonovitch, E. *Photonic Crystals and Photonic nanostructures* 2016 02/10/2016]; Available from: <https://www.youtube.com/watch?v=Ah36cVxtw0I>.
56. Poynting, J.H., *On the transfer of energy in the electromagnetic field*. Philosophical Transactions of the Royal Society 1884. **175**(343).
57. Beth, R.A., *Mechanical detection and measurement of the angular momentum of light*. Physical Review, 1936. **50**(115).
58. Wong, G., et al., *Excitation of orbital angular momentum resonances in helically twisted photonic crystal fiber*. science, 2012. **337**(6093): p. 446-449.
59. de Broglie, L. *Research on the theory of quanta*. in *Annales de Physique*. 1925.
60. Davisson, C.J. and L.H. Germer, *Reflection of Electrons by a Crystal of Nickel*. Proceedings of the National Academy of Sciences of the United States of America, 1928. **14**(4): p. 317.
61. Hall, J.L., M. Zhu, and P. Buch, *Prospects for using laser-prepared atomic fountains for optical frequency standards applications*. JOSA B, 1989. **6**(11): p. 2194-2205.
62. Polimeno, P., et al., *Optical tweezers and their applications*. Journal of Quantitative Spectroscopy and Radiative Transfer, 2018. **218**: p. 131-150.
63. Alshehri, O., Z.-H. Li, and M. Al-Amri, *Basics of quantum communication*, in *Structured Light for Optical Communication*. 2021, Elsevier. p. 1-36.
64. Fabbrichesi, M., E. Gabrielli, and G. Lanfranchi, *The Physics of the Dark Photon: A Primer*. 2021: Springer.

65. Rayleigh, L., *XVII. On the maintenance of vibrations by forces of double frequency, and on the propagation of waves through a medium endowed with a periodic structure*. The London, Edinburgh, and Dublin Philosophical Magazine and Journal of Science, 1887. **24**(147): p. 145-159.
66. Yablonovitch, E., *Inhibited spontaneous emission in solid-state physics and electronics*. Physical Review Letters, 1987. **58**(20): p. 2059-62.
67. John, S., *Strong localization of photons in certain disordered dielectric superlattices*. Physical Review Letters, 1987. **58**(23): p. 2486–2489.
68. Conover, E., *APS Fellow Eli Yablonovitch Wins Institute of Physics' Highest Honor*. 2015, American Physical Society (Physics).
69. Mahon, B., *The man who changed everything: The life of James Clerk Maxwell*. 2004: John Wiley & Sons.
70. Busch-Vishniac, I.J., *Electromechanical sensors and actuators*. 1998: Springer Science & Business Media.
71. Benyus, J.M., *Biomimicry: Innovation inspired by nature*. 1997, Morrow New York.
72. Galusha, J.W., et al., *Discovery of a diamond-based photonic crystal structure in beetle scales*. Physical Review E, 2008. **77**(5): p. 050904.
73. Wei-Che Shiha, Y.-C.C., Wei-Tsai Changa, Chien-Chuan Chengb, Kuo-Sheng Kaoc, Kuo-Hua Chengc, Chih-Ming Wangd, Chih-Yu Wena, Jui-Yang Changa and Po-Wei Tinga. *The Bragg Reflector Layer of Low Surface Roughness Based on Solidly Mounted Resonators*. in *3rd International Conference on Industrial Application Engineering*. 2015. Japan.

74. W.Hergert, R.H.a. *Two-dimensional photonic crystals*. [cited 2016; Available from: <http://www-old.mpi-halle.mpg.de/departement2/research-areas/silicon-photonics-photovoltaics/photonic-crystals-computational-studies/abstract/two-dimensional-photonic-crystals/>].
75. Korkin, A. and F. Rosei, *Nanoelectronics and photonics: from atoms to materials, devices, and architectures*. 2008: Springer Science & Business Media.
76. Hecht, E., *Optics 4 edition San Francisco*. 2002, CA: Addison Wesley.
77. Bjarklev, A., J. Broeng, and A.S. Bjarklev, *Photonic crystal fibres*. 2012: Springer Science & Business Media.
78. Kaiser, P. and H. Astle, *Low-Loss Single-Material Fibers Made From Pure Fused Silica*. Bell System Technical Journal, 1974. **53**(6): p. 1021-1039.
79. Broeng, J., et al., *Highly increased photonic band gaps in silica/air structures*. Optics communications, 1998. **156**(4): p. 240-244.
80. Knight, J.C., et al., *Photonic band gap guidance in optical fibers*. science, 1998. **282**(5393): p. 1476-1478.
81. J. Broeng, S.B., and A. Bjarklev, *Waveguiding by the photonic band gap effect*, in *Topical Meeting on Electromagnetic Optics*. 1998, EOS: Hyeres, France. p. 67-68.
82. Cregan, R., et al., *Single-mode photonic band gap guidance of light in air*. science, 1999. **285**(5433): p. 1537-1539.
83. Broeng, J., et al., *Analysis of air-guiding photonic bandgap fibers*. Optics letters, 2000. **25**(2): p. 96-98.

84. Naumov, A.N. and A.M. Zheltikov, *Optical harmonic generation in hollow-core photonic-crystal fibres: analysis of optical losses and phase-matching conditions*. Quantum Electronics, 2002. **32**(2): p. 129.
85. Ritari, T., *Novel sensor and telecommunication applications of photonic crystal fibers*. 2006: Helsinki University of Technology.
86. Jamois, C., et al., *Silicon-based two-dimensional photonic crystal waveguides*. Photonics and Nanostructures-Fundamentals and Applications, 2003. **1**(1): p. 1-13.
87. Benabid, F., et al., *Compact, stable and efficient all-fibre gas cells using hollow-core photonic crystal fibres*. Nature, 2005. **434**(7032): p. 488-491.
88. Rogers, B., J. Adams, and S. Pennathur, *Nanotechnology: understanding small systems*. 2007: Crc Press.
89. Anderson, M., *Atomic clocks inspire new qubits: Early research explores a more robust quantum computer-[News]*. IEEE Spectrum, 2018. **55**(12): p. 9-10.
90. Wang, Z.-H., et al., *Quantum state manipulation of single-Cesium-atom qubit in a micro-optical trap*. Frontiers of Physics, 2014. **9**(5): p. 634-639.
91. LeibingerLaserPrize. *Philip Russell - Zukunftspreis 2014*. 2014; Available from: <https://www.youtube.com/watch?v=IF011wgF71Y>.
92. Russell, P., *Photonic crystal fibers*. science, 2003. **299**(5605): p. 358-362.
93. Wang, Z., et al., *Designer patterned functional fibers via direct imprinting in thermal drawing*. Nature Communications, 2020. **11**(1): p. 3842.
94. Ghosh, D., et al., *Index-Guided Photonic Crystal Fibers: Study of Fiber Drawing Parameters*. Journal of Optics, 2008. **37**: p. 72-77.

95. Flannery, J., et al., *Implementing Bragg mirrors in a hollow-core photonic-crystal fiber*. *Optical Materials Express*, 2017. **7**(4): p. 1198-1210.
96. ThorLabs. [30/9/2016]; Available from: https://www.thorlabs.com/images/TabImages/MFD_780.jpg.
97. Mihailov, S.J., et al., *Fiber Bragg gratings made with a phase mask and 800-nm femtosecond radiation*. *Optics letters*, 2003. **28**(12): p. 995-997.
98. Couny, F., F. Benabid, and O. Carraz, *Enhanced SRS in H₂ filled hollow core photonic crystal fibre by use of fibre Bragg grating*. *Journal of Optics A: Pure and Applied Optics*, 2007. **9**(2): p. 156.
99. Wang, Y., C. Liao, and D. Wang, *Femtosecond laser-assisted selective infiltration of microstructured optical fibers*. *Optics express*, 2010. **18**(17): p. 18056-18060.
100. Huang, Y., Y. Xu, and A. Yariv, *Fabrication of functional microstructured optical fibers through a selective-filling technique*. *Applied Physics Letters*, 2004. **85**(22): p. 5182-5184.
101. Fini, J.M., *Microstructure fibres for optical sensing in gases and liquids*. *Measurement Science and Technology*, 2004. **15**(6): p. 1120.
102. Xiao, L., et al., *Fabrication of selective injection microstructured optical fibers with a conventional fusion splicer*. *Optics express*, 2005. **13**(22): p. 9014-9022.
103. Cordeiro, C.M., et al., *Lateral access to the holes of photonic crystal fibers—selective filling and sensing applications*. *Optics express*, 2006. **14**(18): p. 8403-8412.
104. Cordeiro, C.M., et al., *Towards practical liquid and gas sensing with photonic crystal fibres: side access to the fibre microstructure and single-mode liquid-core fibre*. *Measurement Science and Technology*, 2007. **18**(10): p. 3075.

105. Martelli, C., et al., *Micromachining structured optical fibers using focused ion beam milling*. Optics letters, 2007. **32**(11): p. 1575-1577.
106. Naeem, K., et al., *High-sensitivity temperature sensor based on a selectively-polymer-filled two-core photonic crystal fiber in-line interferometer*. Sensors Journal, IEEE, 2015. **15**(7): p. 3998-4003.
107. Kuhlmeiy, B.T., B.J. Eggleton, and D.K. Wu, *Fluid-filled solid-core photonic bandgap fibers*. Journal of Lightwave Technology, 2009. **27**(11): p. 1617-1630.
108. Wu, D.K., B.T. Kuhlmeiy, and B.J. Eggleton, *Ultrasensitive photonic crystal fiber refractive index sensor*. Optics letters, 2009. **34**(3): p. 322-324.
109. Canning, J., et al., *White light sources based on multiple precision selective micro-filling of structured optical waveguides*. Optics express, 2008. **16**(20): p. 15700-15708.
110. Martelli, C., et al., *Water-core Fresnel fiber*. Optics express, 2005. **13**(10): p. 3890-3895.
111. Domachuk, P., et al., *Microfluidic tunable photonic band-gap device*. Applied Physics Letters, 2004. **84**(11): p. 1838-1840.
112. Malo, B., et al., *Point-by-point fabrication of micro-Bragg gratings in photosensitive fibre using single excimer pulse refractive index modification techniques*. Electronics Letters, 1993. **29**(18): p. 1668-1669.
113. Iadicicco, A., S. Campopiano, and A. Cusano, *Long-period gratings in hollow core fibers by pressure-assisted arc discharge technique*. IEEE Photonics Technology Letters, 2011. **23**(21): p. 1567-1569.
114. Iadicicco, A., R. Ranjan, and S. Campopiano, *Fabrication and characterization of long-period gratings in hollow core fibers by electric arc discharge*. IEEE Sensors Journal, 2015. **15**(5): p. 3014-3020.

115. Dockney, M.L., S.W. James, and R.P. Tatam, *Fibre Bragg gratings fabricated using a wavelength tuneable laser source and a phase mask based interferometer*. Measurement Science and Technology, 1996. **7**(4): p. 445.
116. Nayak, K. and K. Hakuta, *Photonic crystal formation on optical nanofibers using femtosecond laser ablation technique*. Optics express, 2013. **21**(2): p. 2480-2490.
117. Anderson, D., et al., *Production of in-fibre gratings using a diffractive optical element*. Electronics Letters, 1993. **29**(6): p. 566-568.
118. Hill, K., et al., *Photosensitivity in optical fiber waveguides: Application to reflection filter fabrication*. Applied Physics Letters, 1978. **32**(10): p. 647-649.
119. Meltz, G., W.W. Morey, and W. Glenn, *Formation of Bragg gratings in optical fibers by a transverse holographic method*. Optics letters, 1989. **14**(15): p. 823-825.
120. Askins, C., et al., *Stepped-wavelength optical-fiber Bragg grating arrays fabricated in line on a draw tower*. Optics letters, 1994. **19**(2): p. 147-149.
121. Wolferen, H. and L. Abelmann, *Laser interference lithography*. 2011.
122. Byun, I. and J. Kim, *Cost-effective laser interference lithography using a 405 nm AlInGaN semiconductor laser*. Journal of Micromechanics and Microengineering, 2010. **20**(5): p. 055024.
123. Quimby, R.S., *Photonics and lasers: an introduction*. 2006: John Wiley & Sons.
124. Inc., I.M.M., *i-line/g-line Photoresist Application Guide (0.5 - 6.0 μ m)*. 2022.
125. Li, X., et al. *Low-cost lithography for fabrication of one-dimensional diffraction gratings by using laser diodes*. in *International Conference on Optical Instruments and Technology 2015*. 2015. International Society for Optics and Photonics.
126. 29/09/2016]; Available from: <https://www.newport.com/n/spatial-filters>.

127. Haapamaki, C., et al., *Mesoscale cavities in hollow-core waveguides for quantum optics with atomic ensembles*. Nanophotonics, 2016.
128. Joannopoulos, J.D., et al., *Photonic crystals: molding the flow of light*. 2011: Princeton university press.
129. Baghdasaryan, H., et al., *Absorption loss influence on optical characteristics of multilayer distributed Bragg reflector: wavelength-scale analysis by the method of single expression*. Opto-Electronics Review, 2010. **18**(4): p. 438-445.
130. Fu, L., et al., *Femtosecond laser writing Bragg gratings in pure silica photonic crystal fibres*. Electronics Letters, 2005. **41**(11): p. 1.
131. Martelli, C., et al., *Strain and temperature characterization of photonic crystal fiber Bragg gratings*. Optics letters, 2005. **30**(14): p. 1785-1787.
132. Hood, C.J., H. Kimble, and J. Ye, *Characterization of high-finesse mirrors: Loss, phase shifts, and mode structure in an optical cavity*. Physical Review A, 2001. **64**(3): p. 033804.

Appendix (Permissions)

All figures and tables used in this work that are produced in other literature were reused here with permission: either based on the Fair Use Doctrine, or through privileges given to student publications from academic institutions. However, written permissions were sought whenever possible and listed below.

Permission of Figure 3.

Dear Omar,

I can't help you unfortunately, the mentioned author doesn't work at CSEM anymore. I think you can reuse this figure (as long as it is not for commercial purposes) by referring to the article

Best regards

csem Claudine JULIA-SCHMUTZ • Inbound Marketing Manager • +41 79 551 67 13

Permission of Figure 4.

Hi Omar,

I apologize for not responding to this earlier! The email ended up in the wrong folder, sigh. In any case, if it is not too late, yes, you have our permission to use the probe image. Please credit "Bruker Nano Surfaces and Metrology". And if possible, we would like a copy of your final dissertation for our archive. [Congratulations](#) on your studies!

Best regards,
--Steve

Stephen Hopkins
Content Marketing Manager
Bruker Nano Surfaces and Metrology Division
Phone +1 520 295 4373
Mobile +1 520 415 4511

stephen.hopkins@bruker.com
www.bruker.com

in t f i o

Permission of Figure 5.

5/27/2023, 2:28 PM https://marketplace.copyright.com/ip/view/permissions/1906_4906_4806_1906_4806/2023/04/27/1906_4802_4802...

CCC Marketplace

This is a License Agreement between Omar Alshabi ("User") and Copyright Clearance Center, Inc. (CCC) on behalf of the Rights holder identified in the order details below. The license consists of the order details, the Marketplace Permissions General Terms and Conditions below, and any applicable Terms and Conditions which are included below.

All payments must be made in full to CCC in accordance with the Marketplace Permissions General Terms and Conditions below.

Order Date	11 Apr 2023	Type of Use	Reproduce in a thesis/dissertation
Order License ID	13450211	Publisher Portion	ELIWEI BY Image/photo/illustration
ISSN	0167-0277		

LICENSED CONTENT

Publication Title	Microelectronic engineering	Publication Type	Journal
Article Title	The film stress relaxation using microcantilever structures and their cantilever misalignments	Start Page	219
		End Page	226
		Issue	1-4
		Volume	70
Date	05/01/1983		
Language	Dutch		
Country	Netherlands		
Rights holder	Elsevier Science & Technology Journals		

REQUEST DETAILS

Portion Type	Image/photo/illustration	Distribution	Worldwide
Number of Images / Photos / Illustrations	1	Translation	Original language of publication
Format (select all that apply)	Print, Electronic	Copies for the Disabled?	No
Who Will Republish the Content?	Publisher, not-for-profit	Minor Editing Privileges?	No
Duration of Use	Life of current edition	Incidental Promotional Use?	No
Lifetime Limit Quantity	Up to 499	Currency	USD
Rights Requested	Make product		

NEW WORK DETAILS


Title	New Platform Designs for Enabling Acoustic Interactions in Solid and Geometric Spaces	Institution Name	University of Waterloo
Instructor Name	William	Expected Presentation Date	2023.04.25

ADDITIONAL DETAILS

Order Reference Number	N/A	The Requesting Person/Organization to Appear on the License	Omar Alshabi
------------------------	-----	---	--------------

https://marketplace.copyright.com/ip/view/permissions/1906_4906_4806_1906_4806/2023/04/27/1906_4802_4802...

Permission of Figure 8.



Requesting permission to reuse content from an IEEE publication

Electrostatic curved electrode actuators

Author: R. Legtenberg
 Publication: Journal of Microelectromechanical Systems
 Publisher: IEEE
 Date: September 1997

Copyright © 1997, IEEE

Thesis / Dissertation Reuse

The IEEE does not require individuals working on a thesis to obtain a formal reuse license, however, you may print out this statement to be used as a permission grant:

Requirements to be followed when using any portion (e.g., figure, graph, table, or textual material) of an IEEE copyrighted paper in a thesis:

- 1) In the case of textual material (e.g., using short quotes or referring to the work within these papers) users must give full credit to the original source (author, paper, publication) followed by the IEEE copyright line © 2011 IEEE.
- 2) In the case of illustrations or tabular material, we require that the copyright line © [Year of original publication] IEEE appear prominently with each reprinted figure and/or table.
- 3) If a substantial portion of the original paper is to be used, and if you are not the senior author, also obtain the senior author's approval.

Requirements to be followed when using an entire IEEE copyrighted paper in a thesis:


- 1) The following IEEE copyright/ credit notice should be placed prominently in the references: © [year of original publication] IEEE. Reprinted, with permission, from [author names, paper title, IEEE publication title, and month/year of publication]
- 2) Only the accepted version of an IEEE copyrighted paper can be used when posting the paper or your thesis on-line.
- 3) In placing the thesis on the author's university website, please display the following message in a prominent place on the website: In reference to IEEE copyrighted material which is used with permission in this thesis, the IEEE does not endorse any of [university/educational entity's name goes here]'s products or services. Internal or personal use of this material is permitted. If interested in reprinting/republishing IEEE copyrighted material for advertising or promotional purposes or for creating new collective works for resale or redistribution, please go to http://www.ieee.org/publications_standards/publications/rights/rights_link.html to learn how to obtain a License from RightsLink.

If applicable, University Microfilms and/or ProQuest Library, or the Archives of Canada may supply single copies of the dissertation.

BACK
CLOSE WINDOW

Permission of Figure 9.

5/9/23, 2:47 PM [https://marketplace.copyright.com/cs/ui/webhrp/licensor/31803226-70d8-406d-9a06-09919ea8597b/d5ba414d-4144-490d-999-...](https://marketplace.copyright.com/cs/ui/webhrp/licensor/31803226-70d8-406d-9a06-09919ea8597b/d5ba414d-4144-490d-999-)



This is a License Agreement between Omar Alshehri ("User") and Copyright Clearance Center, Inc. ("CCC") on behalf of the Rightsholder identified in the order details below. The license consists of the order details, the Marketplace Permissions General Terms and Conditions below, and any Rightsholder Terms and Conditions which are included below.
 All payments must be made in full to CCC in accordance with the Marketplace Permissions General Terms and Conditions below.

Order Date	11-Apr-2023	Type of Use	Republish in a thesis/dissertation
Order License ID	1343627-1	Publisher	INSTITUTE OF PHYSICS PUBLISHING
ISSN	0960-1317	Portion	Image/photo/illustration

LICENSED CONTENT

Publication Title	Journal of micromechanics and microengineering: structures, devices, and systems	Country	United Kingdom of Great Britain and Northern Ireland
Author/Editor	Institute of Physics (Great Britain)	Rightsholder	IOP Publishing, Ltd
Date	01/01/1991	Publication Type	Journal
Language	English		

REQUEST DETAILS

Portion Type	Image/photo/illustration	Distribution	Worldwide
Number of Images / Photos / Illustrations	2	Translation	Original language of publication
Format (select all that apply)	Print, Electronic	Copies for the Disabled?	No
Who Will Republish the Content?	Academic institution	Minor Editing Privileges?	No
Duration of Use	Current edition and up to 5 years	Incidental Promotional Use?	No
Lifetime Unit Quantity	Up to 499	Currency	USD
Rights Requested	Main product		

NEW WORK DETAILS

Title	New Platform Designs for Enabling Atomic Interactions in Solid and Gaseous States	Institution Name	University of Waterloo
Instructor Name	William Melek	Expected Presentation Date	2023-04-25

ADDITIONAL DETAILS

Order Reference Number	N/A	The Requesting Person/Organization to Appear on the License	Omar Alshehri
------------------------	-----	---	---------------

REQUESTED CONTENT DETAILS


https://marketplace.copyright.com/cs/ui/webhrp/licensor/31803226-70d8-406d-9a06-09919ea8597b/d5ba414d-4144-490d-999-09d040c3b7c 1/8

Permission of Figure 10.

JOHN WILEY AND SONS LICENSE TERMS AND CONDITIONS	
Mar 19, 2023	
This Agreement between Omar D Alshetri ("You") and John Wiley and Sons ("John Wiley and Sons") consists of your license details and the terms and conditions provided by John Wiley and Sons and Copyright Clearance Center.	
License Number	5512640804213
License date	Mar 19, 2023
Licensed Content Publisher	John Wiley and Sons
Licensed Content Publication	Advanced Engineering Materials
Licensed Content Title	Amorphous Silicon Self-Rolling Micro Electromechanical Systems: From Residual Stress Control to Complex 3D Structures
Licensed Content Author	João Pedro Conde, Virginia Cht, Rui M. R. Pinto
Licensed Content Date	Aug 8, 2019
Licensed Content Volume	21
Licensed Content Issue	9
Licensed Content Pages	11
Type of use	Dissertation/Thesis

Requestor type	
Requestor type	University/Academic
Format	Print and electronic
Portion	Figure/table
Number of figures/tables	7
Will you be translating? No	
Title	New Platform Designs for Enabling Atomic Interactions in Solid and Gaseous States
Institution name	University of Waterloo
Expected presentation date	Apr 2023
Portions	Figures 1 (b)
Requestor Location	Omar D Alshetri Industrial Engineering Department College of Engineering King Saud University Riyadh, Riyadh 11421 Saudi Arabia Attn: Omar D Alshetri
Publisher Tax ID	EU826007151
Total	0.00 USD
Terms and Conditions	
TERMS AND CONDITIONS	
This copyrighted material is owned by or exclusively licensed to John Wiley & Sons, Inc. or one of its group companies (each a "Wiley Company") or handled on behalf of a society with which a Wiley Company has exclusive publishing rights in relation to a particular work	

Permission of Figure 12.



Requesting permission to reuse content from an IEEE publication

A new technique for producing large-area as-deposited zero-stress LPCVD polysilicon films: the MultiPoly process

Author: Jie Yang
 Publication: Journal of Microelectromechanical Systems
 Publisher: IEEE
 Date: December 2000
 Copyright © 2000, IEEE

Thesis / Dissertation Reuse

The IEEE does not require individuals working on a thesis to obtain a formal reuse license, however, you may print out this statement to be used as a permission grant:

Requirements to be followed when using any portion (e.g., figure, graph, table, or textual material) of an IEEE copyrighted paper in a thesis:

- 1) In the case of textual material (e.g., using short quotes or referring to the work within these papers) users must give full credit to the original source (author, paper, publication) followed by the IEEE copyright line © 2011 IEEE.
- 2) In the case of illustrations or tabular material, we require that the copyright line © [Year of original publication] IEEE appear prominently with each reprinted figure and/or table.
- 3) If a substantial portion of the original paper is to be used, and if you are not the senior author, also obtain the senior author's approval.

Requirements to be followed when using an entire IEEE copyrighted paper in a thesis:

- 1) The following IEEE copyright/ credit notice should be placed prominently in the references: © [year of original publication] IEEE. Reprinted, with permission, from [author names, paper title, IEEE publication title, and month/year of publication]
- 2) Only the accepted version of an IEEE copyrighted paper can be used when posting the paper or your thesis on-line.
- 3) In placing the thesis on the author's university website, please display the following message in a prominent place on the website: In reference to IEEE copyrighted material which is used with permission in this thesis, the IEEE does not endorse any of [university/educational entity's name goes here]'s products or services. Internal or personal use of this material is permitted. If interested in reprinting/republishing IEEE copyrighted material for advertising or promotional purposes or for creating new collective works for resale or redistribution, please go to http://www.ieee.org/publications_standards/publications/rights/rights_link.html to learn how to obtain a License from RightsLink.

If applicable, University Microfilms and/or ProQuest Library, or the Archives of Canada may supply single copies of the dissertation.

BACK
CLOSE WINDOW

Permission of Figure 13.

5/9/23, 3:05 PM <https://marketplace.copyright.com/cs/v4-webmp/license/2263f6e6e1c14f56-8325-4562/8f8201790781-016-4066-9646-4...>

CCC Marketplace

This is a License Agreement between Omar Alshehri ("User") and Copyright Clearance Center, Inc. ("CCC") on behalf of the Rightsholder identified in the order details below. The license consists of the order details, the Marketplace Permissions General Terms and Conditions below, and any Rightsholder Terms and Conditions which are included below.
All payments must be made in full to CCC in accordance with the Marketplace Permissions General Terms and Conditions below.

Order Date	29-Mar-2023	Type of Use	Republish in a thesis/dissertation
Order License ID	1339160-1	Publisher Portion	J. Wiley Chart/graph/table/figure
ISBN-13	9780471024784		

LICENSED CONTENT

Publication Title	An introduction to semiconductor microtechnology	Country	United Kingdom of Great Britain and Northern Ireland
Author/Editor	Morgan, D. V., Board, K.	Rightsholder	John Wiley & Sons - Books
Date	01/01/1990	Publication Type	Book
Language	English		

REQUEST DETAILS

Portion Type	Chart/graph/table/figure	Distribution	Canada
Number of Charts / Graphs / Tables / Figures Requested	1	Translation	Original language of publication
Format (select all that apply)	Electronic	Copies for the Disabled?	No
Who Will Republish the Content?	Academic institution	Minor Editing Privileges?	No
Duration of Use	Life of current edition	Incidental Promotional Use?	No
Lifetime Unit Quantity	Up to 499	Currency	CAD
Rights Requested	Main product		

NEW WORK DETAILS

Title	New Platform Designs for Enabling Atomic Interactions in Solid and Gaseous States	Institution Name	University of Waterloo
Instructor Name	Omar Alshehri	Expected Presentation Date	2023-04-08

ADDITIONAL DETAILS

The Requesting Person/Organization to Appear on the License: Omar Alshehri

REQUESTED CONTENT DETAILS

<https://marketplace.copyright.com/cs/v4-webmp/license/2263f6e6e1c14f56-8325-4562/8f8201790781-016-4066-9646-4334106887/3> 1/1

Permission of Figure 14.

3/27/23, 3:16 PM <https://marketplace.copyright.com/cs/v4-webmp/license/7f820172614131-623f-a071aa205f491895-e006-4901-907e-793e...>

CCC Marketplace

This is a License Agreement between Omar Alshehri ("User") and Copyright Clearance Center, Inc. ("CCC") on behalf of the Rightsholder identified in the order details below. The license consists of the order details, the Marketplace Permissions General Terms and Conditions below, and any Rightsholder Terms and Conditions which are included below.
All payments must be made in full to CCC in accordance with the Marketplace Permissions General Terms and Conditions below.

Order Date	19-Mar-2023	Type of Use	Republish in a thesis/dissertation
Order License ID	1333857-1	Publisher Portion	JOHN WILEY & SONS INC Image/photo/illustration
ISBN-13	9780471079354		

LICENSED CONTENT

Publication Title	Introduction to nanotechnology	Country	United States of America
Author/Editor	POOLE	Rightsholder	John Wiley & Sons - Books
Date	01/01/2003	Publication Type	Book
Language	English		

REQUEST DETAILS

Portion Type	Image/photo/illustration	Distribution	Worldwide
Number of Images / Photos / Illustrations	13,11	Translation	Original language of publication
Format (select all that apply)	Print, Electronic	Copies for the Disabled?	No
Who Will Republish the Content?	Publisher, not-for-profit	Minor Editing Privileges?	No
Duration of Use	Life of current edition	Incidental Promotional Use?	No
Lifetime Unit Quantity	Up to 499	Currency	USD
Rights Requested	Main product		

NEW WORK DETAILS

Title	New Platform Designs for Enabling Atomic Interactions in Solid and Gaseous States	Institution Name	University of Waterloo
Instructor Name	William Melek	Expected Presentation Date	2023-04-01

ADDITIONAL DETAILS

The Requesting Person/Organization to Appear on the License: Omar Alshehri

REQUESTED CONTENT DETAILS

<https://marketplace.copyright.com/cs/v4-webmp/license/7f820172614131-623f-a071aa205f491895-e006-4901-907e-793e/3> 1/1

Permission of Figure 15.

3/19/23, 10:38 PM		RightLink Printable License
JOHN WILEY AND SONS LICENSE TERMS AND CONDITIONS		
Mar 19, 2023		
<hr/> <hr/>		
This Agreement between Omar D Alsheshri ("You") and John Wiley and Sons ("John Wiley and Sons") consists of your license details and the terms and conditions provided by John Wiley and Sons and Copyright Clearance Center.		
License Number	5512651217653	
License date	Mar 19, 2023	
Licensed Content Publisher	John Wiley and Sons	
Licensed Content Publication	Advanced Materials Technologies	
Licensed Content Title	Atomic Force Microscope-Based Meniscus-Confined Three-Dimensional Electrodeposition	
Licensed Content Author	David Eliyahu, Eliezer Gileadi, Ehud Golan, et al	
Licensed Content Date	Jan 9, 2020	
Licensed Content Volume	5	
Licensed Content Issue	2	
Licensed Content Pages	9	
Type of use	Dissertation/Thesis	
Requestor type	University/Academic	
https://s100.copyright.com/AppDispatchServlet		

3/19/23, 10:38 PM		RightLink Printable License
Format	Print and electronic	
Portion	Figure/table	
Number of figures/tables	1	
Will you be translating?	No	
Title	New Platform Designs for Enabling Atomic Interactions in Solid and Gaseous States	
Institution name	University of Waterloo	
Expected presentation date	Apr 2023	
Portions	Figures 1 (g)	
Requestor Location	Omar D Alsheshri Industrial Engineering Department College of Engineering King Saud University Riyadh, Riyadh 11421 Saudi Arabia Attn: Omar D Alsheshri	
Publisher Tax ID	EU826007151	
Total	0.00 USD	
Terms and Conditions	<p align="center">TERMS AND CONDITIONS</p> <p>This copyrighted material is owned by or exclusively licensed to John Wiley & Sons, Inc. or one of its group companies (each a "Wiley Company") or handled on behalf of a society with which a Wiley Company has exclusive publishing rights in relation to a particular work (collectively "WILEY"). By clicking "accept" in connection with completing this licensing transaction, you agree that the following terms and conditions apply to this transaction (along with the billing and payment terms and conditions established by the Copyright Clearance Center Inc., ("CCC's Billing and Payment terms and conditions"), at the time that</p>	
https://s100.copyright.com/AppDispatchServlet		

Permission of Figure 16.


3/19/23, 10:41 PM		RightLink Printable License
JOHN WILEY AND SONS LICENSE TERMS AND CONDITIONS		
Mar 19, 2023		
<hr/> <hr/>		
This Agreement between Omar D Alsheshri ("You") and John Wiley and Sons ("John Wiley and Sons") consists of your license details and the terms and conditions provided by John Wiley and Sons and Copyright Clearance Center.		
License Number	5512651431449	
License date	Mar 19, 2023	
Licensed Content Publisher	John Wiley and Sons	
Licensed Content Publication	Small Methods	
Licensed Content Title	Nanopore Formation via Tip-Controlled Local Breakdown Using an Atomic Force Microscope	
Licensed Content Author	Walter Reisner, Peter Grutter, Zezhou Liu, et al	
Licensed Content Date	Apr 24, 2019	
Licensed Content Volume	3	
Licensed Content Issue	7	
Licensed Content Pages	10	
Type of use	Dissertation/Thesis	
Requestor type	University/Academic	
https://s100.copyright.com/AppDispatchServlet		

3/19/23, 10:41 PM		RightLink Printable License
Format	Print and electronic	
Portion	Figure/table	
Number of figures/tables	1	
Will you be translating?	No	
Title	New Platform Designs for Enabling Atomic Interactions in Solid and Gaseous States	
Institution name	University of Waterloo	
Expected presentation date	Apr 2023	
Portions	Figure 1	
Requestor Location	Omar D Alsheshri Industrial Engineering Department College of Engineering King Saud University Riyadh, Riyadh 11421 Saudi Arabia Attn: Omar D Alsheshri	
Publisher Tax ID	EU826007151	
Total	0.00 USD	
Terms and Conditions	<p align="center">TERMS AND CONDITIONS</p> <p>This copyrighted material is owned by or exclusively licensed to John Wiley & Sons, Inc. or one of its group companies (each a "Wiley Company") or handled on behalf of a society with which a Wiley Company has exclusive publishing rights in relation to a particular work (collectively "WILEY"). By clicking "accept" in connection with completing this licensing transaction, you agree that the following terms and conditions apply to this transaction (along with the billing and payment terms and conditions established by the Copyright Clearance Center Inc., ("CCC's Billing and Payment terms and conditions"), at the time that</p>	
https://s100.copyright.com/AppDispatchServlet		

Permission of Figure 18.

<p>09/23, 3:30 PM</p> <p>JOHN WILEY AND SONS LICENSE TERMS AND CONDITIONS</p> <p>May 09, 2023</p> <hr/> <p>This Agreement between Omar D Alshehri ("You") and John Wiley and Sons ("John Wiley and Sons") consists of your license details and the terms and conditions provided by John Wiley and Sons and Copyright Clearance Center.</p> <p>License Number 5513060238861</p> <p>License date Mar 20, 2023</p> <p>Licensed Content Publisher John Wiley and Sons</p> <p>Licensed Content Publication Advanced Functional Materials</p> <p>Licensed Content Title 3D Printing of Functional Magnetic Materials: From Design to Applications</p> <p>Licensed Content Author Yong Chen, Qifa Zhou, Jianzhong Fu, et al</p> <p>Licensed Content Date Jun 17, 2021</p> <p>Licensed Content Volume 31</p> <p>Licensed Content Issue 34</p> <p>Licensed Content Pages 38</p> <p>Type of use Dissertation/Thesis</p> <p>Requestor type University/Academic</p> <p><small>https://onlinelibrary.wiley.com/doi/10.1002/cp.1500 copyright.com/Customers/Admin/P1/P1.jsp?ref=rightslink&id=454814213133861&docid=03506</small></p>	<p>09/23, 3:30 PM</p> <p>RightLink Portable License</p> <p>Format Print and electronic</p> <p>Portion Figure/table</p> <p>Number of figures/tables 18</p> <p>Will you be translating? No</p> <p>Title New Platform Designs for Enabling Atomic Interactions in Solid and Gaseous States</p> <p>Institution name University of Waterloo</p> <p>Expected presentation date Apr 2023</p> <p>Portions Figure 18 (f)</p> <p>Requestor Location Omar D Alshehri Industrial Engineering Department College of Engineering King Saud University Riyadh, Riyadh 11421 Saudi Arabia Attn: Omar D Alshehri</p> <p>Publisher Tax ID EU826007151</p> <p>Total 0.00 USD</p> <p>Terms and Conditions</p> <p>TERMS AND CONDITIONS</p> <p>This copyrighted material is owned by or exclusively licensed to John Wiley & Sons, Inc. or one of its group companies (each a "Wiley Company") or handled on behalf of a society with which a Wiley Company has exclusive publishing rights in relation to a particular work (collectively "WILEY"). By clicking "accept" in connection with completing this licensing transaction, you agree that the following terms</p> <p><small>https://onlinelibrary.wiley.com/doi/10.1002/cp.1500 copyright.com/Customers/Admin/P1/P1.jsp?ref=rightslink&id=454814213133861&docid=03506</small></p>
--	---

Permission of Figure 19.



Requesting permission to reuse content from an IEEE publication

Electrostatic curved electrode actuators

Author: R. Legtenberg
 Publication: Journal of Microelectromechanical Systems
 Publisher: IEEE
 Date: September 1997

Copyright © 1997, IEEE

Thesis / Dissertation Reuse

The IEEE does not require individuals working on a thesis to obtain a formal reuse license, however, you may print out this statement to be used as a permission grant:

Requirements to be followed when using any portion (e.g., figure, graph, table, or textual material) of an IEEE copyrighted paper in a thesis:

- 1) In the case of textual material (e.g., using short quotes or referring to the work within these papers) users must give full credit to the original source (author, paper, publication) followed by the IEEE copyright line © 2011 IEEE.
- 2) In the case of illustrations or tabular material, we require that the copyright line © [Year of original publication] IEEE appear prominently with each reprinted figure and/or table.
- 3) If a substantial portion of the original paper is to be used, and if you are not the senior author, also obtain the senior author's approval.

Requirements to be followed when using an entire IEEE copyrighted paper in a thesis:

- 1) The following IEEE copyright/ credit notice should be placed prominently in the references: © [year of original publication] IEEE. Reprinted, with permission, from [author names, paper title, IEEE publication title, and month/year of publication]
- 2) Only the accepted version of an IEEE copyrighted paper can be used when posting the paper or your thesis on-line.
- 3) In placing the thesis on the author's university website, please display the following message in a prominent place on the website: In reference to IEEE copyrighted material which is used with permission in this thesis, the IEEE does not endorse any of [university/educational entity's name goes here]'s products or services. Internal or personal use of this material is permitted. If interested in reprinting/republishing IEEE copyrighted material for advertising or promotional purposes or for creating new collective works for resale or redistribution, please go to http://www.ieee.org/publications_standards/publications/rights/rights_link.html to learn how to obtain a License from RightsLink.

If applicable, University Microfilms and/or ProQuest Library, or the Archives of Canada may supply single copies of the dissertation.

BACK
CLOSE WINDOW

Permission of Figure 20.

NB Nicolas BERTSCH <Nicolas.BERTSCH@memscap.com>
To: ○ Omar Alshehri

Hello,


Sure, please feel free to use them and give appropriate credits.

Best regards
Nicolas

MEMSCAP S.A.
C.O.O.

Phone Direct. +33 (0)4 7692 85 08
Mobile: +33 (0)6 22 52 51 38

Permission of Figure 27.



Requesting permission to reuse content from an IEEE publication

Prospect of New AFM Probe Design Enabled by Stress Gradient
Conference Proceedings: 2021 21st International Conference on Solid-State Sensors, Actuators and Microsystems (Transducers)
Author: Omar Alshehri
Publisher: IEEE
Date: 20 June 2021
Copyright © 2021, IEEE

Thesis / Dissertation Reuse

The IEEE does not require individuals working on a thesis to obtain a formal reuse license, however, you may print out this statement to be used as a permission grant:

Requirements to be followed when using any portion (e.g., figure, graph, table, or textual material) of an IEEE copyrighted paper in a thesis:

- 1) In the case of textual material (e.g., using short quotes or referring to the work within these papers) users must give full credit to the original source (author, paper, publication) followed by the IEEE copyright line © 2011 IEEE.
- 2) In the case of illustrations or tabular material, we require that the copyright line © [Year of original publication] IEEE appear prominently with each reprinted figure and/or table.
- 3) If a substantial portion of the original paper is to be used, and if you are not the senior author, also obtain the senior author's approval.


Requirements to be followed when using an entire IEEE copyrighted paper in a thesis:

- 1) The following IEEE copyright/ credit notice should be placed prominently in the references: © [Year of original publication] IEEE. Reprinted, with permission, from [author names, paper title, IEEE publication title, and month/year of publication].
- 2) Only the accepted version of an IEEE copyrighted paper can be used when posting the paper or your thesis on-line.
- 3) In placing the thesis on the author's university website, please display the following message in a prominent place on the website: In reference to IEEE copyrighted material which is used with permission in this thesis, the IEEE does not endorse any of [university/educational entity's name goes here]'s products or services. Internal or personal use of this material is permitted. If interested in reprinting/republishing IEEE copyrighted material for advertising or promotional purposes or for creating new collective works for resale or redistribution, please go to http://www.ieee.org/publications_standards/publications/rights/rights_link.html to learn how to obtain a License from RightsLink.

If applicable, University Microfilms and/or ProQuest Library, or the Archives of Canada may supply single copies of the dissertation.

[BACK](#) [CLOSE WINDOW](#)

Permission of Figure 28.



Requesting permission to reuse content from an IEEE publication

Prospect of New AFM Probe Design Enabled by Stress Gradient
Conference Proceedings: 2021 21st International Conference on Solid-State Sensors, Actuators and Microsystems (Transducers)
Author: Omar Alshehri
Publisher: IEEE
Date: 20 June 2021
Copyright © 2021, IEEE

Thesis / Dissertation Reuse

The IEEE does not require individuals working on a thesis to obtain a formal reuse license, however, you may print out this statement to be used as a permission grant:

Requirements to be followed when using any portion (e.g., figure, graph, table, or textual material) of an IEEE copyrighted paper in a thesis:

- 1) In the case of textual material (e.g., using short quotes or referring to the work within these papers) users must give full credit to the original source (author, paper, publication) followed by the IEEE copyright line © 2011 IEEE.
- 2) In the case of illustrations or tabular material, we require that the copyright line © [Year of original publication] IEEE appear prominently with each reprinted figure and/or table.
- 3) If a substantial portion of the original paper is to be used, and if you are not the senior author, also obtain the senior author's approval.


Requirements to be followed when using an entire IEEE copyrighted paper in a thesis:

- 1) The following IEEE copyright/ credit notice should be placed prominently in the references: © [Year of original publication] IEEE. Reprinted, with permission, from [author names, paper title, IEEE publication title, and month/year of publication].
- 2) Only the accepted version of an IEEE copyrighted paper can be used when posting the paper or your thesis on-line.
- 3) In placing the thesis on the author's university website, please display the following message in a prominent place on the website: In reference to IEEE copyrighted material which is used with permission in this thesis, the IEEE does not endorse any of [university/educational entity's name goes here]'s products or services. Internal or personal use of this material is permitted. If interested in reprinting/republishing IEEE copyrighted material for advertising or promotional purposes or for creating new collective works for resale or redistribution, please go to http://www.ieee.org/publications_standards/publications/rights/rights_link.html to learn how to obtain a License from RightsLink.

If applicable, University Microfilms and/or ProQuest Library, or the Archives of Canada may supply single copies of the dissertation.

[BACK](#) [CLOSE WINDOW](#)

Permission of Figure 29.



Prospect of New AFM Probe Design Enabled by Stress Gradient
Conference Proceedings: 2021 21st International Conference on Solid-State Sensors, Actuators and Microsystems (Transducers)
Author: Omar Alshehri
Publisher: IEEE
Date: 20 June 2021
Copyright © 2021, IEEE

Thesis / Dissertation Reuse

The IEEE does not require individuals working on a thesis to obtain a formal reuse license, however, you may print out this statement to be used as a permission grant:

Requirements to be followed when using any portion (e.g., figure, graph, table, or textual material) of an IEEE copyrighted paper in a thesis:

- 1) In the case of textual material (e.g., using short quotes or referring to the work within these papers) users must give full credit to the original source (author, paper, publication) followed by the IEEE copyright line © 2011 IEEE.
- 2) In the case of illustrations or tabular material, we require that the copyright line © [Year of original publication] IEEE appear prominently with each reprinted figure and/or table.
- 3) If a substantial portion of the original paper is to be used, and if you are not the senior author, also obtain the senior author's approval.


Requirements to be followed when using an entire IEEE copyrighted paper in a thesis:

- 1) The following IEEE copyright/ credit notice should be placed prominently in the references: © [Year of original publication] IEEE. Reprinted, with permission, from [author names, paper title, IEEE publication title, and month/year of publication]
- 2) Only the accepted version of an IEEE copyrighted paper can be used when posting the paper or your thesis on-line.
- 3) In placing the thesis on the author's university website, please display the following message in a prominent place on the website: In reference to IEEE copyrighted material which is used with permission in this thesis, the IEEE does not endorse any of [university/educational entity's name goes here]'s products or services. Internal or personal use of this material is permitted. If interested in reprinting/republishing IEEE copyrighted material for advertising or promotional purposes or for creating new collective works for resale or redistribution, please go to http://www.ieee.org/publications_standards/publications/rights/rights_link.html to learn how to obtain a License from RightsLink.

If applicable, University Microfilms and/or ProQuest Library, or the Archives of Canada may supply single copies of the dissertation.

[BACK](#) [CLOSE WINDOW](#)

Permission of Figure 30.



Prospect of New AFM Probe Design Enabled by Stress Gradient
Conference Proceedings: 2021 21st International Conference on Solid-State Sensors, Actuators and Microsystems (Transducers)
Author: Omar Alshehri
Publisher: IEEE
Date: 20 June 2021
Copyright © 2021, IEEE

Thesis / Dissertation Reuse

The IEEE does not require individuals working on a thesis to obtain a formal reuse license, however, you may print out this statement to be used as a permission grant:

Requirements to be followed when using any portion (e.g., figure, graph, table, or textual material) of an IEEE copyrighted paper in a thesis:

- 1) In the case of textual material (e.g., using short quotes or referring to the work within these papers) users must give full credit to the original source (author, paper, publication) followed by the IEEE copyright line © 2011 IEEE.
- 2) In the case of illustrations or tabular material, we require that the copyright line © [Year of original publication] IEEE appear prominently with each reprinted figure and/or table.
- 3) If a substantial portion of the original paper is to be used, and if you are not the senior author, also obtain the senior author's approval.


Requirements to be followed when using an entire IEEE copyrighted paper in a thesis:

- 1) The following IEEE copyright/ credit notice should be placed prominently in the references: © [Year of original publication] IEEE. Reprinted, with permission, from [author names, paper title, IEEE publication title, and month/year of publication]
- 2) Only the accepted version of an IEEE copyrighted paper can be used when posting the paper or your thesis on-line.
- 3) In placing the thesis on the author's university website, please display the following message in a prominent place on the website: In reference to IEEE copyrighted material which is used with permission in this thesis, the IEEE does not endorse any of [university/educational entity's name goes here]'s products or services. Internal or personal use of this material is permitted. If interested in reprinting/republishing IEEE copyrighted material for advertising or promotional purposes or for creating new collective works for resale or redistribution, please go to http://www.ieee.org/publications_standards/publications/rights/rights_link.html to learn how to obtain a License from RightsLink.

If applicable, University Microfilms and/or ProQuest Library, or the Archives of Canada may supply single copies of the dissertation.

[BACK](#) [CLOSE WINDOW](#)

Permission of Figure 31.



Prospect of New AFM Probe Design Enabled by Stress Gradient
Conference Proceedings: 2021 21st International Conference on Solid-State Sensors, Actuators and Microsystems (Transducers)
Author: Omar Alshehri
Publisher: IEEE
Date: 20 June 2021
Copyright © 2021, IEEE

Thesis / Dissertation Reuse

The IEEE does not require individuals working on a thesis to obtain a formal reuse license, however, you may print out this statement to be used as a permission grant:

Requirements to be followed when using any portion (e.g., figure, graph, table, or textual material) of an IEEE copyrighted paper in a thesis:

- 1) In the case of textual material (e.g., using short quotes or referring to the work within these papers) users must give full credit to the original source (author, paper, publication) followed by the IEEE copyright line © 2011 IEEE.
- 2) In the case of illustrations or tabular material, we require that the copyright line © [Year of original publication] IEEE appear prominently with each reprinted figure and/or table.
- 3) If a substantial portion of the original paper is to be used, and if you are not the senior author, also obtain the senior author's approval.

Requirements to be followed when using an entire IEEE copyrighted paper in a thesis:

- 1) The following IEEE copyright/ credit notice should be placed prominently in the references: © [Year of original publication] IEEE. Reprinted, with permission, from [author names, paper title, IEEE publication title, and month/year of publication]
- 2) Only the accepted version of an IEEE copyrighted paper can be used when posting the paper or your thesis on-line.
- 3) In placing the thesis on the author's university website, please display the following message in a prominent place on the website: In reference to IEEE copyrighted material which is used with permission in this thesis, the IEEE does not endorse any of [university/educational entity's name goes here]'s products or services. Internal or personal use of this material is permitted. If interested in reprinting/republishing IEEE copyrighted material for advertising or promotional purposes or for creating new collective works for resale or redistribution, please go to http://www.ieee.org/publications_standards/publications/rights/rights_link.html to learn how to obtain a License from RightsLink.

If applicable, University Microfilms and/or ProQuest Library, or the Archives of Canada may supply single copies of the dissertation.

[BACK](#) [CLOSE WINDOW](#)

Permission of Figure 33.

3/20/23, 4:20 PM		RightsLink Printable License	
SPRINGER NATURE LICENSE TERMS AND CONDITIONS		Will you be translating? no	
Mar 20, 2023		Circulation/distribution 1 - 29	
		Author of this Springer Nature content no	
This Agreement between Omar D Alshehri ("You") and Springer Nature ("Springer Nature") consists of your license details and the terms and conditions provided by Springer Nature and Copyright Clearance Center.		Title New Platform Designs for Enabling Atomic Interactions in Solid and Gaseous States	
License Number 5513071408909		Institution name University of Waterloo	
License date Mar 20, 2023		Expected presentation date Apr 2023	
Licensed Content Publisher Springer Nature		Portions Figure 1 (a) and Figure 3 (a),(b) and (c)	
Licensed Content Publication Nonlinear Dynamics		Requester Location Omar D Alshehri Industrial Engineering Department College of Engineering King Saud University Riyadh, Riyadh 11421 Saudi Arabia Attn: Omar D Alshehri	
Licensed Content Title Lateral pull-in instability of electrostatic MEMS transducers employing repulsive force		Total 0.00 USD	
Licensed Content Author Meysam Daeichin et al		Terms and Conditions	
Licensed Content Date Apr 29, 2020		Springer Nature Customer Service Centre GmbH Terms and Conditions	
Type of Use Thesis/Dissertation		The following terms and conditions ("Terms and Conditions") together with the terms specified in your [RightsLink] constitute the License ("License") between you as Licensee and Springer Nature Customer Service Centre GmbH as Licensor. By clicking 'accept' and completing the transaction for your use of the material ("Licensed Material"), you confirm your acceptance of and obligation to be bound by these Terms and Conditions.	
Requestor type academic/university or research institute		I. Grant and Scope of License	
Format print and electronic		1.1. The Licensor grants you a personal, non-exclusive, non-transferable, non-sublicensable, revocable, world-wide License to reproduce, distribute, communicate to the public, make available, broadcast, electronically transmit or create derivative works using the Licensed Material for the purpose(s) specified in your RightsLink License Details only. Licenses are granted for the specific use requested in the order	
Portion figures/tables/illustrations			
Number of figures/tables/illustrations 3			

Permission of Figure 34.

IEEE Requesting permission to reuse content from an IEEE publication

M-TEST: A test chip for MEMS material property measurement using electrostatically actuated test structures
 Author: P.M. Osterberg
 Publication: Journal of Microelectromechanical Systems
 Publisher: IEEE
 Date: June 1997
 Copyright © 1997, IEEE

Thesis / Dissertation Reuse

The IEEE does not require individuals working on a thesis to obtain a formal reuse license, however, you may print out this statement to be used as a permission grant:

Requirements to be followed when using any portion (e.g., figure, graph, table, or textual material) of an IEEE copyrighted paper in a thesis:

- 1) In the case of textual material (e.g., using short quotes or referring to the work within these papers) users must give full credit to the original source (author, paper, publication) followed by the IEEE copyright line © 2011 IEEE.
- 2) In the case of illustrations or tabular material, we require that the copyright line © [year of original publication] IEEE appear prominently with each reprinted figure and/or table.
- 3) If a substantial portion of the original paper is to be used, and if you are not the senior author, also obtain the senior author's approval.

Requirements to be followed when using an entire IEEE copyrighted paper in a thesis:

- 1) The following IEEE copyright/credit notice should be placed prominently in the references: © [year of original publication] IEEE. Reprinted, with permission, from [author names, paper title, IEEE publication title, and month/year of publication]
- 2) Only the accepted version of an IEEE copyrighted paper can be used when posting the paper or your thesis on-line.
- 3) In placing the thesis on the author's university website, please display the following message in a prominent place on the website: In reference to IEEE copyrighted material which is used with permission in this thesis, the IEEE does not endorse any of [university/educational entity's name goes here's] products or services. Internal or personal use of this material is permitted. If interested in reprinting/republishing IEEE copyrighted material for advertising or promotional purposes or for creating new collective works for resale or redistribution, please go to http://www.ieee.org/publications_standards/publications/rights/rights_link.html to learn how to obtain a License from RightsLink.

If applicable, University Microfilms and/or ProQuest Library, or the Archives of Canada may supply single copies of the dissertation.

BACK
CLOSE WINDOW

Permission of Figure 35.

IEEE Requesting permission to reuse content from an IEEE publication

Capacitance and Force Computation Due to Direct and Fringing Effects in MEMS/NEMS Arrays
 Author: Prashant N. Kambali
 Publication: IEEE Sensors Journal
 Publisher: IEEE
 Date: January 2016
 Copyright © 2016, IEEE

Thesis / Dissertation Reuse

The IEEE does not require individuals working on a thesis to obtain a formal reuse license, however, you may print out this statement to be used as a permission grant:

Requirements to be followed when using any portion (e.g., figure, graph, table, or textual material) of an IEEE copyrighted paper in a thesis:

- 1) In the case of textual material (e.g., using short quotes or referring to the work within these papers) users must give full credit to the original source (author, paper, publication) followed by the IEEE copyright line © 2011 IEEE.
- 2) In the case of illustrations or tabular material, we require that the copyright line © [year of original publication] IEEE appear prominently with each reprinted figure and/or table.
- 3) If a substantial portion of the original paper is to be used, and if you are not the senior author, also obtain the senior author's approval.


Requirements to be followed when using an entire IEEE copyrighted paper in a thesis:

- 1) The following IEEE copyright/credit notice should be placed prominently in the references: © [year of original publication] IEEE. Reprinted, with permission, from [author names, paper title, IEEE publication title, and month/year of publication]
- 2) Only the accepted version of an IEEE copyrighted paper can be used when posting the paper or your thesis on-line.
- 3) In placing the thesis on the author's university website, please display the following message in a prominent place on the website: In reference to IEEE copyrighted material which is used with permission in this thesis, the IEEE does not endorse any of [university/educational entity's name goes here's] products or services. Internal or personal use of this material is permitted. If interested in reprinting/republishing IEEE copyrighted material for advertising or promotional purposes or for creating new collective works for resale or redistribution, please go to http://www.ieee.org/publications_standards/publications/rights/rights_link.html to learn how to obtain a License from RightsLink.

If applicable, University Microfilms and/or ProQuest Library, or the Archives of Canada may supply single copies of the dissertation.

BACK
CLOSE WINDOW

Permission of Figure 36.



Capacitance and Force Computation Due to Direct and Fringing Effects in MEMS/NEMS Arrays

Author: Prashant N. Kambali
 Publication: IEEE Sensors Journal
 Publisher: IEEE
 Date: January 2016

Copyright © 2016, IEEE

Thesis / Dissertation Reuse

The IEEE does not require individuals working on a thesis to obtain a formal reuse license, however, you may print out this statement to be used as a permission grant:

Requirements to be followed when using any portion (e.g., figure, graph, table, or textual material) of an IEEE copyrighted paper in a thesis:

- 1) In the case of textual material (e.g., using short quotes or referring to the work within these papers) users must give full credit to the original source (author, paper, publication) followed by the IEEE copyright line © 2011 IEEE.
- 2) In the case of illustrations or tabular material, we require that the copyright line © [Year of original publication] IEEE appear prominently with each reprinted figure and/or table.
- 3) If a substantial portion of the original paper is to be used, and if you are not the senior author, also obtain the senior author's approval.

Requirements to be followed when using an entire IEEE copyrighted paper in a thesis:

- 1) The following IEEE copyright/ credit notice should be placed prominently in the references: © [Year of original publication] IEEE. Reprinted, with permission, from [author names, paper title, IEEE publication title, and month/year of publication]
- 2) Only the accepted version of an IEEE copyrighted paper can be used when posting the paper or your thesis on-line.
- 3) In placing the thesis on the author's university website, please display the following message in a prominent place on the website: In reference to IEEE copyrighted material which is used with permission in this thesis, the IEEE does not endorse any of [university/educational entity's name goes here]'s products or services. Internal or personal use of this material is permitted. If interested in reprinting/republishing IEEE copyrighted material for advertising or promotional purposes or for creating new collective works for resale or redistribution, please go to http://www.ieee.org/publications_standards/publications/rights/rights_link.html to learn how to obtain a License from RightsLink.

If applicable, University Microfilms and/or ProQuest Library, or the Archives of Canada may supply single copies of the dissertation.

BACK
CLOSE WINDOW

Permission of Figure 43.



TOPLINE CORPORATION
 95 HIGHWAY 22 W.
 MILLEDGEVILLE, GA. 31061 USA
 Tel 1-800-776-9888
 Tel 1-478-451-5000
 www.topline.tv

Statement of Work


Contact: Omar Alshehri
Company: UNIVERSITY OF WATERLOO
Address: 200 UNIVERSITY AVE WEST
City, State: WATERLOO ONTAR
Country:
Tel:
Email: oalshetri@uwaterloo.ca
CC:

Date: Mar, 29 2023
Quotation# 126265 A
Customer# 793512

From: Jennifer Thigpen
Tel: 800-776-9888 x709
Email: Jennifer@topline.tv

Item	Subject	DWG
01A	LCC52B50SQ.75-N350	169872

Permission of Figure 46.



Prospect of New AFM Probe Design Enabled by Stress Gradient

Conference Proceedings: 2021 21st International Conference on Solid-State Sensors, Actuators and Microsystems (Transducers)
 Author: Omar Alshehri
 Publisher: IEEE
 Date: 20 June 2021

Copyright © 2021, IEEE

Thesis / Dissertation Reuse

The IEEE does not require individuals working on a thesis to obtain a formal reuse license, however, you may print out this statement to be used as a permission grant:

Requirements to be followed when using any portion (e.g., figure, graph, table, or textual material) of an IEEE copyrighted paper in a thesis:

- 1) In the case of textual material (e.g., using short quotes or referring to the work within these papers) users must give full credit to the original source (author, paper, publication) followed by the IEEE copyright line © 2011 IEEE.
- 2) In the case of illustrations or tabular material, we require that the copyright line © [Year of original publication] IEEE appear prominently with each reprinted figure and/or table.
- 3) If a substantial portion of the original paper is to be used, and if you are not the senior author, also obtain the senior author's approval.

Requirements to be followed when using an entire IEEE copyrighted paper in a thesis:

- 1) The following IEEE copyright/ credit notice should be placed prominently in the references: © [Year of original publication] IEEE. Reprinted, with permission, from [author names, paper title, IEEE publication title, and month/year of publication]
- 2) Only the accepted version of an IEEE copyrighted paper can be used when posting the paper or your thesis on-line.
- 3) In placing the thesis on the author's university website, please display the following message in a prominent place on the website: In reference to IEEE copyrighted material which is used with permission in this thesis, the IEEE does not endorse any of [university/educational entity's name goes here]'s products or services. Internal or personal use of this material is permitted. If interested in reprinting/republishing IEEE copyrighted material for advertising or promotional purposes or for creating new collective works for resale or redistribution, please go to http://www.ieee.org/publications_standards/publications/rights/rights_link.html to learn how to obtain a License from RightsLink.

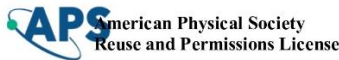
If applicable, University Microfilms and/or ProQuest Library, or the Archives of Canada may supply single copies of the dissertation.

BACK
CLOSE WINDOW

Permission of Figure 55.

<p>4/11/23, 9:01 AM</p> <p>RightLink Printable License</p> <p>Number of figures/tables/illustrations: 1</p> <p>Will you be translating?: no</p> <p>Circulation/distribution: 1 - 29</p> <p>Author of this Springer Nature content: no</p> <p>Title: New Platform Designs for Enabling Atomic Interactions in Solid and Gaseous States</p> <p>Institution name: University of Waterloo</p> <p>Expected presentation date: Apr 2023</p> <p>Portions: figure 8.6.</p> <p>Requestor Location: Omar D Alshehri Industrial Engineering Department College of Engineering King Saud University Riyadh, Riyadh 11421 Saudi Arabia Attn: Omar D Alshehri</p> <p>Total: 0.00 USD</p> <p>Terms and Conditions</p> <p>https://s100.copyright.com/AppDispatchServlet</p>	<p>4/11/23, 9:01 AM</p> <p>RightLink Printable License</p> <p>SPRINGER NATURE LICENSE TERMS AND CONDITIONS</p> <p>Apr 11, 2023</p> <hr/> <p>This Agreement between Omar D Alshehri ("You") and Springer Nature ("Springer Nature") consists of your license details and the terms and conditions provided by Springer Nature and Copyright Clearance Center.</p> <p>License Number: 5525760389978</p> <p>License date: Apr 11, 2023</p> <p>Licensed Content Publisher: Springer Nature</p> <p>Licensed Content Publication: Springer eBook</p> <p>Licensed Content Title: Energy-conserving Transducers</p> <p>Licensed Content Date: Jan 1, 2002</p> <p>Type of Use: Thesis/Dissertation</p> <p>Requestor type: non-commercial (non-profit)</p> <p>Format: print and electronic</p> <p>Portion: figures/tables/illustrations</p> <p>https://s100.copyright.com/AppDispatchServlet</p>
---	--

Permissions of Figure 61.



01-May-2023
This license agreement between the American Physical Society ("APS") and Omar Alshehri ("You") consists of your license details and the terms and conditions provided by the American Physical Society and SciPm.

Licensed Content Information

License Number: RNP:23MAY065886
 License date: 01 May 2023
 DOI: 10.1103/PhysRevLett.139.024602
 Title: Reconfigurable Optothermal Microsphere Trap in Air-Filled Hollow-Core Photonic Crystal Fiber
 Author: O. A. Schmidt et al.
 Publication: Physical Review Letters
 Publisher: American Physical Society
 Cost: USD \$ 0.00

Request Details

Does your reuse require significant modifications: No

Specify intended distribution locations: Worldwide

Reuse Category: Reuse in a thesis/dissertation

Requestor Type: Student

Items for Reuse: Figures/Tables

Number of Figure/Tables: 1

Figure/Tables Details: Particle guided in hollow-core PCF approaching a thermal hotspot, shown at several different positions.

Format for Reuse: Print and Electronic



Total number of print copies: Up to 1000

Information about New Publication:

University/Publisher: University of Waterloo
 Title of dissertation/thesis: New Platform Designs for Enabling Atomic Interactions in Solid and Gaseous States
 Author(s): Omar Alshehri
 Expected completion date: May 2023

License Requestor Information

Name: Omar Alshehri
 Affiliation: Individual
 Email Id: oalshehr@uwaterloo.ca
 Country: Canada

 Lincoln Connor <Lincoln.Connor@nktphotonics.com>
To:  Omar Alshehri

Hello Omar,

Yes, feel free to use the figure, as long as you reference its source.

Best of luck!

Lincoln Connor
Senior Sales Manager for Central North America

NKT Photonics Inc.
 110 16th St. Mall, Unit 1300 • Denver, CO • USA
 Tel: (303) 817-8799
www.nktphotonics.com

Permission of Figure 62.

APS American Physical Society
Reuse and Permissions License

01-May-2023

This license agreement between the American Physical Society ("APS") and Omar Alshahri ("You") consists of your license details and the terms and conditions provided by the American Physical Society and APSRe.

Licensed Content Information

License Number: RNP-23-MAY-065897
 License date: 01-May-2023
 DOI: 10.1103/PhysRevE.77.050904
 Title: Discovery of a diamond-based photonic crystal structure in boron nitride
 Author: Jeremy W. Gohshi et al.
 Publication: Physical Review E
 Publisher: American Physical Society
 Cost: USD \$ 0.00

Request Details

Does your reuse require significant modifications? No
 Are you intended distribution locations: Worldwide
 Reuse Category: Reuse in a thesis/dissertation
 Requester Type: Student
 Items for Reuse: Figure/Titles
 Number of Figure/Titles: 1
 Figure/Titles Details: Boron and its photonic crystal
 Format for Reuse: Print and Electronic
 Total number of print copies: Up to 1000

Information about New Publication

University/Publisher: University of Waterloo
 Title of dissertation/thesis: New Platform Designs for Enabling Atomic Interactions in Solid and Gaseous States
 Author(s): Omar Alshahri
 Expected completion date: May, 2023

License Requestor Information

Name: Omar Alshahri
 Affiliation: Jado Akad
 Email Id: oalshah@uwaterloo.ca
 Country: Canada

Page 1 of 2

Permission of Figure 63.

Berger <berger@mpi-halle.mpg.de>
 To: Omar Alshahri

Dear Mr. Alshahri,

You may use the named image for non-commercial purposes in your dissertation. The correct indication of authorship/copyright is assumed.

Best regards,
 Andreas Berger

Dr. Andreas Berger
 Verwaltungsbüro/Forschungsadministrator
 Head of Administration/Research Coordination
 Max-Planck-Institut für Mikrostrukturphysik
 Weinberg 2, 06120 Halle (Saale), Germany
 Besucheradresse: Weinberg 11, 06120 Halle (Saale)
 Phone: +49-345-5582 600
 Fax: +49-345-5582 588

Permission of Figure 65.

NOKIA

Intellectual Property Department 650 Mountain Avenue, Murray Hill, NJ 07974 (908) 610-8063

PERMISSION AGREEMENT
 Req. No.: 0423-04

Permission is granted to Omar Alshahri Student at University of Waterloo Ontario, Canada oalshahri@uwaterloo.ca April 11, 2023

To adapt the following images: Figure 1 (a) and 17 (a) from Bell System Technical Journal paper:
 "Low-loss Single-Material Fibers Made From Pure Fused Silica"

It is agreed that the purpose for which the images is being used is: In a Ph. D Thesis "New Platform Designs for Enabling Atomic Interactions in Solid and Gaseous States"

End credit reading: "Nokia Corporation and AT&T Archives." Permission to reproduce an adaptation of the figures for the license of the product, worldwide, in all languages, and in the format (DVI, streaming, and downloading) originally requested, and must not be contained in a further license to use the images for other purposes or to reproduce other Nokia images. Nokia does not endorse your products.

Nokia reserves the right to withdraw permission to reproduce material whenever, in its discretion, it feels the privilege of reproducing its material is being used in a way detrimental to its interest or the above terms are not being followed.

Images are not for use in or in conjunction with any legal proceeding.

No permission is granted to use trademarks, trade dress, service marks, names or other indicia or origin ("marks") of Nokia or its affiliates apart from the incidental appearance of such marks in the figures.

This Agreement shall be governed by the laws of the State of New York, without regard to the conflict of law provisions. The parties hereto submit to the exclusive jurisdiction of the courts located in New York, New York.

Nokia Corporation
 By: _____ Name: Edward Dickert
 Title: Nokia Intellectual Property
 Date: April 4, 2023

By: _____ Name: _____
 Title: _____
 Date: _____

IP Department 07-14-17

Permission of Figure 68.

RM Rehbinder Maria <maria.rehbinder@aalto.fi>
To: Omar Alshehri

Dear Omar Alshehri,

If you use the figure in your PhD thesis as a citation, and cite the author and the source according to good scientific practice, you may reproduce the figure.

Maria Elisabeth Rehbinder
Senior Legal Counsel
Certified Information Privacy Professional (CIPP/E)
<https://www.linkedin.com/in/maria-elisabeth-rehbinder-9a807321/>
ORCID: <https://orcid.org/0000-0001-8427-9421>

maria.rehbinder@aalto.fi
+35850570 3396
Aalto-yliopisto - Aalto University
Otaniementie 14, Väre Q303
Academic Legal Services

Permission of Figure 69.

ELSEVIER LICENSE TERMS AND CONDITIONS	
Mar 22, 2023	
This Agreement between Omar D Alshehri ("You") and Elsevier ("Elsevier") consists of your license details and the terms and conditions provided by Elsevier and Copyright Clearance Center.	
License Number	5514200165684
License date	Mar 22, 2023
Licensed Content Publisher	Elsevier
Licensed Content Publication	Photonics and Nanostructures - Fundamentals and Applications
Licensed Content Title	Silicon-based two-dimensional photonic crystal waveguides
Licensed Content Author	C. Jamois, R.B. Wehrspohn, J.C. Andreani, C. Hermann, O. Hess, U. Gösele
Licensed Content Date	Dec 1, 2003
Licensed Content Volume	1
Licensed Content Issue	1
Licensed Content Pages	13
Start Page	1
End Page	13

<https://is100.copyright.com/AppDispatchServlet>

1/8

RightsLink Printable License	
Type of Use	reuse in a thesis/dissertation
Portion	figures/tables/illustrations
Number of figures/tables/illustrations	2
Format	both print and electronic
Are you the author of this Elsevier article?	No
Will you be translating?	No
Title	New Platform Designs for Enabling Atomic Interactions in Solid and Gaseous States
Institution name	University of Waterloo
Expected presentation date	Apr 2023
Portions	Figures 2
Requestor Location	Omar D Alshehri Industrial Engineering Department College of Engineering King Saud University Riyadh, Riyadh 11421 Saudi Arabia Attn: Omar D Alshehri
Publisher Tax ID	GB 494 6272 12
Total	0.00 USD
Terms and Conditions	INTRODUCTION

<https://is100.copyright.com/AppDispatchServlet>

2/8

Permission of Figure 70.

Atomic clocks inspire new qubits: Early research explores a more robust quantum computer - [News]

Author: Mark Anderson
Publication: IEEE Spectrum
Publisher: IEEE
Date: December 2018
Copyright © 2018, IEEE

Requesting permission to reuse content from an IEEE publication

Thesis / Dissertation Reuse

The IEEE does not require individuals working on a thesis to obtain a formal reuse license, however, you may print out this statement to be used as a permission grant:

Requirements to be followed when using any portion (e.g., figure, graph, table, or textual material) of an IEEE copyrighted paper in a thesis:


- 1) In the case of textual material (e.g., using short quotes or referring to the work within these papers) users must give full credit to the original source (author, paper, publication) followed by the IEEE copyright line © 2011, IEEE.
- 2) In the case of illustrations or tabular material, we require that the copyright line © [Year of original publication] IEEE appear prominently with each reprinted figure and/or table.
- 3) If a substantial portion of the original paper is to be used, and if you are not the senior author, also obtain the senior author's approval.

Requirements to be followed when using an entire IEEE copyrighted paper in a thesis:

- 1) The following IEEE copyright/ credit notice should be placed prominently in the references: © [year of original publication] IEEE. Reprinted, with permission, from [author names, paper title, IEEE publication title, and month/year of publication]
- 2) Only the accepted version of an IEEE copyrighted paper can be used when posting the paper or your thesis on-line.
- 3) In placing the thesis on the author's university website, please display the following message in a prominent place on the website: In reference to IEEE copyrighted material which is used with permission in this thesis, the IEEE does not endorse any of [university/educational entity's name goes here]'s products or services. Internal or personal use of this material is permitted. If interested in reprinting/republishing IEEE copyrighted material for advertising or promotional purposes or for creating new collective works for resale or redistribution, please go to http://www.ieee.org/publications_standards/publications/rights/rights_link.html to learn how to obtain a License from RightsLink.

If applicable, University Microfilms and/or ProQuest Library, or the Archives of Canada may supply single copies of the dissertation.

Permission of Figure 71

 Lincoln Connor <Lincoln.Connor@nktphotonics.com>
To: ○ Omar Alshehri

Hello Omar,

Yes, feel free to use the figure, as long as you reference its source.

Best of luck!

Lincoln Connor
Senior Sales Manager for Central North America

NKT Photonics Inc.
110 16th St. Mall, Unit 1300 • Denver, CO • USA
Tel: (303) 817-8799
www.nktphotonics.com

Permission of Figure 72.

 Sven Ederer <svener@leibinger-stiftung.de>
To: ○ Omar Alshehri
Cc: ○ Markus Wener <markus.wener@leibinger-stiftung.de>

 Mon 17/04/2023 11:32 AM

Dear Omar,

thank you for your request. Permission is granted as requested.
Good luck and all the best for your dissertation,

Best regards,
Sven

Dipl.-Phys. Sven Ederer
Berthold Leibinger Stiftung GmbH

Telefon: +49 7156 303-35202, svener@leibinger-stiftung.de
Berthold Leibinger Stiftung GmbH, Johann-Maus-Strasse 2, 71254 Ditzingen, Deutschland, www.leibinger-stiftung.de

Berthold Leibinger Stiftung GmbH, Sitz Ditzingen, Amtsgericht Stuttgart HRB 204041
Geschäftsführung: Markus Wener

Die Informationen zur Erhebung Ihrer personenbezogenen Daten nach Art. 13 DSGVO können Sie unserer Website unter <https://www.leibinger-stiftung.de/de/datenschutz> entnehmen.

Permission of Figure 74.

DATE March 30, 2023

Name of Publication: New Platform Designs for Enabling Atomic Interactions in Solid and Gaseous States)

Author: Omar Alshehri

Publisher: University of Waterloo (the "Publisher")

Description or sample of Material: Dissertation requirement for the degree of Doctor of Philosophy In Mechanical and Mechatronics Engineering (Nanotechnology)

Thorlabs, Inc. hereby grants permission to Publisher under a Creative Commons Attribution License (CC BY) to include the Material in the Work, and in all future editions and revisions thereof, without restriction, and to create derivative and ancillary works therefrom for research and academic purposes only subject to making such derivative work generally available under the grant of a similar license, and to publish such derivative work in all media now known or hereafter discovered throughout the world and in all languages, whether published by the Publisher or its licensees.

A credit line to acknowledge use of the material is required and shall reference "Thorlabs, Inc." and the product part number(s).

Agreed and Accepted:

THORLABS, INC.


By:  Digitally signed by Christopher Russo
Date: 2023.03.30 09:00:48 -0400

Date: March 30, 2023

Name: Christopher Russo

Title: Corporate Counsel

Permission of Figure 80.



Fluid-Filled Solid-Core Photonic Bandgap Fibers
Author: Boris T. Kuhlmeiy
Publication: Journal of Lightwave Technology
Publisher: IEEE
Date: June 2009
Copyright © 2009, IEEE

Thesis / Dissertation Reuse

The IEEE does not require individuals working on a thesis to obtain a formal reuse license, however, you may print out this statement to be used as a permission grant:

Requirements to be followed when using any portion (e.g., figure, graph, table, or textual material) of an IEEE copyrighted paper in a thesis:

- 1) In the case of textual material (e.g., using short quotes or referring to the work within these papers) users must give full credit to the original source (author, paper, publication) followed by the IEEE copyright line © 2011 IEEE.
- 2) In the case of illustrations or tabular material, we require that the copyright line © [Year of original publication] IEEE appear prominently with each reprinted figure and/or table.
- 3) If a substantial portion of the original paper is to be used, and if you are not the senior author, also obtain the senior author's approval.


Requirements to be followed when using an entire IEEE copyrighted paper in a thesis:

- 1) The following IEEE copyright/ credit notice should be placed prominently in the references: © [year of original publication] IEEE. Reprinted, with permission, from [author names, paper title, IEEE publication title, and month/year of publication]
- 2) Only the accepted version of an IEEE copyrighted paper can be used when posting the paper or your thesis on-line.
- 3) In placing the thesis on the author's university website, please display the following message in a prominent place on the website: In reference to IEEE copyrighted material which is used with permission in this thesis, the IEEE does not endorse any of [university/educational entity's name goes here]'s products or services. Internal or personal use of this material is permitted. If interested in reprinting/republishing IEEE copyrighted material for advertising or promotional purposes or for creating new collective works for resale or redistribution, please go to http://www.ieee.org/publications_standards/publications/rights/rights_link.html to learn how to obtain a License from RightsLink.

If applicable, University Microfilms and/or ProQuest Library, or the Archives of Canada may supply single copies of the dissertation.

[BACK](#) [CLOSE WINDOW](#)

Permission of Figure 81.



High-Sensitivity Temperature Sensor Based on a Selectively-Polymer-Filled Two-Core Photonic Crystal Fiber In-Line Interferometer
Author: Khurram Naeem
Publication: IEEE Sensors Journal
Publisher: IEEE
Date: July 2015
Copyright © 2015, IEEE

Thesis / Dissertation Reuse

The IEEE does not require individuals working on a thesis to obtain a formal reuse license, however, you may print out this statement to be used as a permission grant:

Requirements to be followed when using any portion (e.g., figure, graph, table, or textual material) of an IEEE copyrighted paper in a thesis:

- 1) In the case of textual material (e.g., using short quotes or referring to the work within these papers) users must give full credit to the original source (author, paper, publication) followed by the IEEE copyright line © 2011 IEEE.
- 2) In the case of illustrations or tabular material, we require that the copyright line © [Year of original publication] IEEE appear prominently with each reprinted figure and/or table.
- 3) If a substantial portion of the original paper is to be used, and if you are not the senior author, also obtain the senior author's approval.


Requirements to be followed when using an entire IEEE copyrighted paper in a thesis:

- 1) The following IEEE copyright/ credit notice should be placed prominently in the references: © [year of original publication] IEEE. Reprinted, with permission, from [author names, paper title, IEEE publication title, and month/year of publication]
- 2) Only the accepted version of an IEEE copyrighted paper can be used when posting the paper or your thesis on-line.
- 3) In placing the thesis on the author's university website, please display the following message in a prominent place on the website: In reference to IEEE copyrighted material which is used with permission in this thesis, the IEEE does not endorse any of [university/educational entity's name goes here]'s products or services. Internal or personal use of this material is permitted. If interested in reprinting/republishing IEEE copyrighted material for advertising or promotional purposes or for creating new collective works for resale or redistribution, please go to http://www.ieee.org/publications_standards/publications/rights/rights_link.html to learn how to obtain a License from RightsLink.

If applicable, University Microfilms and/or ProQuest Library, or the Archives of Canada may supply single copies of the dissertation.

[BACK](#) [CLOSE WINDOW](#)

Permission of Figure 84.

 Cicero Martelli <cmartelli@utfpr.edu.br>
To: Omar Alshehri

Hello Omar,

yes, no problem.

Regards,
Cicero

Permission of Figure 90.


AIP PUBLISHING LICENSE TERMS AND CONDITIONS	
Mar 22, 2023	
This Agreement between Omar D Alshchri ("You") and AIP Publishing ("AIP Publishing") consists of your license details and the terms and conditions provided by AIP Publishing and Copyright Clearance Center.	
License Number	5514250536042
License date	Mar 22, 2023
Licensed Content Publisher	AIP Publishing
Licensed Content Publication	Applied Physics Letters
Licensed Content Title	Microfluidic tunable photonic band-gap device
Licensed Content Author	P. Domachuk, H. C. Nguyen, B. J. Eggleton, et al
Licensed Content Date	Mar 15, 2004
Licensed Content Volume	84
Licensed Content Issue	11
Type of Use	Thesis/Dissertation
Requestor type	Student
Format	Print and electronic

<https://i100.copyright.com/App/DispatchServlet>

RightsLink Printable License	
Portion	Figure/Table
Number of figures/tables	3
Will you be translating?	No
Title	New Platform Designs for Enabling Atomic Interactions in Solid and Gaseous States
Institution name	University of Waterloo
Expected presentation date	Apr 2023
Portions	Figure 3
Requestor Location	Omar D Alshchri Industrial Engineering Department College of Engineering King Saud University Riyadh, Riyadh 11421 Saudi Arabia Attn: Omar D Alshchri
Total	0.00 USD
Terms and Conditions	AIP Publishing -- Terms and Conditions: Permissions Uses
AIP Publishing hereby grants to you the non-exclusive right and license to use and/or distribute the Material according to the use specified in your order, on a one-time basis, for the specified term, with a maximum distribution equal to the number that you have ordered. Any links or other content accompanying the Material are not the subject of this license.	
<ol style="list-style-type: none"> 1. You agree to include the following copyright and permission notice with the reproduction of the Material: "Reprinted from [FULL CITIATION], with the permission of AIP Publishing." For an article, the credit line and permission notice must be printed on the first page of the article or book chapter. For photographs, covers, or tables, the notice may appear with the Material, in a footnote, or in the reference list. 2. If you have licensed reuse of a figure, photograph, cover, or table, it is your responsibility to ensure that the material is original to AIP Publishing and does not contain the copyright of another entity, and that the copyright notice of the figure, photograph, cover, or table does not indicate that it was reprinted by AIP Publishing. 	

<https://i100.copyright.com/App/DispatchServlet>

Permission of Figure 95.



Fabrication and Characterization of Long-Period Gratings in Hollow Core Fibers by Electric Arc Discharge

Author: Agostino Iadicicco
 Publication: IEEE Sensors Journal
 Publisher: IEEE
 Date: May 2015

Copyright © 2015, IEEE

Thesis / Dissertation Reuse

The IEEE does not require individuals working on a thesis to obtain a formal reuse license, however, you may print out this statement to be used as a permission grant:

Requirements to be followed when using any portion (e.g., figure, graph, table, or textual material) of an IEEE copyrighted paper in a thesis:

- 1) In the case of textual material (e.g., using short quotes or referring to the work within these papers) users must give full credit to the original source (author, paper, publication) followed by the IEEE copyright line © 2011 IEEE.
- 2) In the case of illustrations or tabular material, we require that the copyright line © [Year of original publication] IEEE appear prominently with each reprinted figure and/or table.
- 3) If a substantial portion of the original paper is to be used, and if you are not the senior author, also obtain the senior author's approval.

Requirements to be followed when using an entire IEEE copyrighted paper in a thesis:

- 1) The following IEEE copyright/ credit notice should be placed prominently in the references: © [year of original publication] IEEE. Reprinted, with permission, from [author names, paper title, IEEE publication title, and month/year of publication]
- 2) Only the accepted version of an IEEE copyrighted paper can be used when posting the paper or your thesis on-line.
- 3) In placing the thesis on the author's university website, please display the following message in a prominent place on the website: In reference to IEEE copyrighted material which is used with permission in this thesis, the IEEE does not endorse any of [university/educational entity's name goes here]'s products or services. Internal or personal use of this material is permitted. If interested in reprinting/republishing IEEE copyrighted material for advertising or promotional purposes or for creating new collective works for resale or redistribution, please go to http://www.ieee.org/publications_standards/publications/rights/rights_link.html to learn how to obtain a License from RightsLink.

If applicable, University Microfilms and/or ProQuest Library, or the Archives of Canada may supply single copies of the dissertation.

BACK
CLOSE WINDOW

Permission of Figure 97.

3/27/23, 3:09 PM <https://marketplace.copyright.com/cs-ui-web/mp/license/5b1e181e-d40a-15ed-e115-54582a475a29e89b3a2-950-49a-b70c-4a...>

CCC Marketplace

This is a License Agreement between Omar Alshehri ("User") and Copyright Clearance Center, Inc. ("CCC") on behalf of the Rightsholder identified in the order details below. The license consists of the order details, the Marketplace Permissions General Terms and Conditions below, and any Rightsholder Terms and Conditions which are included below.
All payments must be made in full to CCC in accordance with the Marketplace Permissions General Terms and Conditions below.

Order Date	23-Mar-2023	Type of Use	Republish in a thesis/dissertation
Order License ID	1337393-1	Publisher	INSTITUTE OF PHYSICS PUBLISHING
ISSN	0950-1317	Portion	Image/photo/illustration

LICENSED CONTENT

Publication Title	Journal of micromechanics and microengineering: structures, devices, and systems	Country	United Kingdom of Great Britain and Northern Ireland
Author/Editor	Institute of Physics (Great Britain)	Rightsholder	IOP Publishing, Ltd
Date	01/01/1991	Publication Type	Journal
Language	English		

REQUEST DETAILS

Portion Type	Image/photo/illustration	Distribution	Worldwide
Number of Images / Photos / Illustrations	1	Translation	Original language of publication
Format (select all that apply)	Print, Electronic	Copies for the Disabled?	No
Who Will Republish the Content?	Publisher, not-for-profit	Minor Editing Privileges?	No
Duration of Use	Life of current edition	Incidental Promotional Use?	No
Lifetime Unit Quantity	Up to 499	Currency	USD
Rights Requested	Main product		

NEW WORK DETAILS

Title	New Platform Designs for Enabling Atomic Interactions in Solid and Gaseous States	Institution Name	University of Waterloo
Instructor Name	William Melek	Expected Presentation Date	2024-04-01

ADDITIONAL DETAILS

Order Reference Number	N/A
-------------------------------	-----

<https://marketplace.copyright.com/cs-ui-web/mp/license/5b1e181e-d40a-15ed-e115-54582a475a29e89b3a2-950-49a-b70c-4a/2175/042d> 1/8

Permission of Figure 99.

ZX #ZHU XIANGWEN# <XIANGWEN001@e.ntu.edu.sg>
To: Omar Alshehri

Yes, you have my permission.

Regards
Xiangwen


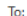
Permission of Figure 100.

AR Adam Rimshaw <adam.rimshaw@mksinst.com>
To: Omar Alshehri

Hi Omar,
Yes, that's fine. Good luck writing!
Regards,
Adam

Adam Rimshaw, PhD, MBA
Senior Inside Sales Engineer
Photonics Solutions Division
MKS Instruments, Inc.
Main:1-949-979-7098
adam.rimshaw@mksinst.com
www.mksinst.com

Permission of Figure 105.

 Lincoln Connor <Lincoln.Connor@nktphotronics.com>
To:  Omar Alshehri

Hello Omar,

Yes, feel free to use the figure, as long as you reference its source.

Best of luck!

Lincoln Connor
Senior Sales Manager for Central North America

NKT Photonics Inc.
110 16th St. Mall, Unit 1300 • Denver, CO • USA
Tel: (303) 817-8799
www.nktphotronics.com

Permission of Table 1

02/23, 2:57 PM RightsLink Printable License

SPRINGER NATURE LICENSE
TERMS AND CONDITIONS

Mar 27, 2023

This Agreement between Omar D Alshehri ("You") and Springer Nature ("Springer Nature") consists of your license details and the terms and conditions provided by Springer Nature and Copyright Clearance Center.

License Number	5517030430883
License date	Mar 27, 2023
Licensed Content Publisher	Springer Nature
Licensed Content Publication	MRS Online Proceedings Library
Licensed Content Title	Residual Stress of Silicon Films Deposited by LPCVD From Silane
Licensed Content Author	P. Temple-Boyer et al
Licensed Content Date	Dec 1, 1998
Type of Use	Thesis/Dissertation
Requestor type	non-commercial (non-profit)
Format	print and electronic
Portion	figures/tables/illustrations
Number of figures/tables/illustrations	1



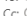
https://o1100.copyright.com/CustomerAdmin/PIF.jsp?refno=23a079_c5c:46be-b078-1bdf6d64300

02/23, 2:57 PM RightsLink Printable License

Will you be translating?	no
Circulation/distribution	1 - 29
Author of this Springer Nature content	no
Title	New Platform Designs for Enabling Atomic Interactions in Solid and Gaseous States
Institution name	University of Waterloo
Expected presentation date	Apr 2023
Portions	tables 1 and 2
Requestor Location	Omar D Alshehri Industrial Engineering Department College of Engineering King Saud University Riyadh, Riyadh 11421 Saudi Arabia Attn: Omar D Alshehri
Total	0.00 USD
Terms and Conditions	Springer Nature Customer Service Centre GmbH Terms and Conditions The following terms and conditions ("Terms and Conditions") together with the terms specified in your [RightsLink] constitute the License ("License") between you as Licensee and Springer Nature Customer Service Centre GmbH as Licensor. By clicking "accept" and completing the transaction for your use of the material ("Licensed Material"), you confirm your acceptance of and obligation to be bound by these Terms and Conditions. 1. Grant and Scope of License 1.1. The Licensor grants you a personal, non-exclusive, non-transferable, non-sublicensable, revocable, world-wide License to reproduce, distribute, communicate to the public, make available, broadcast, electronically transmit or create derivative works using the Licensed Material for the purpose(s) specified in your RightsLink License Details only. Licenses are granted for the specific use requested in the order

https://o1100.copyright.com/CustomerAdmin/PIF.jsp?refno=23a079_c5c:46be-b078-1bdf6d64300

Permission of Table 3 and Table 4.

 Nicolas BERTSCH <Nicolas.BERTSCH@memscap.com>
To:  Omar Alshehri
Cc:  Christine Schmid <christines@science.xyz>

Hi Omar,

As MEMSCAP, we are definitely OK with your request.
Please credit the company for the content that you extract and that will be fine.
You may also contact Christine Schmid from Science as MEMSCAP recently sold its MUMPS business to Science and I am not 100% sure what the MUMPS naming will be in the future.

Best regards
Nicolas

MEMSCAP S.A.
C.O.O.

Phone Direct: +33 (0)4 7692 85 08
Mobile: +33 (0)6 22 52 51 38


Mon 20/03/2023 04:25 PM